Efficacy evaluation of multiple Parkinson's disease vaccine candidates

Inaugural-Dissertation

zur Erlangung des Doktorgrades
der Mathematisch-Naturwissenschaftlichen Fakultät
der Heinrich-Heine-Universität Düsseldorf

vorgelegt von

Liang Ma
aus Liaoning, China

Düsseldorf, April 2024

aus dem Institut für Physikalische Biologie
der Heinrich-Heine-Universität Düsseldorf

Gedruckt mit der Genehmigung der
Mathematisch-Naturwissenschaftlichen Fakultät der
Heinrich-Heine-Universität Düsseldorf

Berichterstatter:

1. Prof. Dr. Gültekin Tamgüney

2. Prof. Dr. Dieter Willbold

Tag der mündlichen Prüfung: 21. Juni 2024

Affidavit

I hereby declare on oath that I have produced my thesis independently and without any undue assistance by third parties under consideration of the 'Principles for Safeguarding Good Scientific Practice at Heinrich Heine University Düsseldorf.'

Furthermore, I declare that I have not attempted to submit this dissertation in any other dissertation procedure, with or without success.

Düsseldorf, April 22, 2024

_____

Liang Ma

Table of Content

Abstract

Parkinson's disease is a neurodegenerative disease that is becoming increasingly prevalent throughout the world and is disabling, debilitating, and fatal. Since aging is the main risk factor for the disease and no cure or prevention has been found, it is a significant problem in an aging population. It involves the oligomerization and fibrillization of the protein α-synuclein. These oligomers act as seeds, recruiting native α-synuclein monomers into insoluble aggregates. This leads to the death of dopaminergic neurons in the substantia nigra through a variety of toxic effects, ultimately resulting in neurological disease.

Currently, only symptomatic treatment is available. Therefore, the development of a vaccine for prevention or treatment would be of great importance. Several vaccine candidates have been tested in both preclinical and clinical studies. Although immunization studies targeting native α-synuclein have shown promising efficacy in mouse models, the transition of these vaccines into clinical phases is challenging due to the significant risk of autoimmune reactions. Therefore, shorter epitopes of α-synuclein have been explored to mitigate T helper cell activation and the potential for subsequent autoimmune responses.

A novel methodology was used in this study. The fibril-forming fungal prion HET-s was modified to display four distinct epitopes present on the surface of synthetic α-synuclein fibrils, resulting in the creation of four individual vaccines. The efficacy of these vaccines was then evaluated in the TgM83$^{+/-}$ mice modeling either brain-first or body-first Parkinson's disease. All vaccinated mice showed sustained weight gain, but only mice used to model body-first Parkinson's disease showed improved performance in motor behavior, and prolonged life expectancy compared to the non-vaccinated mice.

In conclusion: Immunization with the developed vaccine candidates delayed disease onset and improved motor behavior in mice modeling body-first Parkinson's disease. Subsequently, but much later, vaccinated mice developed identical pathology and neuroinflammation as non-vaccinated mice. In addition, this study shows that antibodies in the plasma of vaccinated mice effectively identify vaccines, α-synuclein fibrils, and brain homogenates from patients with various synucleinopathies. The vaccines developed and tested in this study show promising potential for clinical trials, as the induced antibodies exhibit recognition of human pathogenic α-synuclein.

List of Figures

List of Tables

List of Abbreviations

Abbreviation	Meaning
α-syn	α-Synuclein
ATP	Adenosine triphosphate
BBB	Blood brain barrier
BSA	Bovine serum albumin
CB	Citric buffer
CNS	Central nervous system
DAB	3-3′-diaminobenzidine
DAPI	4',6-diamidino-2-phenylindole
DBS	Deep brain stimulation
DLB	Dementia with Lewy bodies
dmX	Dorsal motor nucleus of the vagus nerve
DNA	Deoxyribonucleic acid
E. coli	Escherichia coli
ELISA	Enzyme-linked immunosorbent assay
ENS	Enteric nervous system
ER	Endoplasmic reticulum
GFAP	Glial fibrillary acidic protein
HRP	Horseradish peroxidase
Iba1	Ionized calcium-binding adaptor molecule 1
IG	Intragastric injection
IP	Intraperitoneal injection
IPTG	Isopropyl-beta-D-1-thiogalactopyranoside
iRBD	Isolated rapid eye movement (REM) sleep behavior disorder
IC	Intracerebral injection

kDa	Kilodalton
LBs	Lewy bodies
LNs	Lewy neurites
MSA	Multiple system atrophy
NAC	Non-amyloid-β component
NGS	Normal goat serum
NMR	Nuclear magnetic resonance spectroscopy
OD	Optical density
PARK	Parkinson's disease related genes
PBS	Phosphate-buffered saline
PCR	Polymerase chain reaction
PD	Parkinson's disease
PDD	Parkinson's disease dementia
PFA	Paraformaldehyde
PTMs	Posttranslational modifications
ROS	Reactive oxygen species
rpm	Revolutions per minute
RT	Room temperature
SCNA	Gene encoding mouse α-syn
SDS	Sodium dodecyl sulfate
SN	Substantia nigra
Siah-1	Seven in absentia homologue-1
SUMO	Small ubiquitin-like modifiers
Tg	Transgenic
TLRs	Toll-like receptors
TOM	Translocase of the outer membrane
TR-FRET	Time-resolved fluorescence resonance energy transfer

VAPB	Vesicle-associated membrane protein B
v/v	Volume per volume
w/v	Weight per volume
WB	Western blot
wt	Wild-type

1 Introduction

1.1 Synucleinopathies and Parkinson's disease

Synucleinopathies are a group of neurodegenerative diseases characterized by aggregation of the protein α-synuclein (α-syn). The synucleinopathies include Parkinson's disease (PD), dementia with Lewy bodies (DLB) and multiple system atrophy (MSA). The hallmark pathological features are the presence of α-syn aggregates in neuronal cell bodies (Lewy bodies, LBs), which also contain other components, and in neurites (Lewy neurites, LNs). Glial cytoplasmic inclusions are also observed in oligodendrocytes of MSA patients (Fujiwara *et al*., 2002; Koga *et al*., 2021; Spillantini *et al*., 1997; Spillantini and Goedert, 2000). These α-syn aggregates cause the death of dopaminergic neurons in the substantia nigra, resulting in a dopamine deficit (Gómez-Benito *et al*., 2020; Taschenberger *et al*., 2012). PD is one of the most common neurodegenerative diseases, along with Alzheimer's disease, and its incidence increases with age. In addition to aging, several external factors are associated with an increased risk of developing PD. These factors include exposure to environmental toxins, drugs, pesticides, dairy consumption, and a history of traumatic brain injury or melanoma (Hubble *et al*., 1993; Park *et al*., 2005; Ascherio and Schwarzschild, 2016; Tysnes and Storstein, 2017).

The incidence of PD increases from 1% in individuals in their sixties to 3% in individuals in their eighties. Notably, men are more likely to develop the disease than women (Pringsheim *et al*., 2014; Lee and Gilbert, 2016). While most cases of PD are sporadic, 10-15% of cases are genetically predisposed due to multiplications or missense mutations in the SNCA gene, which is located on human chromosome 4q21-q23 and codes for α-syn (Fig. 1). Several additional genetic mutations have been identified in other Parkinson's disease-related genes (PARK), also known as familial PD genes (Polymeropoulos *et al*., 1997; Pankratz and Foroud, 2004; Hyun *et al*., 2013; Chan *et al*., 2017).

Braak and colleagues observed a stereotypical pattern of α-syn accumulation in the brain. In postmortem PD brains, LBs were first found in the olfactory bulb and the dorsal motor nucleus of the vagal nerve (dmX) prior to motor impairment. As the disease progresses, connected brain areas are also affected. Braak and colleagues classified the spreading of α-syn within the brain into six stages (Braak *et al*., 2003). They hypothesized that aggregated α-syn pathology is present in the olfactory bulb and the dorsal motor nucleus of the vagus nerve, including connected areas of the lower brainstem, in stages I and II. Patients in these stages may experience symptoms such as loss of smell, emotional disturbance, and sleep disorders. In stage III, Lewy body pathology spreads into midbrain regions, such as the amygdala and substantia nigra (SN). Additionally, patients may experience thermoregulation disorders. In

stage IV of PD, LBs begin to appear in the thalamus and associated meso- and allocortex, marking the onset of the symptomatic phase. At this stage, the dopaminergic neurons of the SN are already severely damaged, leading to the appearance of major clinical symptoms: bradykinesia, resting tremor, rigidity, and instability. In stages V and VI, LBs are present in the neocortex and frontal lobe, affecting all motor and sensory brain regions. At the final stage, patients experience psychiatric symptoms, visual hallucinations, and dementia, in addition to the clinical motor symptoms (Braak *et al*., 2003; Goedert, Clavaguera and Tolnay, 2010; Goedert *et al.*, 2014; Braak and Del Tredici, 2016).

PD is characterized by motor symptoms including bradykinesia, resting tremor, rigidity, and changes in posture and gait. In addition to these symptoms, patients may also experience sleep disturbance, anosmia, difficulty swallowing, and digestive problems such as constipation (Tolosa *et al*., 2021; Jankovic, 2008; Chung and Pfeiffer, 2021; Ali *et al*., 1996). Currently, there is no cure for PD, and only the motor symptoms can be treated. Symptomatic treatment for PD relies heavily on the administration of levodopa, a dopamine precursor, to replace the missing dopamine (Katzenschlager and Lees, 2002; Schapira *et al*. 2009). Levodopa treatment can be supplemented with monoamine oxidase inhibitors, such as selegiline and rasagiline, which reduce the breakdown of dopamine and improve motor function (Young *et al*., 1997; Alborghetti and Nicoletti, 2019). Deep brain stimulation (DBS) is a therapeutic approach in which electrodes are surgically placed in specific areas of the brain. These electrodes are then stimulated at high frequencies. In the treatment of PD, the subthalamic nucleus and globus pallidus internus are targeted. However, both medications and DBS focus on managing symptoms and do not stop the disease from progressing (Benabid, 2003; Kalia *et al*., 2013).

1.2 Native α-syn

α-Syn was first described in the electric torpedo ray by (Maroteaux *et al*. 1988). Shortly after its discovery, two additional members of the synuclein family were discovered: β-syn and γ-syn (Nakajo *et al*., 1993; Jakes *et al*., 1994; Lavedan *et al*., 1998). Native α-syn is only present in vertebrates (George, 2002) and is mainly expressed in the brain (Jakes *et al*., 1994; Iwai *et al*., 1995). Physiological α-syn exists as both an intrinsically disordered monomer and a stable tetramer, present in the cytosol and membrane-bound in neurons (Tong *et al*., 2010; George, 2002; Jakes *et al*., 1994; Bartels *et al*., 2011). The human protein α-syn consists of 140 amino acids divided into three major domains. The N-terminal domain (amino acids 1-60) is the membrane-binding domain and forms an amphipathic α-helix (Davidson *et al*., 1998; Eliezer *et al*., 2001; Chandra *et al*., 2003). This domain also contains most of the missense mutations associated with familial PD. These mutations include A18T, A29S, A30P, E46K, H50Q, G51D,

A53E, and A53T among others (Polymeropoulos *et al.*, 1997; Krüger *et al.*, 1998; Conway *et al*., 1998; Zarranz *et al*., 2004; Proukakis *et al*., 2013; Kiely *et al*., 2013; Pasanen *et al*., 2014). Amino acids 61 to 95 form the hydrophobic 'non-amyloid-β component', shortened to 'NAC domain'. This domain is primarily responsible for the formation of α-syn aggregates by inducing a conformational change from random coil to β-sheets (Uéda *et al.*, 1993). Recently, another familial mutation, E83Q, was found in this region marking the first familial mutation found outside the N-terminal domain (Kumar *et al*., 2022). The C-terminal domain (amino acids 96-140) is acidic and can be truncated. One of the most important post-translational modifications (PTMs) is also found here. Serine 129 is phosphorylated in many pathological α-syn species. This domain also contains a calcium binding site (Uéda *et al*., 1993; Crowther *et al*., 1998; Li *et al*., 2002; Nielsen *et al.,* 2001). The exact function of α-syn is not yet fully understood, however, its presynaptic localization suggests that it plays a role in vesicle recycling. The protein also binds to phospholipids and synaptobrevin-2, playing a role in the assembly of the SNARE complex (Burré *et al.*, 2010; Nakajo *et al.*, 1993) (Fig. 1).

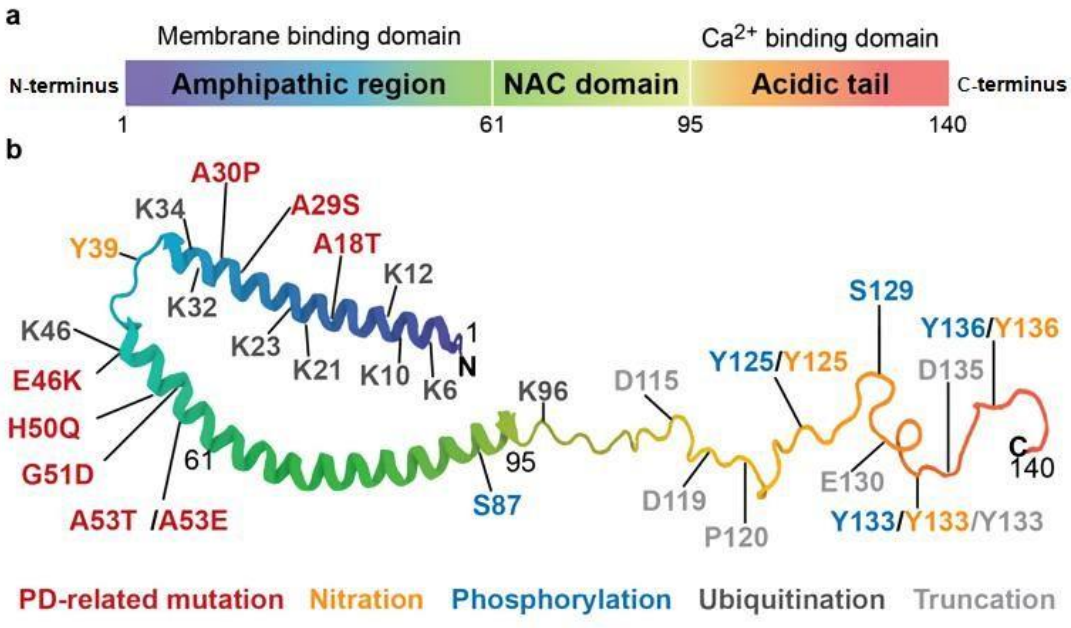

Fig. 1 Structure of membrane-bound α-syn and posttranslational modifications. Native α-syn can be divided into three domains: **(a)** N-terminal domain, NAC domain, and C-terminal domain. Some of the missense mutations associated with familial PD are in the N-terminal domain. **(b)** Additionally, there are posttranslational modifications at various amino acids of the protein.

1.3 Aggregation of α-syn

Under various conditions, the α-syn can adopt different conformations (Fig. 2). Physiologically, α-syn exists as a monomer. However, under pathological conditions, the monomers can adopt

β-sheet structures and form oligomers, which act as seeds and recruit more and more α-syn monomers, resulting in the formation of protofibrils. These protofibrils form long, insoluble amyloid fibrils that are rich in β-sheet structures and are neurotoxic (Smith *et al*., 2006). Furthermore, fibrillar α-syn is resistant to degradation by Proteinase K (Spillantini *et al.*, 1998; Neumann *et al*., 2004).

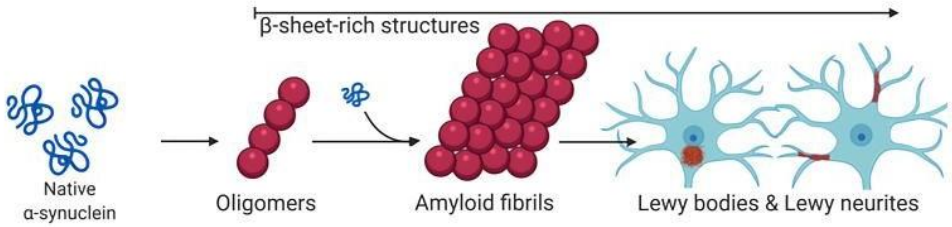

Fig. 2 α-Syn aggregation. Typically, α-syn exists as an unfolded monomer, which is either in a free form or membrane-bound. However, under pathological conditions, monomeric α-syn can spontaneously misfold and form oligomers that assemble into α-syn fibrils, ultimately depositing in LBs and LNs.

1.4 Posttranslational modifications contributing to α-syn aggregation

PTMs alter certain characteristics of α-syn, affecting its physiological functions, but also aggregate formation and neurotoxicity. Most of these modification sites are located in either the N- or C-terminal domain (Uversky and Eliezer, 2009; Oueslati, Fournier and Lashuel, 2010).

1.4.1 Phosphorylation

Phosphorylation of serine 129 is the most common PTMs of pathological α-syn (Anderson *et al*., 2006; Foulds *et al.*, 2013). This process involves various kinases, such as casein kinase I and II, G-protein-coupled receptor kinases, and Polo-like kinase 2, which catalyze the transfer of the γ-phosphate of adenosine triphosphate (ATP) to serine or tyrosine residues (Pratt *et al.*, 2015; Inglis *et al*., 2009; Okochi *et al*., 2000; Pronin *et al*., 2000). Phosphorylation at serine 129 is thought to enhance fibril formation (Anderson *et al*., 2006; Iwatsubo, 2003). However, phosphorylation at serine 87 reduces aggregation while simultaneously diminishing the binding capability of α-syn to membranes (Paleologou *et al.*, 2010). Additionally, tyrosine residues at positions 39, 125, 133, and 136 are known to be phosphorylated (Ellis *et al*., 2001; Negro *et al*., 2002; Mahul-Mellier *et al*., 2014).

1.4.2 Nitration and oxidation

Nitration and oxidation are additional common PTMs observed in α-syn. During this modification, a nitro group replaces the hydrogen atom at the 3'-position of the tyrosine phenol ring, resulting in the formation of 3-nitrotyrosine (Chavarría and Souza, 2013; Giasson *et al*., 2000). This modification specifically occurs at the tyrosine residues Y39, Y125, Y133, and Y136 of α-syn (Sevcsik *et al.,* 2011; Burai *et al.,* 2015). Each of these nitrated monomeric α-syn species contributes to the increased accumulation of α-syn, potentially facilitating fibril formation (Hodara *et al.,* 2004; Danielson *et al.,* 2009).

1.4.3 Truncation

In LBs and LNs, in addition to full-length α-syn, truncated forms of α-syn ranging in size from 10 to 15 kDa are present (Baba *et al*., 1998; Crowther *et al.,* 1998; Campbell *et al*., 2001). Approximately 15% of the existing α-syn pool is truncated. These truncated forms of α-syn show an increased tendency to form pathological cellular inclusions and accelerate fibril formation. Additionally, C-terminally truncated α-syn has been demonstrated to enhance the accumulation of full-length α-syn, exhibiting a seeding property (Murray *et al*., 2003; Tofaris *et al*., 2003; Hoyer *et al*., 2004).

1.4.4 Ubiquitination and SUMOylation

Ubiquitin, which consists of 76 amino acids, functions as a modification attached to lysine residues (Welchman *et al*., 2005). Ubiquitination plays a significant role in PD, as evidenced by the presence of ubiquitin in LBs (Gómez-Tortosa *et al.,* 2000; Kuzuhara *et al*., 1988). In the context of α-syn, ubiquitination appears to have pathological implications (Tofaris *et al*., 2003). Ubiquitination of α-syn can occur at nine different lysine residues (K6, K10, K12, K21, K23, K32, K34, K46, and K96). K6, K10, and K12 can also be ubiquitinated after aggregate formation (Nonaka, Iwatsubo, and Hasegawa, 2005; Rott *et al*., 2008). The ubiquitination of α-syn is primarily mediated by the ubiquitin-protein ligase seven in absentia homolog-1 (Siah-1) and can be observed as single, double, or triple modifications. Siah-1-mediated ubiquitination has been associated with increased α-syn aggregation in dopaminergic neurons (Lee *et al*., 2008b; Rott *et al.,* 2008; Hasegawa *et al*., 2002; Sampathu *et al*., 2003). Additionally, small ubiquitin-like modifiers (SUMO), including SUMO1, 2, and 3, can be attached to lysine residues and interact prominently with α-syn. SUMOylation also enhances α-syn accumulation by inhibiting the ubiquitin-dependent degradation pathway.

1.5 The toxicity of α-syn aggregates

1.5.1 Cellular stress

It is known that α-syn oligomers as well as α-syn fibrils are toxic (Peelaerts *et al*., 2015; Winner *et al.,* 2011). The oligomerization of α-syn plays a key role in mitochondrial dysfunction. It has

been demonstrated that α-syn oligomers disrupt mitochondrial-associated membranes, inhibit mitochondrial complexes, induce permeabilization of mitochondrial-like membranes, and increase mitochondrial fragmentation (Guardia-Laguarta *et al.*, 2014; Plotegher, Gratton, and Bubacco, 2014; Stefanovic *et al.*, 2014; Subramaniam *et al.*, 2014). Additionally, these oligomers initiate ATP synthase oxidation, leading to cellular demise (Ludtmann *et al.*, 2018) and impair protein import by binding to translocase of the outer membrane (TOM) 20 receptors (Di Maio *et al.*, 2016). Specific missense mutations in α-syn exacerbate mitochondrial damage. For instance, the H50Q mutation triggers oligomerization and mitochondrial fragmentation in hippocampal neurons (Appel-Cresswell *et al.*, 2013; Khalaf *et al.*, 2014). In contrast, the A53T mutation, in combination with phosphorylation at S129, increases intracellular reactive oxygen species (ROS) levels and enhances mitochondrial fragmentation (Perfeito *et al.*, 2014).

Due to its membrane-binding ability, α-syn directly interacts with synaptic vesicles and the endoplasmic reticulum (ER) membrane. The ER plays a crucial role in protein synthesis, folding, and transport within the cell. Toxic α-syn oligomers accumulate in the ER, causing significant stress to this cellular compartment (Colla *et al.*, 2012). These oligomers disrupt the interaction between the ER and mitochondria by binding to vesicle-associated membrane protein B (VAPB), leading to ER stress from disrupted calcium homeostasis. Heightened ER stress also promotes the aggregation of wild-type α-syn (Jiang *et al.*, 2010).

As previously mentioned, monomeric α-syn is involved in the formation of the SNARE complex. However, α-syn oligomers often bind to the N-terminal domain of Synaptobrevin-2, causing vesicle clustering, which restricts synaptobrevin in the synapse and prevents SNARE complex formation and exocytosis. This hinders the release of dopamine, leading to the typical symptoms of synucleinopathies (Nemani *et al.*, 2010; Choi *et al.*, 2013). Furthermore, α-syn oligomers disrupt the collaboration between microtubules and kinesin, leading to microtubule destabilization and impaired axonal transport. Furthermore, they impede tubulin polymerization, leading to cellular apoptosis (Chen *et al.*, 2007; Prots *et al.*, 2013).

1.5.2 Inflammatory responses mediated by microgliosis and astrogliosis

Neurodegenerative diseases are associated with neuroinflammation characterized by microgliosis and astrogliosis (Hirsch and Hunot, 2009). Inflammation is induced when α-syn aggregates, leading to neurotoxicity of the protein.

Microglia, the tissue-resident macrophages, are the primary immune cells in the central nervous system (CNS), maintaining homeostasis of the microenvironment through

chemotaxis, phagocytosis, and secretion of various inflammatory mediators. Astrocytes are the most abundant glial cells in the brain. They actively communicate with microglia, oligodendrocytes, other glial cells, and neurons. Additionally, astrocytes play a crucial role in maintaining the homeostasis of the brain microenvironment. They regulate synaptic transmission, control the permeability of the blood-brain barrier (BBB), and manage the homeostasis of water and ions. In addition, astrocytes are involved in the secretion of neurotrophins (Lee *et al.,* 2003; Sofroniew and Vinters, 2010; Allaman, Bélanger, and Magistretti, 2011; Wilton, Dissing-Olesen, and Stevens, 2019).

Microglia and astrocytes play crucial roles in the toxicity of α-syn oligomers, leading to neurodegeneration (Wu *et al*., 2002; Hirsch and Hunot, 2009; Lee *et al.*, 2010). Activation of microglia, triggered by α-syn oligomers through Toll-like receptors (TLRs), leads to increased levels of ROS and subsequent neuronal damage (Hughes *et al.*, 2019; Daniele *et al.*, 2015). Inhibition of microglial activation reduces cell death (Zhang *et al*., 2005; Shavali *et al*., 2006; Wilms *et al*., 2009). Activated microglia release proinflammatory cytokines, which exacerbate neuroinflammation (Theodore *et al*., 2008; Mitra *et al*., 2011). Astrocytes respond to microglial activation by forming a protective barrier around injured tissue. This process, known as astrogliosis, helps regulate microglial activity and protect neurons from oxidative stress. Although α-syn is expressed in small amounts in astrocytes, they take up α-syn resealed from neurons in a TLRs 4-independent way and induce neuroinflammation. (Fellner *et al*., 2013; Rannikko, Weber and Kahle, 2015).

1.5.3 Loss of dopaminergic neurons

Various cellular toxicity mechanisms follow α-syn aggregation, causing damage to vulnerable neurons in different brain areas. Including the dorsal motor nucleus of the vagus, the putamen, and especially the SN pars compacta (Hirsch, 1994; Dickson, 2007; Sulzer and Surmeier, 2013). However, the most affected neurons are dopaminergic neurons in the SN (Hirsch, Graybiel, and Agid, 1988; Petrucelli *et al.*, 2002; Chung *et al.*, 2005). The toxicity of α-syn aggregation to dopaminergic neurons has been demonstrated in various models, ranging from Drosophila, C. elegans, rodents, various cell culture models, to PD patients (Feany and Bender, 2000; Masliah *et al*., 2000a; Zhou *et al.,* 2000; Lakso *et al*., 2003; Hoban *et al*., 2020). Ultimately, the aggregation of α-syn and the degeneration of dopaminergic neurons in the SN lead to dopamine loss in the basal ganglia. The loss of function is projected onto the striatum and motor cortex, which are responsible for motor behavior and movement. resulting in the characteristic motor symptoms of PD (Hirsch, Graybiel, and Agid, 1988; Michel, Hirsch, and Hunot, 2016).

1.6 Transmission of α-syn aggregates

The prion-like behavior of misfolded α-syn has been discussed extensively. Similar to prions, α-syn oligomers recruit normal α-syn and form distinct β-sheet structures, leading to self-propagation (Luk *et al.*, 2009; Masuda-Suzukake *et al.,* 2013). α-Syn oligomers can be transmitted through various mechanisms, facilitating both short-distance cell-to-cell transmission and long-distance propagation to distant anatomical regions. Therefore, α-syn pathology can be observed not only in the CNS but also in the periphery, particularly in the enteric nervous system (ENS) (Annerino *et al.*, 2012; Recasens and Dehay, 2014).

1.6.1 Intercellular transmission

Cellular transmission of aggregated α-syn to neighboring neurons has been demonstrated in both cell culture and mouse models. Oligomeric α-syn may be released from the donor neuron into the extracellular space, from where it can enter a recipient neuron. Several mechanisms have been proposed for this cell-to-cell transmission (Fig. 3). Extracellular α-syn can be transferred to neighboring cells by clathrin-mediated endocytosis (Sung *et al.*, 2001), direct diffusion across the plasma membrane, or receptor-mediated endocytosis (Mao *et al.*, 2016). Another demonstrated transmission mechanism in cell culture is calcium-dependent exocytosis (Danzer *et al.*, 2012). Lysosomal-vesicle trafficking through tunneling nanotubes spanning from one neuron to another is considered another potential transmission route (Abounit *et al.*, 2016). Neuronal uptake of oligomeric α-syn, also called seeds, leads to recruitment of endogenous monomeric α-syn to form larger α-syn aggregates and fibrils, and this process leads to the formation of LBs, LNs, and eventual neuronal death (Luk *et al.*, 2009; Volpicelli-Daley *et al.*, 2011).

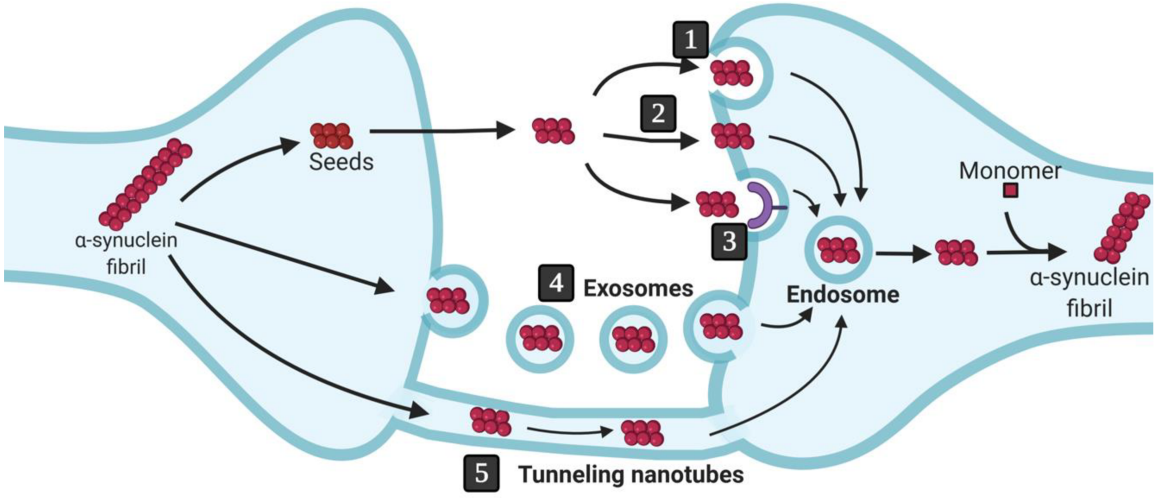

Fig. 3 Transmission pathways of α-syn between neurons. In its oligomeric form, α-syn can spread from one neuron to another, acting as a seed to induce fibril formation. This occurs through five possible pathways: (1) endocytosis, (2) diffusion or membrane penetration, (3) receptor-mediated endocytosis,

(4) exocytosis, or (5) via nanotunnels extending from one neuron to the next. Figure based on Guo and Lee, 2014.

1.6.2 Transmission via the gut-brain axis

The intercellular transmission ability of α-syn enables it to reach different areas that are neuronally connected. Neurons in the olfactory bulb can uptake aggregated forms of α-syn, which can then be transported to various brain regions (Rey *et al*., 2013). Furthermore, there is evidence that PD pathology can also originate in the gastrointestinal tract and spread from the ENS via the dmX to the CNS. PD pathology has been detected in the gastrointestinal tract in the early stages of PD and in patients with isolated rapid eye movement (REM) sleep behavior disorder (iRBD), with approximately 80% of iRBD patients subsequently developing PD, suggesting iRBD as a potential precursor to PD (Braak *et al*., 2006; Sprenger *et al*., 2015). The transmission via the gut-brain axis has been experimentally demonstrated in mice and rats through various challenge methods with α-syn fibrils, including intraperitoneal, intragastric, intramuscular, and intravenous injections and oral challenge (Breid *et al*., 2017; Lohmann *et al*., 2019; Uemura *et al*., 2018; Kim *et al*., 2019; Sacino *et al*., 2014). Additionally, it has been demonstrated that after seeding in the duodenum, α-syn pathology exhibits bidirectional trans-synaptic parasympathetic and sympathetic spread to the brain, as well as retrograde spread to the stomach and heart (Van den Berge *et al*., 2019).

1.7 The structure of α-syn fibrils

1.7.1 The structure of synthetic α-syn fibrils

The structures of synthetic α-syn fibrils to design the vaccine candidates used in this study have been determined using solid-state nuclear magnetic resonance (NMR) spectroscopy (PDB ID: 2N0A) (Tuttle *et al*., 2016) and cryo-electron microscopy (PDB ID: 6H6B) (Guerrero-Ferreira *et al.,* 2018). The structure determined by Tuttle et al. showed a single protofilament with a width of 5 nm. In contrast, the structure determined by Guerrero-Ferreira et al. showed that α-syn fibrils were 10 nm wide and composed of two adjacent protofilaments (Fig. 4a). Each α-syn (1-121) molecule consists of eight parallel β-strands arranged in a Greek key-like topology (Tuttle *et al*., 2016). The β-strands β2-β7 form a hydrophobic intramolecular core, which contributes to the stability of the protofilament. The hydrophobic core is surrounded by two hydrophilic regions, to which the less well-defined β1 and β8 strands attach (Fig. 4b). The N-terminal residues 1-41 and C-terminal residues 103-121 exhibit a flexible random coil arrangement. The α-syn subunits within each protofilament align along an approximately 2_1 screw-axis with a helical twist of -0.72° and a rise of 4.8 Å-4.9 Å (Guerrero-Ferreira *et al.,* 2018; Meade *et al.*, 2019; Li *et al*., 2018).

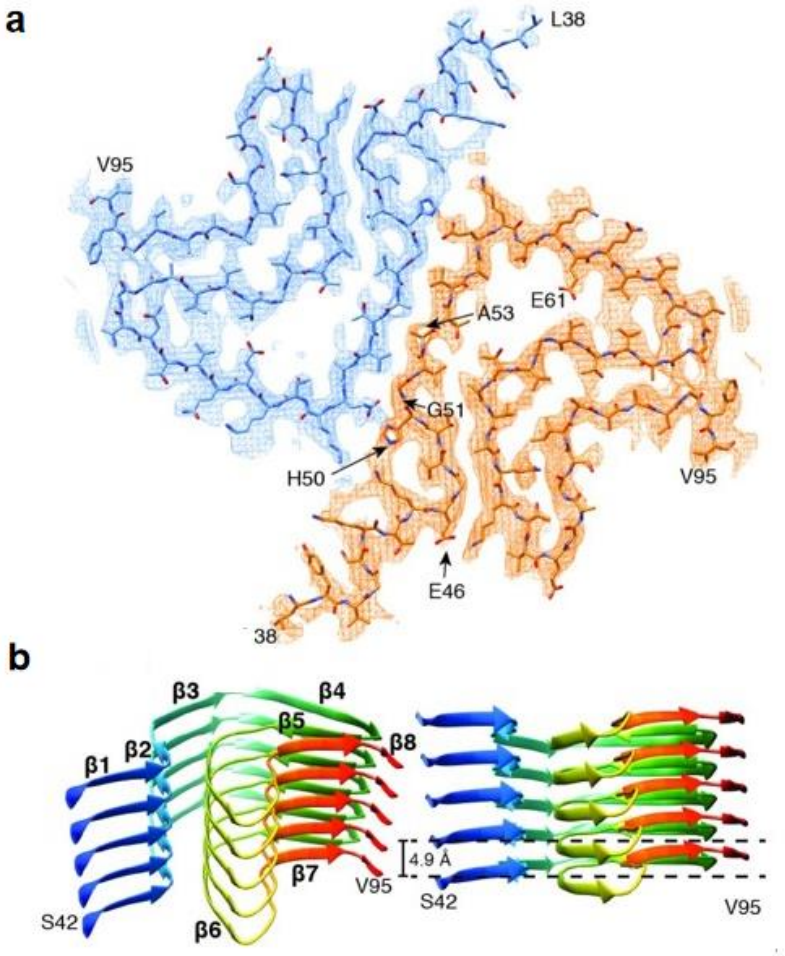

Fig. 4 Structure of synthetic α-syn fibril. (a) The schematic shows two protofilaments (in blue and orange) spanning from residues L38 to V95, along with the NAC domain (E61 to V95). Arrows indicate the positions of four of the five residues associated with familial mutations linked to PD (E46K, H50Q, G51D, and A53T/E). **(b)** The distribution of β-strands in a single protofilament of the α-syn fibril corresponds to residues S42 to V95. Figure based on Guerrero-Ferreira *et al.*, 2018.

1.7.2 The structures of α-syn fibrils isolated from patient brains with synucleinopathies

Recently, the structure of α-syn fibrils isolated from patients has been solved by cryo-electron microscopy, which highlight the existence of distinct molecular structures of aggregated α-syn in neurodegenerative disease. Distinct types of α-syn filament structures have been observed in the brains of patients with PD, Parkinson's disease dementia (PDD), and DLB versus patients with MSA.

The α-syn filaments obtained from PD, PDD, and DLB comprise a single protofilament referred to as the 'Lewy fold' (Fig. 5a). The Lewy fold is constituted by residues 31-100 of α-syn arranged into nine β-strands (β1-9) within a three-layered structure. The first two layers are corrugated, with the first layer including β1-5 and the second layer comprising β6-8. The third

layer consists solely of β9. Additionally, two partial layers are formed by densities that are not interconnected with the remainder of the structured core. Island A interacts with β5, while island B interacts with the N-terminal portion of β9. Reconstructed densities for both islands suggest they are peptides, but their precise identification is hindered by lack of discernible side-chain densities (Yang *et al.*, 2022).

In contrast, the structural characteristics of MSA filaments observed in human brains differs from the Lewy fold. The α-syn filaments from MSA patients' brains are comprised of two filament types, each composed of two distinct protofilaments (Fig. 5b). Both Type I and Type II filaments are asymmetric and consist of two protofilaments each. The larger protofilament of Type I filaments (PF-IA) is composed of residues G14–F94 of α-syn, while the smaller protofilament (PF-IB) is composed of residues K21–Q99. For Type II filaments, PF-IIA and PF-IIB are composed of residues G14–F94 and G36–Q99, respectively. Protofilament folds exhibit variability within and between filament types. MSA type I and type II filaments are composed of four distinct protofilaments. Two non-identical protofilaments interact through an extended interface, creating a cavity surrounded by the side chains of K43, K45, and H50 from each protofilament. This cavity encloses an additional density not connected to the protein density, the chemical nature of which remains to be determined (Schweighauser *et al.*, 2020).

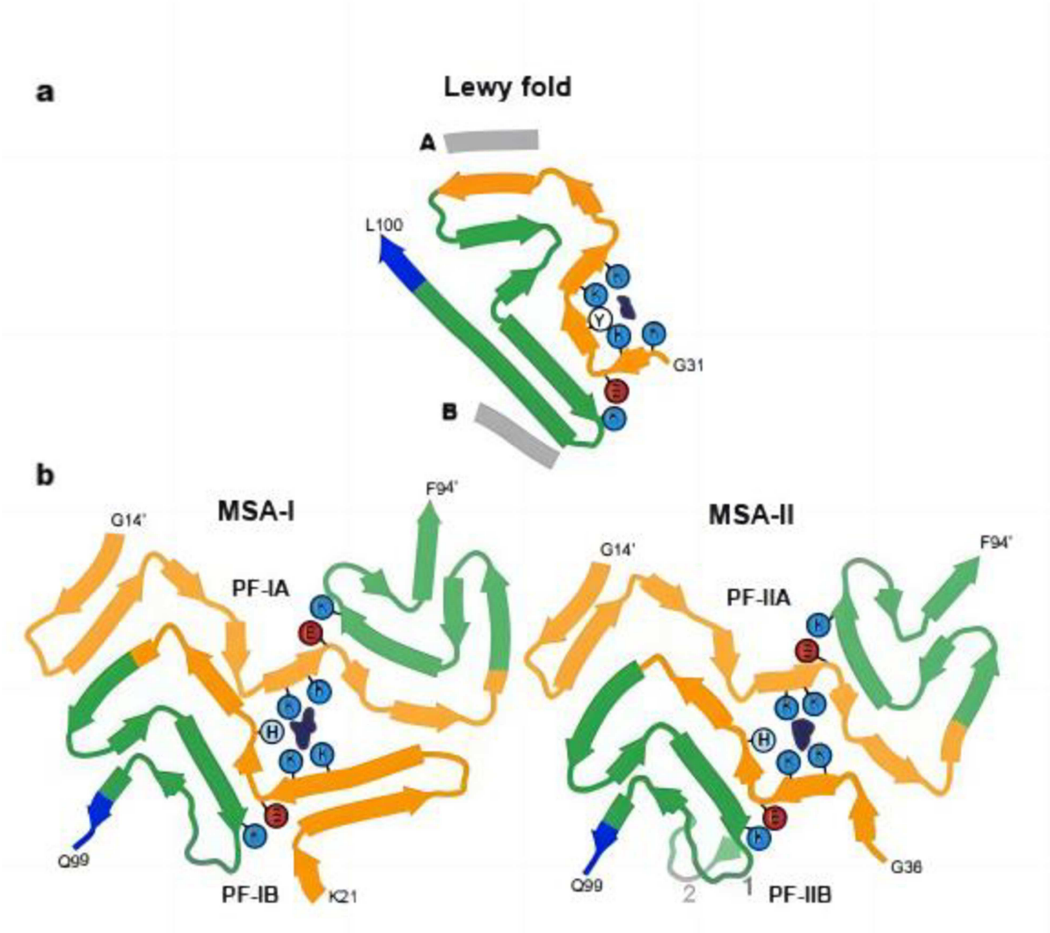

Fig. 5 Structures of α-syn filaments from human brains with Lewy pathology and MSA. (a) The α-syn filaments from PD, PDD, and DLB are identical and consist of a single protofilament. Two reconstructed densities (islands) are shown in light gray. **(b)** Schematic representation of type I and type II α-syn filaments in MSA. The non-proteinaceous density at the protofilament interface is indicated in dark blue. Figure based on Yang *et al*., 2022.

1.8 Parkinson's disease in mouse models

The clinical manifestations of PD can be modeled in mice using a variety of approaches. These include local or systemic delivery of neurotoxins or α-syn fibrils, the use of transgenic mouse lines, or a combination of both. The models aim to mimic the key pathological features of PD, including neuroinflammation and neurodegeneration, which lead to the development of severe PD-like motor symptoms.

1.8.1 TgM83 mouse models

Synucleinopathies can be mimicked by the overexpression of α-syn or by the induced overexpression of α-syn in transgenic (Tg) mouse models. Genetic mouse models provide a detailed representation of several characteristics of PD. For example, Tg mouse lines overexpressing human A53T or A30P mutant α-syn under the murine prion promoter exhibit high expression levels in the brain and spinal cord, as well as slightly elevated expression levels throughout other tissues (Giasson *et al*., 2002; Lee *et al*., 2002).

TgM83$^{+/-}$ mice express human α-syn with the familial A53T mutation but do not naturally develop any neuropathology or disease for up to 650 days. Injection of patient-derived and synthetic α-syn fibrils induces a PD-like neuropathology and disease in these mice with variable incubation times depending on the dose and route of injection. The phenotype manifests after injection of α-syn fibrils. Before movement impairment, mice may experience lax grooming, weight loss, and diminished mobility. As the condition progresses, they may develop partial limb paralysis, trembling, and an inability to stand. Immunohistochemistry analysis of mutants between 8 to 12 months of age reveals widely distributed α-syn inclusions, with dense accumulation in the spinal cord, brainstem, cerebellum, and thalamus. The appearance of α-syn inclusions parallels the onset of the motor impairment phenotype (Watts *et al*.,2013; Lohmann *et al*., 2019; Pesch *et al*.,2024).

In TgM83$^{+/-}$ mice, aggregation of α-syn causes a toxic gain-of-function for aggregated α-syn (Giasson *et al*., 2002; Lee *et al*., 2002), characterized by ER stress, oxidative stress, and mitochondrial dysfunction, which trigger the activation of cell death pathways and ultimately result in neurodegeneration, and behavioral impairment, thus modelling cellular mechanisms and symptoms present in familial PD (Singleton *et al.,* 2003; Farrer *et al*., 2004).

Synucleinopathy models, which involve inoculation with preformed α-syn fibrils, provide an opportunity to explore the mechanisms of transmission or prion-like spreading of α-syn observed in synucleinopathies (Lohmann *et al.*, 2019; Luk *et al.*, 2012b; Pesch *et al.*, 2024).

1.9 Immunization against PD

Considering the lack of a preventive measure for PD, there is a growing interest in exploring prevention or treatment options, including immunization. Currently, both preclinical and clinical studies are underway for passive and active immunization (Knecht *et al.*, 2022). For instance, it has been demonstrated that antibodies targeting α-syn can bind not only extracellular but also intracellular α-syn. This binding inhibits intercellular transmission of pathological α-syn and has the potential to destruction of oligomers (Tran *et al.*, 2014; Masliah *et al.*, 2005; Bae *et al.*, 2012).

1.9.1 Passive immunization against PD

Passive immunization is a therapeutic strategy for PD that focuses on treatment rather than prevention. This approach involves the administration of antibodies specifically targeting α-syn oligomers or fibrils via injections, aiming to rapidly intercept and clear aggregated α-syn (Bergström *et al.*, 2016). Preclinical investigations have shown promising results, with experimental models demonstrating improvements in motor function and reductions in α-syn pathology (Masliah *et al.*, 2011; Games *et al.*, 2014). Moving on to clinical trials, certain antibodies have progressed to Phase I trials, showing favorable tolerability profiles and a significant decrease in serum levels of α-syn (Jankovic *et al.*, 2018; Brys *et al.*, 2019). However, passive immunization has a significant drawback: the need for regular administration of antibodies. This not only increases the overall cost of treatment but also adds a considerable time burden for both patients and healthcare providers (Schneeberger *et al.*, 2016). Thus, although offering promising therapeutic potential, the practical implications of sustained antibody dosing pose substantial challenges for widespread implementation and accessibility.

1.9.2 Active immunization against PD

Active immunization is a distinct approach from passive immunization, as it obviates the need for regular administrations and provides lifelong protection. Initial investigations in mouse models have demonstrated the feasibility of active immunization against α-syn (Masliah *et al.*, 2005). However, direct translation to clinical studies has posed challenges due to the substantial risk of autoimmunity against α-syn. Clinical trials of an experimental vaccine targeting β-amyloid encountered autoimmunity, including meningoencephalitis induced by T-helper cells (Orgogozo *et al.*, 2003).

To address these concerns, vaccine development shifted towards utilizing individual short epitopes to minimize autoimmune risks. Integration of a foreign helper epitope with the α-syn epitopes facilitated antibody production while mitigating autoimmunity by T-helper cells (Ghochikyan *et al*., 2014). Consequently, vaccines that include these short epitopes have undergone initial clinical evaluations and have demonstrated good tolerability profiles (Poewe *et al.,* 2021; Volc *et al*., 2020).

However, challenges remain in ensuring both efficacy and safety in larger-scale clinical trials. Ongoing research aims to improve active immunization strategies against α-syn while minimizing the risk of adverse autoimmunity, advancing the prospects for PD disease-modifying therapies.

1.10 HET-s-derived vaccine candidates targeting α-syn fibrils

HET-s is a prion protein domain from the fungus Podospora anserina. It consists of 289 amino acids. The prion domain of HET-s, spanning amino acid residues 218-289, has the ability to form amyloid fibrils (Coustou *et al*., 1997; Balguerie *et al*., 2003). These fibrils have a left-handed, two-rung beta-solenoid folded structure with a distance of 4.8 ± 0.2 Å between each β-rung. Within these fibrils, each molecule of HET-s(218-289) forms eight β-sheet structures. Four β-sheets in one rung are on top of the other four in the second rung, creating a triangular β-solenoid shape (Wasmer *et al*., 2008) (Fig. 6A-C). To model specific antigenic determinants, selected amino acids from the synthetic surface of α-syn fibrils were introduced into the inert HET-s(218-289) scaffold protein in a structurally controlled, discontinuous manner.

Four vaccine candidates, namely α-SC3, α-SC6, α-SC8 and α-SC9 fibrils (Fig. 6D-G), were designed based on the structures of two synthetic α-syn fibrils, which were determined by cryo-electron microscopy (Guerrero-Ferreira *et al.*, 2018) and solid-state NMR spectroscopy (Tuttle *et al*., 2016). Specific amino acids were exchanged through targeted mutagenesis to create conformational epitopes present on the surface of fibrillar α-syn. All four vaccine candidates have the ability to self-assemble into typical amyloid fibrils (Fig. 7A-D).

1.11 Aim of the study

The objective of this study was to assess the efficacy of each of the four HET-s-derived fibrils as potential vaccine candidates for PD. Based on this, three questions were defined.

i. Whether each vaccine candidate can elicit an immune response against pathological α-syn aggregates in TgM83$^{+/-}$ mice.

ii. Whether each vaccine candidate can prevent or delay neurological disease in a TgM83$^{+/-}$ mouse model of brain-first PD.

iii. Whether each vaccine candidate can prevent or delay neurological disease in two different TgM83$^{+/-}$ mouse models of body-first PD.

To this aim, groups of 6-8 weeks old TgM83$^{+/-}$ mice were intraperitoneally immunized with a primary and three follow-up booster vaccinations at two-week intervals to induce active immunity. Groups of control mice were left unvaccinated. Blood samples were collected before each vaccination and two weeks after the final booster for enzyme-linked immunosorbent assay (ELISA). Two weeks after the last booster, synucleinopathy was seeded by the injection of α-syn fibrils (Lohmann *et al*., 2019). To model brain-first PD, groups of mice were injected intracerebrally with α-syn fibrils. Two routes of challenge with α-syn fibrils were used to model body-first PD. In one body-first PD model, TgM83$^{+/-}$ mice were injected intraperitoneally with α-syn fibrils, and in the other body-first PD model, groups of TgM83$^{+/-}$ mice were injected intragastrically with α-syn fibrils. The effects of vaccination on weight gain, performance in behavioral test, and survival of the mice were then examined. Furthermore, neuropathology was compared through immunohistochemistry and immunofluorescence analyses of brain sections, and by biochemical analyses of brain homogenates. The humoral immune response of the mice was assessed through ELISA.

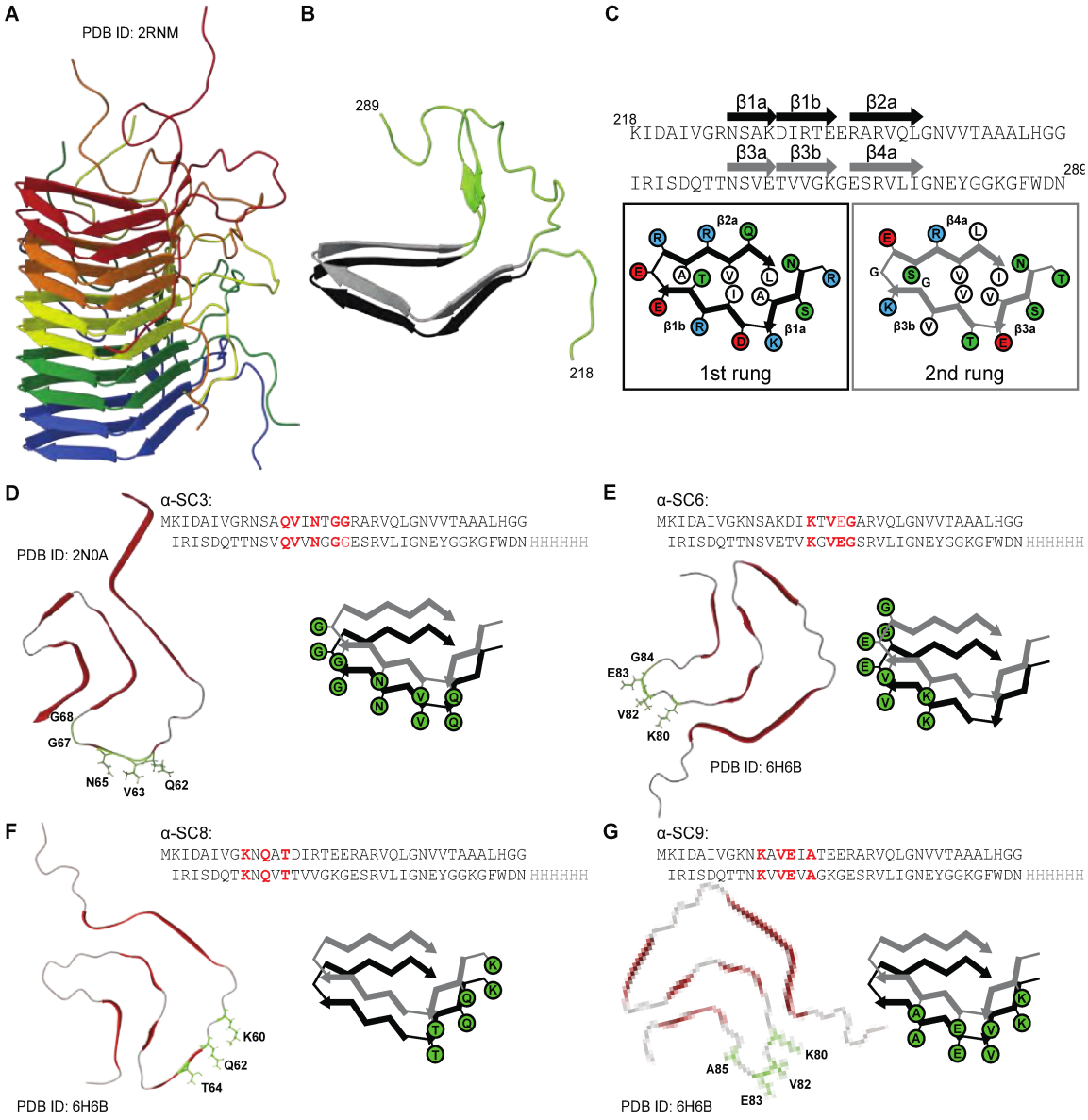

Fig. 6 The four vaccine candidates containing different epitopes of α-syn fibrils. (**A**) HET-s(218–289) forms fibrils in a triangular β-solenoid structure. The different colors represent individual HET-s (218-289) monomers (Wasmer *et al.,* 2008). (**B**) A single HET-s(218-289) monomer contains eight β-sheets, which are layered on top of each other in a triangular structure (black and gray layers). This triangular structure forms a hydrophobic core. (**C**) Shown is the sequence of HET-s(218-289) highlighting the amino acids that form β-sheets in both layers with black and gray arrows. The two images below highlight amino acids with polar (green), hydrophobic (white), negatively charged (red), and positively charged (blue) residues. (**D**) For the creation of α-SC3 fibrils, residues K229, D230, R232, E234, and E235 in the first loop and E265, T266, V268, K270, and G271 in the second loop of HET-s were replaced by Q62, V63, N65, G67, and G68 of α-syn to model a conformational epitope on the surface of a synthetic α-syn fibril with the PDB ID 2N0A (Tuttle *et al.*, 2016). (**E**) For the creation of α-SC6 fibrils, residues R232, E234, (E235), and R236 in the first loop and V268, K270, G271, and E272 in the second loop of HET-s were replaced by the amino acids K80, V82, E83, and G84 of α-syn to model a conformational epitope of an α-syn fibril with the PDB ID 6H6B (Guerrero-Ferreira *et al.*, 2018). (**F**) For the creation of α-SC8 fibrils, residues R225, S227, and K229 in the first loop and T261, S263, and E265 in the second loop of HET-s were replaced by K60, Q62, and T64 of α-syn to model another epitope of the α-syn fibril with the PDB ID 6H6B (Guerrero-Ferreira *et al.*, 2018). (**G**) For the creation of α-SC9 fibrils, residues S227, K229, D230, and R232 in the first loop and S263, E265, T266, and V268 in the second loop of HET-s were replaced by K80, V82, E83, and A85 of α-syn to model yet another

epitope of α-syn fibril with the PDB ID 6H6B (Guerrero-Ferreira *et al.,* 2018). Figure based on Pesch *et al*., 2024

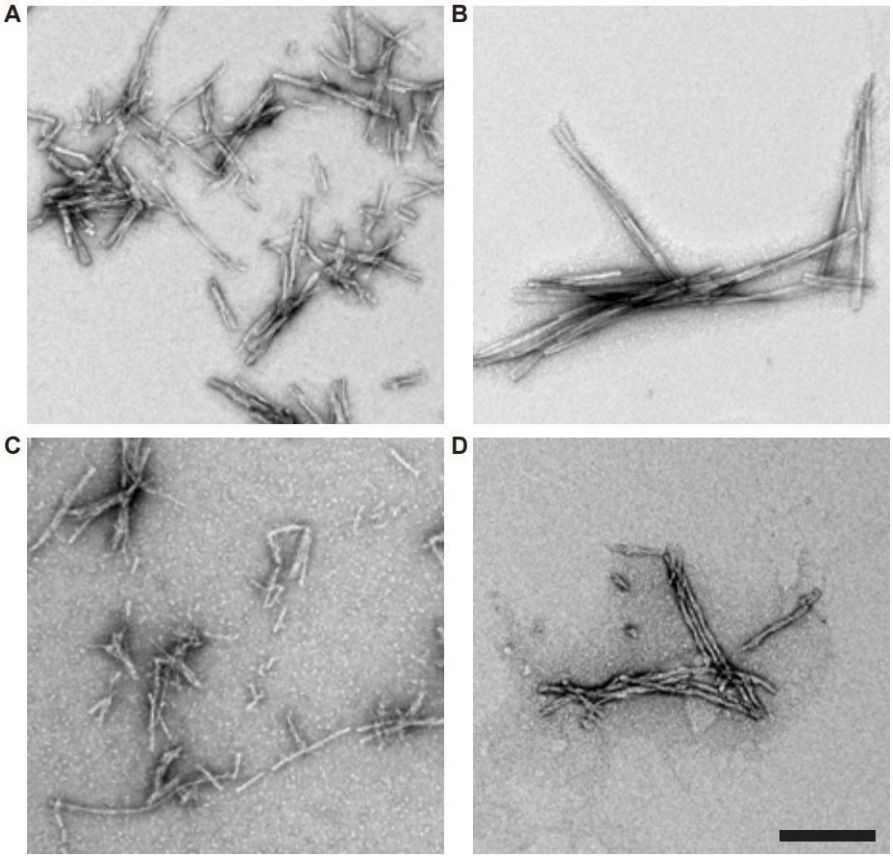

Fig. 7 HET-s-derived vaccine candidates form fibrils. (**A–D**) Negative stain transmission electron microscopy revealed that all four vaccine candidates, (**A**) α-SC3, (**B**) α-SC6, (**C**) α-SC8, and (**D**) α-SC9, readily formed fibrils. Scale bars represent 200 nm (A-C) or 500 nm (D).

2. Materials and Methods

2.1. Materials

The chemicals used were, unless otherwise stated, obtained from Carl Roth or Sigma Aldrich.

2.1.1 Buffers

Table 1 Used buffers and solutions

Buffer	Composition	
Blocking buffer	20% (v/v) 1% (w/v) 0.5% (v/v) 1x	Normal goat serum (NGS)（Sigma） Bovine serum albumin (BSA) (Sigma) Triton X-100 Phosphate-buffered saline (PBS)
Citric buffer (CB)	9 mL 41 mL 450 mL	Citric acid 0.1M Sodium citrate dehydrate ddH_2O
Copper sulfate solution	10 mM 50 mM	$CuSO_4$ Ammonium acetate ddH_2O pH 5.0
Paraformaldehyde (PFA) 0.4%	0.4% (w/v) 1x	Paraformaldehyde PBS
Primary antibody buffer	1% (v/v) 1% (w/v) 0.25% (v/v) 1x	NGS BSA Triton X-100 PBS
Secondary antibody buffer	1% (v/v) 1% (w/v) 1x	NGS BSA PBS
PBST (0.1 %)	0.1% (v/v) 1x	Tween-20 PBS
TBST (0.05 %)	0.05% (v/v) 1x	Tween-20 Tris-buffered saline (TBS)
Homogenization buffer	0.1% (v/v) 0.1% (v/v) 0.1% (v/v) 1x	Protease inhibitor (Thermo Fisher Scientific) Phosphatase inhibitor (Thermo Fisher Scientific) Benzonase (Sigma) PBS
TD4215 buffer	4% (w/v) 2% (v/v) 192 mM 25 mM 5% (w/v)	Sodium dodecyl sulfate (SDS) β-Mercaptoethanol Glycine TRIS Sucrose
Transfer buffer stock (10x)	60.4 g 288 g Up to 2L	Trizma base Glycin ddH_2O
Transfer buffer	50 mL 50 mL 400 mL	Transfer-buffer (10x) Methanol ddH_2O
Wash-Buffer	0.25% (v/v)	Triton X-100

	1x	PBS

2.1.2 Primary antibodies

Table 2 Used primary antibodies and their dilution

Target antigen (alternative name) [Clone number]	Reference	Host	Dilution (IF/IHC)	Antigen retrieval	Dilution (WB)
alpha-Synuclein (phospho S129) [EP1536Y]	AB51253 Abcam	Rabbit	1:200	CB	1:1000
alpha-Synuclein (phospho S129) [pSyn#64]	015-25191 Wako	Mouse	1:1200	CB	–
alpha-Synuclein (phospho S129) [pSyn#64], biotin-conjugated	010-26481 Wako	Mouse	1:1000	CB	–
Glial fibrillary acidic protein (GFAP)	Z0334 Dako	Rabbit	1:1000	CB	–
Ionized calcium-binding adapter molecule 1 (Iba-1)	019-19741 Wako	Rabbit	1:500	CB	–

2.1.3 Secondary antibodies

Table 3 Used secondary antibodies and their dilution

Secondary antibody	Reference	Host	Dilution (IF/IHC)	Dilution (WB)
AlexaFluor 488, Anti-Mouse IgG	A-11001, Thermo Fisher Scientific	Goat	1:1000	–
AlexaFluor 568, Anti-Rabbit IgG	A-11011, Thermo Fisher Scientific	Goat	1:1000	–
Anti-Rabbit IgG, Horseradish peroxidase, HRP)-conjugated	Cay100004301, Cayman Chemicals	Goat	–	1:10000
Anti-Mouse IgG, HRP-conjugated	31430, Invitrogen	Goat	–	1:5000

2.1.4 Primers used with sequence

Table 4 Used primers and their sequences.

Primer	Description	Sequence	Final Concentration	For 1 Probe
oIMR1544	**IC forward**	CAC GTG GGC TCC AGC ATT	0.40 µM	0.15 µL

oIMR3580	**IC reverse**	TCA CCA GTC ATT TCT GCC TTT G	0.40 µM	0.15 µL
oIMR1770	**Tg forward**	TGA CGG GTG TGA CAG CAG TAG	0.40 µM	0.15 µL
oIMR1771	**Tg reverse**	CAG TGG CTG CTG CAA TG	0.40 µM	0.15 µL
TmoIMR0025	**Tg Probe**	6-FAM CCC TGC TCC CTC CAC TGT CTT CTG G - BHQ1	0.15 µM	0.45 µL
TmoIMR0105	**IC Probe**	Cy5- CCA ATG GTC GGG CAC TGC TCA A - BBQ	0.15 µM	0.45 µL

2.2 Methods

If no temperature is specified, the steps were carried out at room temperature (RT).

2.2.1 Mice

Approval for all animal experiments was obtained from the State Agency for Nature, Environment and Consumer Protection of North Rhine-Westphalia (LANUV). The mice were housed in groups with a 12 h light/dark cycle and provided with food and water *ad libitum*. Heterozygous offspring were generated by crossing B6;C3-g(Prnp-SNCA*A53T)83Vle/J (TgM83) mice, which express human α-syn with the A53T mutation (Giasson *et al.,* 2002), with wild type C57BL/6 J mice. Genotyping was performed to confirm the presence of the transgene.

2.2.2 Genotyping

2.2.2.1 DNA-isolation

DNA was isolated from ear punches using the DNeasy Blood & Tissue Kit (Qiagen) according to the manufacturer's instructions. The biopsies were lysed in a proteinase K-containing buffer at 56 °C overnight with agitation. After centrifugation to remove cell debris, RNase A was added to the supernatant, followed by a brief incubation. The sample was mixed with a combination of 200 µL buffer AL and 200 µL ethanol. The mixture was briefly mixed and loaded onto silica-membrane spin columns. DNA purification was achieved through centrifugation steps with two washes using 500 µL buffer AW1, followed by a final wash with buffer AW2. DNA elution was performed using 45 µL buffer AE, followed by a final centrifugation step. The concentration of the isolated DNA was determined with a NanoPhotometer (IMPLEN). Subsequently, the extracted DNA was used for genotyping through real-time polymerase chain reaction (PCR).

2.2.2.2 Real-time polymerase chain reaction

To determine the genotypes of murine progeny, 10 ng of isolated DNA was amplified by real-time PCR. All primer sequences used for the internal positive control, the amplification of the

transgene, and the labeled oligonucleotides are listed in Table 4. The master mix containing the primers and Taq polymerase was pipetted onto a PCR plate in duplicates before the sample was added. The master mix was mixed with 5 µL of DNA (10 ng) and amplified using the program shown in Table 5 on a PCR cycler (BioRad). Afterwards, the samples were compared with the controls to genotype them.

Table 5 PCR-cycler settings

Steps	Temperature (°C)	Time (min)	Number of cycles
1	95	3:00	1
2	95	0:05	40
3	60	0:30	
4	72	0:30	
5	72	2:00	1
6	10	∞	

2.2.3 Preparation of α-syn monomers and fibrils

N-terminally acetylated human wild-type α-syn was expressed in *Escherichia coli* (*E. coli*) strain BL21(DE3) cells carrying the pT7 vector for codon-optimized α-syn and the pNatB vector of the Schizosaccharomyces pombe N-terminal acetyltransferase B complex (Johnson *et al*., 2010). Glycerol stocks of these bacteria were streaked onto agar plates containing 100 µg/mL ampicillin and 34 µg/mL chloramphenicol, followed by overnight incubation at 37 °C and 120 revolutions per minute (rpm). The next day, the optical density (OD) of the preculture was measured, and 1 L of LB medium with ampicillin/chloramphenicol was inoculated at an OD of 0.1 and incubated again at 37 °C and 120 rpm until an OD of 1.0-1.2 was reached. Expression was induced with 1 mM isopropyl-beta-D-1-thiogalactopyranoside (IPTG). After 4.5 h, the cells were pelleted at 5000 × g and 4 °C for 20 min. The pellets were then resuspended in 20 mM Tris (pH 8.0) containing protease inhibitor (Roche), boiled for 2 × 15 min, and centrifuged at 20,000 × g and 4 °C for 30 min. For ammonium precipitation, the supernatant was adjusted with ammonium sulfate salt (0.45 g/mL) and incubated at 4 °C for 30 min. The solution was then centrifuged as before and the pellet was stored at −20 °C.

α-Syn was then purified using a HiPrep QFF 16/10 anion-exchange chromatography column with a linear gradient from 20 mM Tris-HCl binding buffer (pH 8.0) to 1 M NaCl in 20 mM Tris-HCl elution buffer (pH 8.0) on an ÄKTA Pure chromatography system (GE Healthcare). Ammonium precipitation was repeated and the pellet was resuspended in 50 mM Tris-HCl (pH 7.2) and then purified by size exclusion chromatography on a HiLoad 16/60 Superdex 75 pg column (Cytiva) in 50 mM Tris-HCl and 150 mM NaCl. The protein was concentrated to 5 mg/mL using a Vivaspin concentrator (Sartorius) and fibrillated by incubation at 37 °C and 1000 rpm on a Thermomixer (Eppendorf) for 7 d. The fibrils were sonicated four times for 15

s each with a 2 min break between steps using a Sonoplus Mini20 ultrasound probe (Bandelin) and the MS 1.5 microtip.

2.3 Challenge of TgM83$^{+/-}$ mice with α-syn fibrils

2.3.1 Intracerebral transmission

For intracerebral challenge (IC) with α-syn fibrils, mice were weighed and administered subcutaneous carprofen (5 mg/kg) as an analgesic 30 min prior to surgery according to their body weight. Subsequently, mice were anesthetized with 1.5-2.0% isoflurane and oxygen gas mixture, and the depth of anesthesia was assessed by the absence of the hindlimb withdrawal reflex. The mouse was fixed by a palate bar and two additional ear bars. Eyes were covered with ophthalmic and nasal ointment (Bepanthen) to prevent drying, and hypothermia was prevented by placing the mice on a 37 °C warming pad in the stereotaxic frame. The head was shaved, and the skin was disinfected with iodine solution (Betaisodona). A 1 cm incision was made on the scalp, and the landmarks lambda and bregma were identified. To minimize pain, 1-2 drops of 1% lidocaine were applied to the skull. The injection site was located in the right striatum at coordinates +0.2 mm relative to bregma and +2.0 mm relative to the midline. A hole was drilled through the skull and the needle of a 10 µL syringe (Hamilton) was inserted to a depth of 2.6 mm below the dura to start the injection. Each mouse was administered a dose of 10 µg α-syn fibrils, with 4 µL of fibrils (2.5 µg/µL) injected at a flow rate of 1.0 µL/min. Blood sampling was conducted during the injection. Following completion of the injection, the needle was left in place for an additional minute before being slowly withdrawn over 5 min. The incision was closed with tissue adhesive (3M Animal Care Products), and the mouse was placed in a separate and heated cage for recovery.

2.3.2 Intraperitoneal transmission

For the intraperitoneal challenge (IP) with α-syn fibrils, mice were restrained using standard tail and scruff handling in the head-down position. A 20 µL suspension of α-syn fibrils, with a concentration of 2.5 µg/µL (50 µg in total), was injected into the right peritoneum using a 30-gauge disposable hypodermic insulin syringe (B. Braun). The mice were then allowed to return to their home cages.

2.3.3 Intragastric transmission

For the intragastric challenge (IG) with α-syn fibrils, a sterile laparotomy procedure was performed. Prior to this, the animal was weighed and administered subcutaneous buprenorphine (0.05 mg/kg, Bayer) for analgesia. The animal was then anesthetized using 1.5-2% isoflurane and oxygen gas mixture. To prevent dryness, the eyes were covered with an eye and nose ointment (Bepanthen), while hypothermia was averted by positioning the mice on a 37 °C warm heating pad. The surgical procedure began with shaving and

disinfecting the abdomen, followed by a small incision made with surgical scissors. The stomach was then exposed, and α-syn fibrils were injected into both the pylorus and duodenal wall at four separate locations, each spaced 0.5 cm apart, using a 10 µL syringe (Hamilton). A dose of 6.25 µg (2.5 µL) of α-syn fibrils was administered at each injection site (25 µg in total). After the injection, the abdominal wall was sutured and the skin was closed with wound clips, which were removed two weeks later. The animals received a single subcutaneous injection of carprofen (5 mg/kg) and a mixture of metamizole (0.5 mg/mL, WDT) and 10% (w/v) sucrose in their drinking water for 3 d. Daily monitoring of the drinking water was conducted to quantify consumption.

2.4 Behavioral test (Grip strength test)

To assess motor function, mice were tested using a grid connected to a grip strength meter (Ugo Basil) to grasp with all four paws. The mouse was then gently pulled by its tail until it released the grid, and the maximal grip strength value displayed on the screen was recorded. Grip strength measurements were taken three times for each mouse, with a 15 min break between each measurement session. The average of the three measurements was calculated as the result for each mouse. The behavioral performance of vaccinated and non-vaccinated TgM83$^{+/-}$ mice was assessed at different time points after challenge with α-syn fibrils using the grip strength test. The mice that were intracerebrally challenged were tested after 2 and 5 months, while those that were intragastrically and intraperitoneally challenged were tested after 3 and 7 months. The percentage of each animal's average performance in the test was calculated relative to its average performance at an earlier time point. Statistical analysis was performed using Graphpad Prism version 10.1.1. Outliers were identified and removed using the ROUT function with Q set to 2%. The significance of the performance of vaccinated and non-vaccinated mice was determined using a one-way ANOVA followed by Dunnett's multiple comparisons test.

2.5 Mouse tissue preparation

Animals displaying signs of disease or a weight loss exceeding 20% of their maximum weight were euthanized by either spinal dislocation or an overdose of ketamine/xylazine.

For histological analysis, mice were sacrificed by intraperitoneal overdose with ketamine and xylazine and transcardially perfused with ice-cold PBS and 4% PFA solution using a perfusion pump (ISMATEC) until they were fixed. After perfusion, the brains were dissected and post-fixed overnight in 4% PFA solution, followed by replacement with 1% PFA solution. For biochemical analysis, mice were sacrificed by spinal dislocation and the brains were dissected, snap-frozen in 2-methylbutane, and stored at −80 °C.

For tissue embedding, the brains were dehydrated in a series of graded ethanol baths with concentrations of 70%, 85%, 95%, and 100%, each applied for 1 h. Subsequently, the tissues were immersed in 100% ROTI-Histol twice for 30 min each, followed by overnight incubation in the same solution. The next day, the brain tissues were incubated in a 1:1 mixture of ROTI-Histol and paraffin at 56 °C for 1 h. The brain tissues were then transferred to fresh paraffin and incubated for three additional 1 h incubations. Afterward, each brain was embedded using an embedding machine (Zhejiang Jinhua Kedee Instrumental Equipment Co. Ltd). Finally, the tissues were cut into 8-µm thick coronal sections using a microtome (Microm). The sections were mounted on SuperFrost Plus adhesive slides (Thermo Fisher Scientific), dried overnight at RT, and stored at 4 °C.

2.5.1 Histological examinations of the tissues

2.5.1.1 Immunohistochemical analysis

For immunohistochemical analysis, tissue sections were first deparaffinized and then rehydrated by incubation in ROTI-Histol and a series of decreasing concentrations of ethanol. Antigen retrieval was achieved by heat-induced antigen retrieval using citric buffer for 10 min, followed by microwave boiling for another 10 min. To deactivate endogenous peroxidases, the sections were incubated for 30 min in 5% H_2O_2 in methanol. The sections were then blocked with 20% (v/v) NGS and 1% (w/v) BSA in 0.5% (v/v) Triton X-100 in PBS at RT for 1 h. The appropriate primary antibody was diluted in 1% (v/v) NGS, 1% (w/v) BSA, and 0.25% (v/v) Triton X-100 in PBS (PBST) and incubated overnight at RT. After washing once with wash buffer and twice with PBS, the tissue sections were incubated for 1 h at RT with peroxidase-conjugated secondary antibody using the Mouse on Mouse kit (Vector Labs) diluted in 1% (v/v) NGS and 1% (w/v) BSA in PBS. After washing once with PBST and twice with PBS, peroxidase-positive structures were visualized by incubating with DAB (3-3'- diaminobenzidine, Vector Labs) for 20-40 s. The reaction was stopped directly with 3% (v/v) hydrogen peroxide solution. The sections were washed three times with ddH_2O and counterstained with hematoxylin. Finally, the sections were coverslipped with Aqua-Poly/Mount (Polysciences). Images were captured using a Leica DM 6000 B microscope and Leica Application Suite 4.0 (Leica).

2.5.1.2 Immunofluorescence analysis

For immunofluorescence, the 8-µm thick brain sections were deparaffinized as described previously. The tissue sections underwent heat-induced antigen retrieval with citric buffer. After washing twice with PBS, autofluorescence from the mouse tissue was quenched by incubating it in $CuSO_4$ solution for 90 min at RT in the dark. The sections were washed once with PBS and then blocked with a blocking buffer for 1 h. Primary antibodies were then applied to the sections in primary antibody buffer and incubated overnight at RT. The following day,

after washing with PBST and twice with PBS, the tissue sections were incubated with the corresponding secondary antibodies in the secondary antibody buffer, as well as the appropriate Alexa Fluor 488- and Alexa Fluor 568-conjugated secondary antibodies (1:1,000, Thermo Fischer Scientific) for 1 h. Cell nuclei were stained with DAPI (4′,6-diamidino-2-phenylindole) (1:1,000, Thermo Fisher Scientific) in PBS for 5 min. The sections were washed with ddH_2O and then coverslipped with Fluoromount (Sigma). Fluorescence images were captured using a confocal laser-scanning microscope LSM 710 (Carl Zeiss).

2.5.2 Biochemical analysis of tissues

Mice that were not used for histological examination were euthanized using cervical dislocation, and their brains were rapidly frozen after extraction.

2.5.2.1 Preparation of brain homogenates

The brains were homogenized using a $Ca2^{+}$- and Mg^{2+}-free buffer containing phosphatase and protease inhibitors. Homogenization was performed by two 30 s cycles at 6500 rpm in a Precellys 24-Dual Homogenizer (Peqlab). The homogenates were then appropriately diluted to achieve a final concentration of 25% (w/v). To remove larger tissue particles, the homogenates were centrifuged at 1000 × g for 5 min at 4 °C. The concentration of total protein was determined using the Pierce BCA Protein Assay Kit (Thermo Fischer Scientific). All samples were analyzed in triplicate. To each well of a 96-well plate, 15 µL of sample was added, followed by 150 µL of detection solution (a mixture of solution A and solution B at a 40:1 ratio). The plate was gently mixed on a shaker for 30 s, then incubated at 37 °C for 30 min in the dark. The plate was cooled to RT before measuring fluorescence emission at 562 nm using a FLUOstar omega microplate reader (BMG Labtech).

2.5.2.2 Sarkosyl precipitation of α-syn aggregates

To separate sarkosyl-soluble from insoluble α-syn aggregates, brain homogenates containing 1 mg total protein were adjusted to 750 mM NaCl and incubated with 10% (w/v) N-lauroylsarcosyl for 15 min on ice. The sample was then supplemented with a 20% (w/v) solution of sarkosyl to reach a final concentration of 10% (w/v) sarkosyl. The mixture was incubated on ice for 15 min. The samples were centrifuged using 10% sucrose cushion at 465,000 g for 1 h at 4 °C in a TLA-110 rotor (Beckman-Coulter). The pellets containing the sarkosyl-insoluble proteins were then resuspended in 50 µL TD4215 buffer and stored at −20 °C.

2.5.2.3 SDS-page and western blot

To separate proteins from sarkosyl-insoluble fractions according to their molecular weight, samples were thawed, boiled at 99 °C for 5 min at 700 rpm, and loaded onto Novex NuPAGE Bis-Tris Mini Gels (Invitrogen). Subsequently, SeeBlue Plus2 Pre-stained Protein Standard

(Life Technologies) was used as a molecular weight reference. Proteins were separated by gel electrophoresis for 30 min at 80 V, then 90 min at 120 V. Proteins were then transferred to a polyvinylidene difluoride membrane for 75 min using a semi-dry blotting device. After fixing with 0.4% PFA for 30 min, the membranes were blocked with 5% (w/v) milk in TBS containing 0.05% Tween 20 (TBST) for 1 h to reduce unspecific antibody binding. The membranes were incubated overnight at 4 °C in 5% (w/v) milk powder in TBST with a primary antibody for phosphorylated α-syn (EP1536Y). The membranes were washed three times with 0.05% TBST and then incubated with specific anti-rabbit horseradish peroxidase-linked (HRP) secondary antibody (1:10,000) in 5% (w/v) milk powder in 0.05% TBST for 1 h at RT. After being washed three times for 10 min in TBST, the membrane was developed using Super Signal ECL West Dura (Thermo Fisher Scientific) and a chemiluminescence imaging system (Gel Doc XR+ Imaging System, Bio-Rad).

2.5.3 Enzyme-linked immunosorbent assay (ELISA)

2.5.3.1 Indirect ELISA

The 96-well high-binding ELISA plate (Corning, Cat# 9018) was coated with 100 µL/well of each vaccine fibrils or α-syn fibrils (5 µg/mL) overnight at 4 °C with gentle shaking. The next day, following washing twice with 0.1% PBST and once with PBS, the plate was blocked in 5% (w/v) milk powder in 1x PBS for 90 min with gentle shaking. The plate was then washed twice with 0.1% PBST and once with PBS. After blocking, the plate was washed five times with 0.1% PBST and once with PBS before being incubated overnight at 4 °C with gentle shaking. For tests involving plasma samples from five different time points, a 1:330,000 dilution in PBS was used. The next day, the plate was washed five times with 0.1% PBST and once with PBS, followed by incubation with an anti-mouse antibody conjugated to HRP at a dilution of 1:5000 in PBS for 2 h with gentle shaking. Following another round of washing, the plate was incubated with 100 µL/well of the TMB Substrate (Thermo Fisher Scientific). The color reaction was halted with 2 M sulfuric acid after 50 min, and the absorbance at 450 nm was measured using a CLARIOstar microplate reader (BMG Labtech).

2.5.3.2 Competitive ELISA

To evaluate how well the antibodies present in plasma samples to recognize pathological α-syn in brain homogenates from patients with synucleinopathies, a competitive ELISA was conducted (Fig. 8). A 96-well high-binding ELISA plate (Corning, Cat# 9018) was coated with 100 µL/well of individual vaccine candidates (5 µg/mL), and incubated overnight at 4 °C with gentle shaking. A low-binding 96-well plate was used to mix 75 µL of mouse serum at a final dilution of 1:330,000 with 66.67 µg/mL (5 µg) of brain homogenate from patients (DLB, MSA, PD or healthy control). The following day, the vaccine-coated plate was blocked with 3% BSA for 90 min. The mixture was incubated with gentle shaking overnight at 4 °C. After washing

twice with 0.1% PBST and once with PBS, 100 µL/well of the plasma and homogenate mixture was added to the plate and incubated overnight at 4 °C with gentle shaking. After washing the plate twice with 0.1% PBST and once with PBS, a secondary antibody bound to HRP in a 1:5000 dilution in 3% BSA was added. The plate was then incubated for 2 h at RT. Following this, the plate was washed four more times with 0.1% PBST and once with PBS. Next, 100 µL/well of TMB substrate was added and the plate was incubated for 30 min. The color reaction was stopped with 2 M sulfuric acid and the absorbance at 450 nm was measured using a CLARIOstar microplate reader.

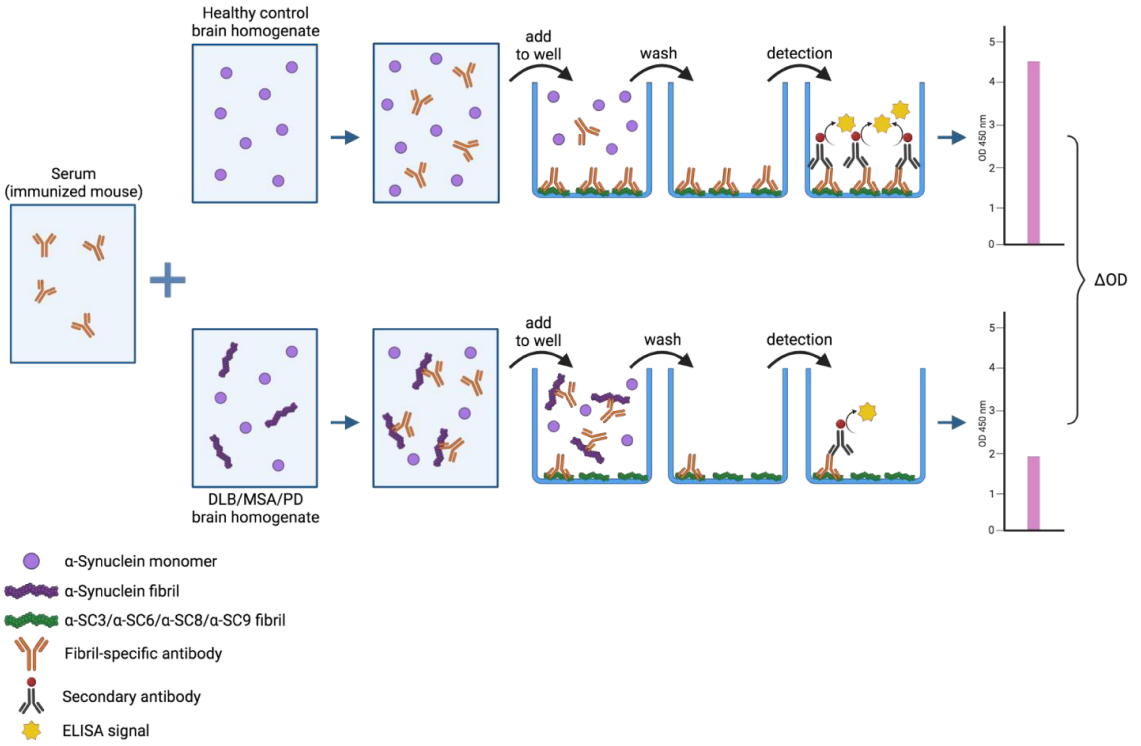

Fig. 8 Principle of the competitive ELISA. For the competitive ELISA, plasma of immunized mice was mixed with brain homogenates of healthy controls and those of patients with DLB, MSA, and PD. Since brain homogenates of healthy controls only harbor monomeric α-syn and no α-syn fibrils, most of the antibodies in the plasma of immunized mice are free to bind to wells precoated with α-SC3, α-SC6, α-SC8, or α-SC9 fibrils, yielding a relatively high ELISA signal [OD 450 nm (HC)]. In contrast, brain homogenates of patients with synucleinopathies harbor pathologic α-syn fibrils that are bound by antibodies in the plasma of immunized mice, thereby reducing the number of antibodies that are free to bind to wells precoated with α-SC3, α-SC6, α-SC8, or α-SC9 fibrils, resulting in a relatively low ELISA signal [OD 450 nm (DLB/MSA/PD)]. The competitive ELISA signal ΔOD 450 nm, is the difference between the two ELISA signals [OD 450 nm (HC)−OD 450 nm (DLB/MSA/PD)]. ΔOD 450 nm values above zero indicate the presence of antibodies in the plasma of fully immunized mice recognizing pathologic α-syn fibrils.

2.5.4 Immunoprecipitations

The specificity of the antibodies was tested by immunoprecipitation with magnetic beads. Briefly, 50 µL of plasma was incubated with 16.7 µL Dynabeads Protein G (Invitrogen) for 1 hour with rotation at room temperature. As positive control, the beads were incubated in a

0.0135 µg/µL solution of the anti-α-synuclein aggregate antibody [MJFR-14-6-4-2] - Conformation-Specific (abcam) in PBS with 0.02 % Tween 20. The beads were washed 3 times with 50 µL PBS. The beads were suspended in 50 µL samples with one of the patient extracts. After overnight incubation with rotation at 4 °C, the remaining oligomers and aggregates of α-syn in the samples were quantified by time-resolved fluorescence resonance energy transfer (TR-FRET).

2.5.5 TR-FRET assay

The quantification of α-syn oligomers and aggregates in brain homogenates was performed using a commercially available kit (Revvity) and TR-FRET. Briefly, 10 µL samples with 1 µg total protein were prepared from 10% (w/v) brain homogenates in 1 x lysis buffer. To each sample, 10 µL of a pre-mixed antibody solution containing anti-h-α-Synuclein-d2 (acceptor) and anti-h-α-Synuclein-Tb-Cryptate (donor) were added. The negative control, Cryptate control, and buffer control were prepared according to the company's instructions. Next, 20 µL of the final mixture containing the sample and antibody, along with the controls, were transferred onto a HTRF 96-well low volume plate (Revvity). The plate was then covered with a plate sealer and incubated for 20 h at RT. Fluorescence emission was measured at 665 nm for FRET-dependent acceptor fluorescence and at 620 nm for FRET-independent donor fluorescence using a CLARIOstar microplate reader (BMG Labtech). The amount of human α-syn oligomers and aggregates in each sample is directly proportional to the ratio of both fluorescence emission values multiplied by 10,000. The signal-to-background ratio of the assay is represented by the Delta F (%) value. This value is calculated by dividing the difference between the ratio of the sample and the ratio of the negative control by the ratio of the negative control multiplied by 100. An internal control is provided by the negative control.

3. Results

3.1 Vaccination of TgM83$^{+/-}$ mice with HET-s-based vaccine candidates

To evaluate the effect of each of the HET-s-based vaccine fibrils on PD outcome, groups of adult TgM83$^{+/-}$ mice were vaccinated with unmodified HET-s fibrils or one of the four different HET-s-derived vaccine candidates α-SC3, α-SC6, α-SC8, or α-SC9. Non-vaccinated mice served as controls. After a primary immunization dose, each mouse received three additional booster doses at two-week intervals by single interaperitoneal injections of 100 µg of antigen, which is four times the amount of antigen used in a previous study (Fig. 9) (Pesch *et al.*, 2024). To assess the immune response, blood was collected from each mouse before each injection and two weeks after the third booster. To induce a synucleinopathy, fully vaccinated mice and non-vaccinated controls were challenged with α-syn fibrils. To model brain-first PD, α-syn fibrils were injected intracerebrally. To model body-first PD, α-syn fibrils were injected either intraperitoneally or into the wall of the stomach and pylorus during laparotomy.

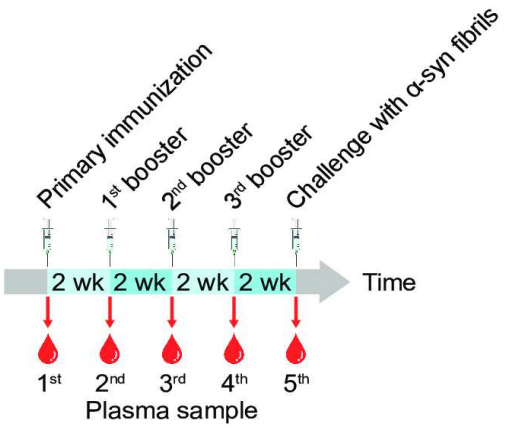

Fig. 9 Vaccination schedule. Animals received a total of four antigen injections at two-week intervals. Blood samples were collected before each injection and two weeks after the third and final booster.

3.2 Vaccination protects mice from early weight loss

To detect early signs of disease in TgM83$^{+/-}$ mice, the weight of the experimental mice was monitored weekly (Fig. 10). Both vaccinated and non-vaccinated mice challenged with α-syn fibrils initially gained weight before reaching a maximum weight and then began to lose weight and develop neurological disease. For all three challenge routes, vaccinated mice showed a longer duration of weight gain compared to non-vaccinated mice (Fig. 11). In the case of intracerebral challenge, all vaccinated mice continued to gain weight two months after injection. At three months, this was reduced to 91% and 92% for HET-s- and α-SC9- vaccinated mice, respectively, and to 82% for non-vaccinated mice, while α-SC3-, α-SC6-, and α-SC8-

vaccinated mice still gained weight. Four months post-injection, these values further decreased to 64% for HET-s-vaccinated mice, 40% for α-SC3-, 82% for α-SC6-, 60% for α-SC8-, 67% for α-SC9-vaccinated mice, and 37% for non-vaccinated animals. In intraperitoneally challenged mice, all α-SC9-vaccinated mice continued to gain weight up to five months post-injection. This decreased to 83% for HET-s-, 83% for α-SC3-, 92% for α-SC6-, 73% for α-SC8-vaccinated mice, and 58% for non-vaccinated mice. After seven months, these values further decreased to 50% for HET-s-, 42% for α-SC3-, 83% for α-SC6-, 46% for α-SC8-, and 64% for α-SC9-vaccinated mice, while only 21% of non-vaccinated mice continued to gain weight. After nine months, these rates decreased further to 50% for α-SC6-, 18% for α-SC8-, and 55% for α-SC9-vaccinated mice. In contrast, none of the HET-s- and α-SC3-vaccinated mice or non-vaccinated animals gained weight at this time point. Similar trends were observed in intragastrically injected mice, where at five months all HET-s-, α-SC8- and α-SC9-vaccinated mice continued to gain weight. This decreased to 91% for α-SC3-, 83% for α-SC6-vaccinated mice, and 90% for non-vaccinated mice. After seven months, these values decreased to 67% for HET-s-, 91% for α-SC3-, 75% for α-SC6-, 80% for α-SC8-, and 91% for α-SC9-vaccinated mice, while only 32% of non-vaccinated mice continued to gain weight. At nine months, 33% of HET-s-, 36% of α-SC3-, 33% of α-SC6-, 40% of α-SC8-, and 64% of α-SC9-vaccinated mice continued to gain weight, while only 16% of non-vaccinated mice did. In conclusion, these results show that vaccination with any of the four HET-s-derived vaccine candidates, or even with unmodified HET-s fibrils, provides protection against early weight loss in the brain-first and both body-first animal models of PD.

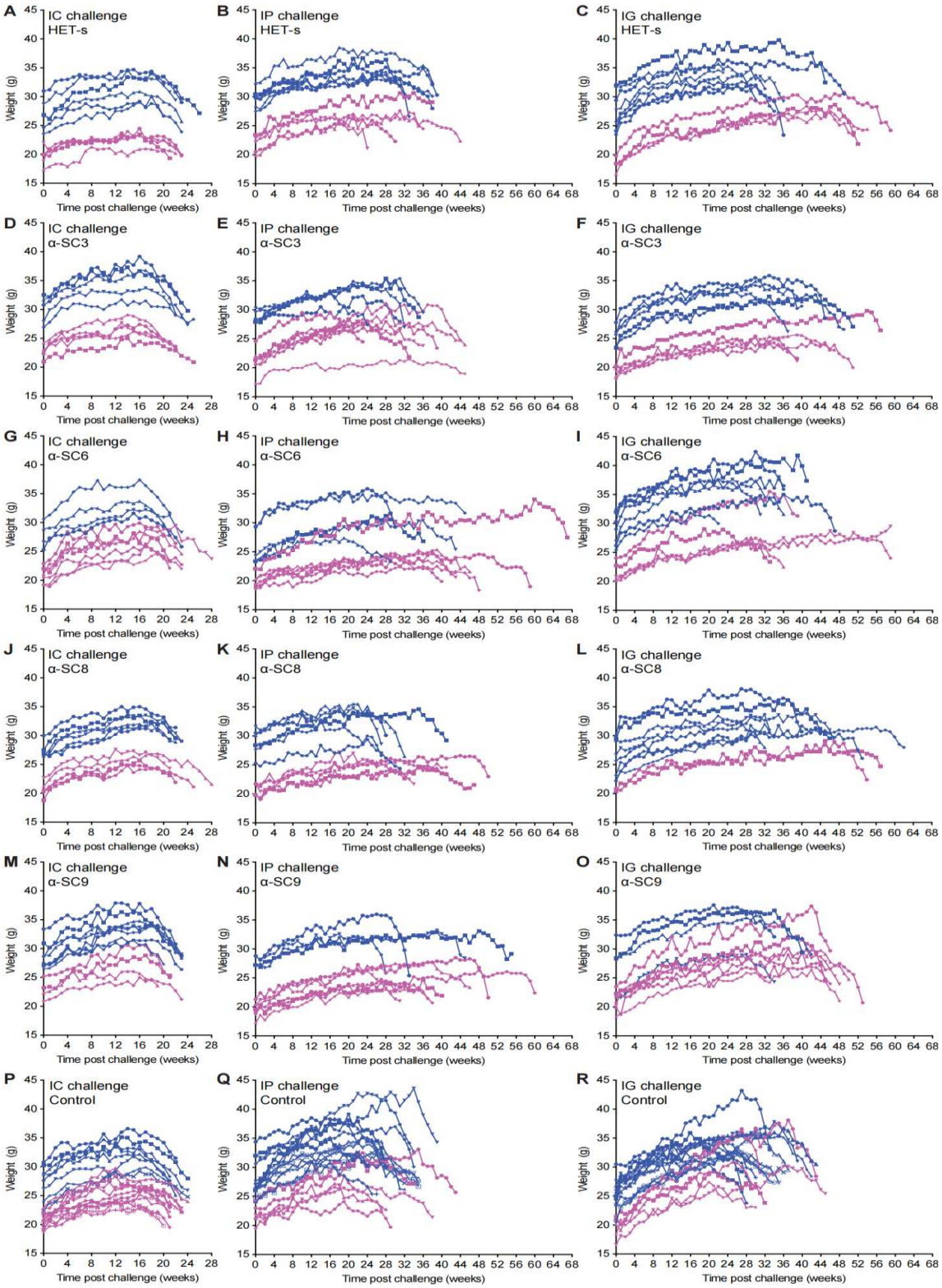

Fig. 10 Weights of TgM83$^{+/-}$ mice injected with α-syn fibrils. Shown is the weight of immunized and non-immunized control mice after intracerebral, intraperitoneal and intragastric injection of α-syn fibrils. Both immunized and non-immunized TgM83$^{+/-}$mice challenged with α-syn fibrils initially gained weight before reaching a maximum weight and then began to lose weight. In all three models of brain-first and body-first PD, immunized mice gained weight for longer periods of time than non-immunized mice. Weight of male mice is depicted in blue and weight of female mice is depicted in magenta.

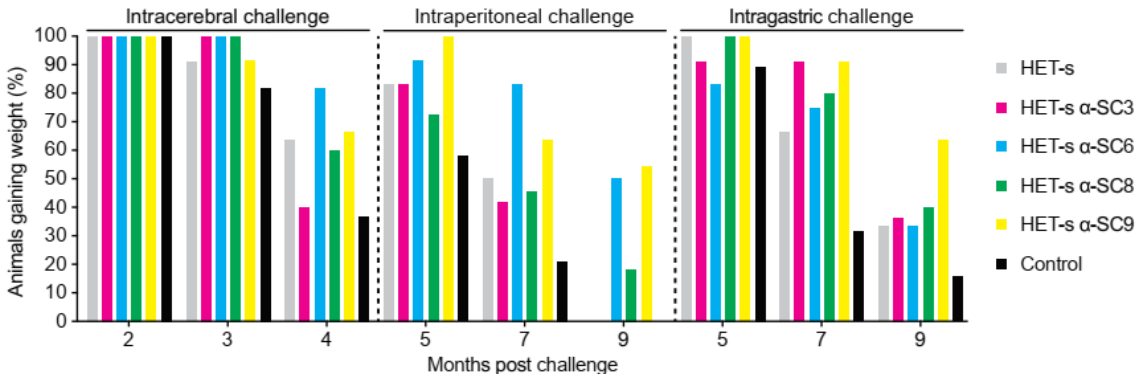

Fig. 11 Vaccinated TgM83$^{+/-}$ mice show prolonged weight gain. After challenge with α-syn fibrils, all mice initially showed weight gain. Vaccinated mice showed prolonged weight gain across all challenge routes compared to non-vaccinated mice. Data for intracerebrally (IC) challenged mice are presented for months 2, 3 and 4 post injection. For mice challenged intraperitoneally (IP) and intragastrically (IG), data are presented for months 5, 7, and 9 post-challenge.

3.3 Vaccination protects peripherally challenged mice from motor impairment

To assess the motor function of all TgM83$^{+/-}$ mice challenged with α-syn fibrils, the grip strength test was performed at specific time points: mice were tested 2 and 5 months after intracerebral injections with α-syn fibrils, and 3 and 7 months after intraperitoneal injections or injections into the gut wall (Fig. 12).

In animals subjected to intracerebral challenge with α-syn fibrils, the relative performance of HET-s-vaccinated mice decreased to 46%, and to 65% for α-SC3-, 83% for α-SC6-, 70% for α-SC8-, and 56% for α-SC9-vaccinated mice at 5 months post-challenge compared to 2 months post-challenge with α-syn fibrils. In contrast, the relative performance of non-vaccinated control mice decreased to 68% (Fig. 12A). None of these changes reached statistical significance. In animals intraperitoneally injected with α-syn fibrils, HET-s-vaccinated mice showed a significant increase in relative performance to 111% ($P < 0.0001$) at 7 months post-challenge compared to 3 months post-challenge. Similarly, α-SC3-vaccinated mice showed an increase to 103% ($P < 0.0001$), which was 109% ($P < 0.0001$) for α-SC6-, 105% ($P < 0.001$) for α-SC8-, and 101% ($P < 0.0001$) for α-SC9-vaccinated mice. In contrast, non-vaccinated mice showed a decrease to 90% at 7 months post-challenge compared to 5 months post-challenge (Fig. 12B). In animals injected with α-syn fibrils into the gut wall, HET-s-vaccinated animals showed a significant increase in relative performance to 105% ($P < 0.001$) at 7 months post-challenge compared to 3 months post-challenge. In addition, α-SC3-vaccinated mice increased to 109% ($P < 0.05$), which was 107% ($P < 0.001$) for α-SC6-, 105% ($P < 0.05$) for α-SC8-, and 107% ($P < 0.05$) for α-SC9-vaccinated mice, while non-vaccinated mice decreased to 92% (Fig. 12C).

Overall, vaccinated mice showed improved behavioral performance for longer periods of time after α-syn fibril challenge than non-vaccinated mice, suggesting that vaccination provides protection against motor deficits in two body-first PD models.

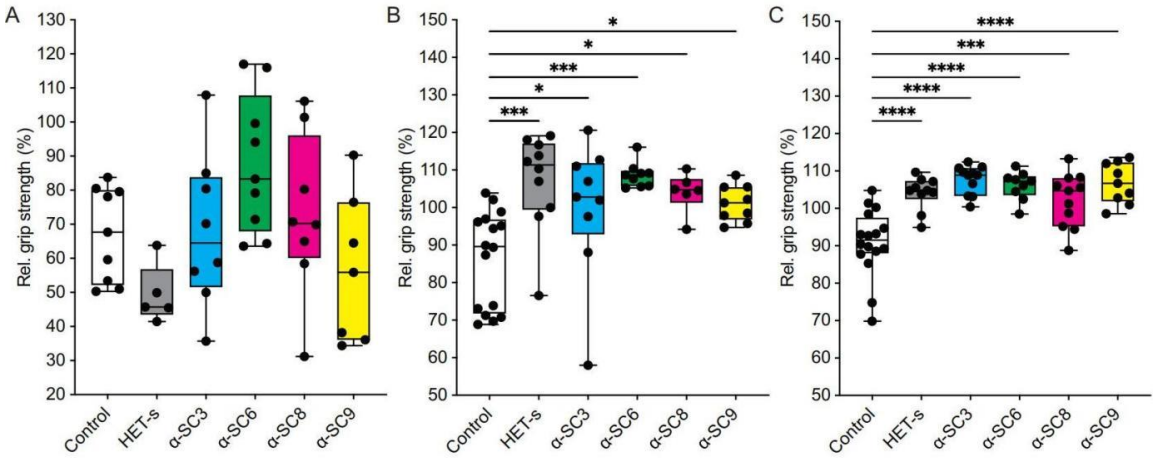

Fig. 12 Vaccinated TgM83$^{+/-}$ mice show improved grip strength. The grip strength of mice was measured at 2 and 5 months after intracerebral challenge **(A)**, and 3 and 7 months after intraperitoneal **(B)** or intragastric challenge **(C)** with α-syn fibrils. Vaccination with HET-s, α-SC3, α-SC6, α-SC8, and α-SC9 fibrils resulted in significant improvement of the grip strength at later time points relative to earlier time points for intraperitoneally and intragastrically challenged mice but not intracerebrally challenged mice in comparison to non-vaccinated control mice. Boxes indicate 25th to 75th percentiles. Lines in the center of the boxes indicate the median. Whiskers indicate minimum and maximum values. Significance was calculated using one-way ANOVA followed by Dunnett's multiple comparison test. *P < 0.05, ***P < 0.001, **** P < 0.0001

3.4 Vaccination induces antibodies against each of the vaccine candidates, including HET-s and α-syn fibrils

To evaluate the immune response elicited by HET-s fibrils or any of its four derivatives α-SC3, α-SC6, α-SC8 and α-SC9 fibrils, antibodies to these antigens were measured in the collected blood samples (Fig. 9) by indirect ELISA (Fig. 13). Both the primary immunization and the three subsequent booster vaccinations led to a progressive increase in antibody titers specific for HET-s fibrils and the four vaccine candidates. Significantly increased antibody titers were measured after the third booster.

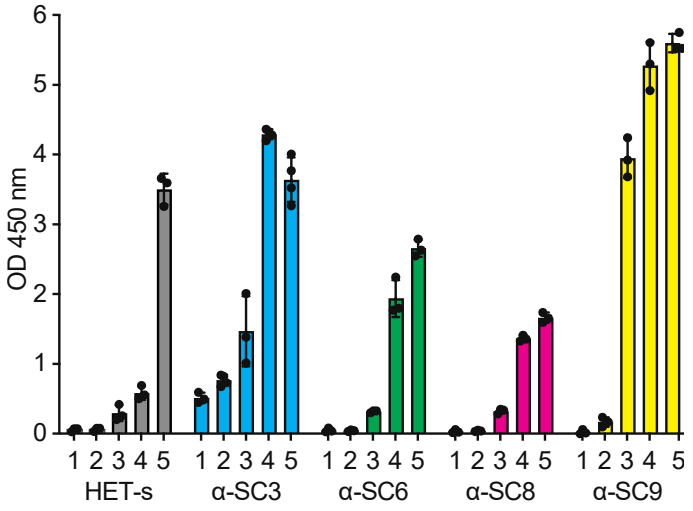

Fig. 13 Vaccinated mice produce antibodies against HET-s fibrils and all four vaccine candidates. ELISA measurements of plasma samples collected from three to four TgM83$^{+/-}$ mice each showed that, in contrast to pre-immune plasma samples (1:10,000 dilution) collected from non-vaccinated mice (1), plasma samples (1:330,000 dilution) collected from sequentially boostered mice (2-5) had much higher antibody titers against HET-s fibrils and all four vaccine candidates. The final booster vaccination significantly increased titers.

Additionally, it was crucial to determine whether the generated antibodies also recognize α-syn aggregates. For this purpose, another indirect ELISA was conducted, in which plasma samples were tested against synthetic α-syn fibrils (Fig. 14). Plasma from fully vaccinated animals had much higher antibody titers against α-syn fibrils compared to non-vaccinated animals. This observation underscores that HET-s-based vaccine candidates and HET-s fibrils themselves can induce a significant immune response against pathological α-syn aggregates.

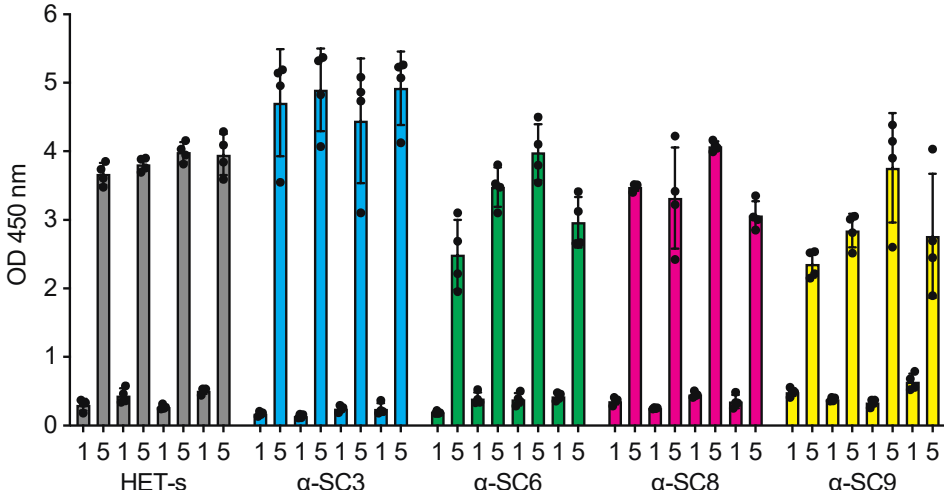

Fig. 14 Vaccinated mice produce antibodies against synthetic α-syn fibrils. ELISA measurements of plasma samples collected from four TgM83$^{+/-}$ mice each showed that, in contrast to pre-immune plasma samples (1:1000 dilution) collected from non-vaccinated mice (1), plasma samples (1:1000 dilution) collected from fully immunized mice two weeks after the third booster (5) with either HET-s, α-SC3, α-SC6, α-SC8 or α-SC9 fibrils had much higher antibody titers towards synthetic α-syn fibrils.

3.5 Vaccination results in a significant extension of survival in both body-first PD models, but not in the brain-first PD model.

In intracerebrally challenged TgM83$^{+/-}$ mice (Fig. 15A), median survival after vaccination with HET-s fibrils was 162 d (n = 11), with α-SC3 fibrils 158.5 d (n = 10), with α-SC6 fibrils 161 d (n = 11), with α-SC8 fibrils 158 d (n = 11), and with α-SC9 fibrils 159 d (n = 12) compared to non-vaccinated animals where it was 154 days (n = 19). Each vaccine candidate and HET-s fibrils also resulted in modest but insignificant increases in survival time compared to non-vaccinated animals.

Intraperitoneally challenged mice (Fig. 15B) had a median survival of 261 d after vaccination with HET-s fibrils (n = 12), representing a significant 17% increase ($P < 0.05$) compared to non-vaccinated animals with a median survival of 223 d (n = 19). Similarly, mice vaccinated with α-SC3 fibrils had a median survival of 249 d (n = 12), representing a 12% increase ($P < 0.05$), while mice vaccinated with α-SC6 fibrils had a median survival of 307 d (n = 12), representing a 38% increase ($P < 0.0001$). Mice vaccinated with α-SC8 fibrils (n = 11) had a median survival of 236 d, a modest but insignificant increase of 6%. Mice vaccinated with α-SC9 fibrils (n = 11) had a median survival of 288 d, with a 29% increase ($P < 0.01$).

Similarly, intragastrically challenged animals (Fig. 15C) also had a significantly longer lifespan, with a median survival of 316 d for HET-s fibrils (n = 11), representing a 37% increase ($P < 0.01$), compared to non-vaccinated animals with a median survival of 231 d (n = 20). Mice vaccinated with α-SC3 fibrils had a median survival of 316 d (n = 12), representing a 37% increase ($P < 0.001$), while mice vaccinated with α-SC6 fibrils (n = 12) had a median survival of 264 d, representing a 14% increase ($P < 0.05$). Mice vaccinated with α-SC8 fibrils (n = 10) had a median survival of 328.5 d, representing a 42% increase ($P < 0.01$), and those vaccinated with α-SC9 fibrils (n = 11) had a median survival of 321 d, representing a 39% increase ($P < 0.001$).

In general, the lifespan of vaccinated mice was significantly prolonged only in those challenged either intraperitoneally or intragastrically, but not intracerebrally.

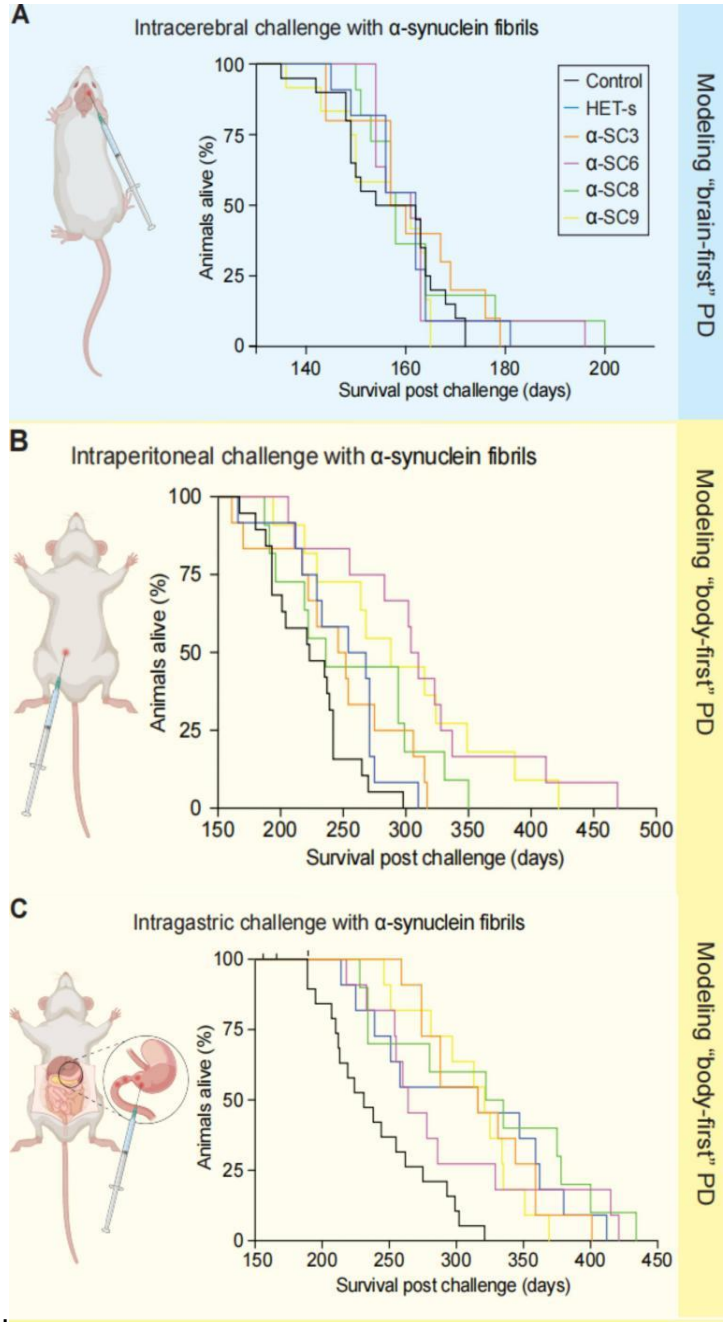

Fig. 15 In two body-first models of PD, vaccinated mice survive longer than non-vaccinated mice. **(A)** In intracerebrally challenged TgM83$^{+/-}$ mice, a model for the brain-first subtype of PD, none of the vaccine candidates led to significantly prolonged survival. Vaccinated mice showed a median survival of 162 d for the HET-s fibrils (n = 11), 158.5 d for α-SC3 fibrils (n = 10), 161 d for α-SC6 fibrils (n = 11), 158 d for α-SC8 fibrils (n = 11), and 159 d for α-SC9 fibrils (n = 12) compared to non-vaccinated mice with a median survival of 154 d (n = 19). **(B and C)** Body-first PD was modeled by challenging TgM83$^{+/-}$ mice with α-syn fibrils intraperitoneally or intragastrically. (**B**) The median survival of vaccinated TgM83$^{+/-}$ mice challenged intraperitoneally was significantly longer for all vaccine candidates except α-SC8 fibrils, with a median survival of 261 d for HET-s fibrils (n = 12), 249 d for α-SC3 fibrils (n = 12), 307 d for α-SC6 fibrils (n = 12), 236 d for α-SC8 fibrils (n = 11), and 288 d for α-SC9 fibrils (n = 11) compared to non-vaccinated animals with a median survival of 223 d (n = 19). (**C**) In intragastrically challenged mice, all vaccine candidates significantly extended lifespan from a median survival of 231 d in non-vaccinated mice (n = 20) to 316 d in mice vaccinated with HET-s fibrils (n = 12), 316 d with α-SC3 fibrils (n = 11), 264 d with α-SC6 fibrils (n = 12), 328.5 d with α-SC8 fibrils (n = 10), and 321 d with α-SC9 fibrils (n = 11). Survival was analyzed using Kaplan-Meier curves and the Log-Rank test (Mantel-Cox).

3.6 Both vaccinated and non-vaccinated mice develop α-syn pathology and neuroinflammation in the CNS

To analyze the effect of vaccination with HET-s fibrils and the four derived vaccine candidates on neurodegeneration, brain homogenates from diseased mice were first examined biochemically. The ability of α-syn to form detergent-insoluble aggregates in the CNS of diseased mice was demonstrated by immunoblotting sarkosyl-insoluble fractions of brain homogenates against the EP1536Y antibody. This antibody recognizes phosphorylation at serine 129 of α-syn, which is the most commonly used modification to detect synucleinopathy lesions (Fujiwara *et al*., 2002; Anderson *et al*., 2006). Western blot analysis revealed sarkosyl-insoluble phosphorylated α-syn in brain tissue from all challenged mice. There was no observable difference between non-vaccinated and vaccinated mice (Fig. 16). In both cases, several molecular species of pathological α-syn were detected, including phosphorylated monomers and larger aggregates.

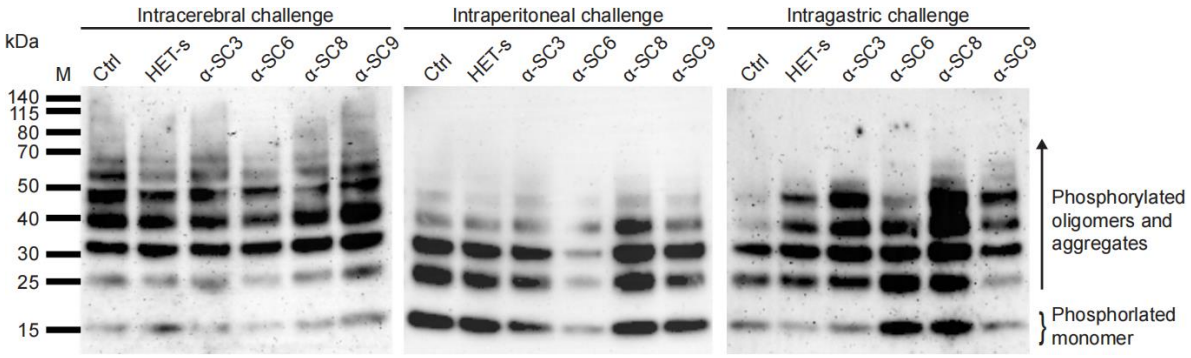

Fig. 16 Diseased TgM83$^{+/-}$ mice accumulate sarkosyl-insoluble aggregates of phosphorylated α-syn in the CNS. Western blot analysis with an antibody against α-syn phosphorylated at serine 129 revealed various pathological α-syn species, ranging from monomers to oligomers and larger aggregates with higher molecular weight bands, regardless of whether the mice were non-vaccinated (Ctrl) or vaccinated with HET-s, α-SC3, α-SC6, α-SC8, or α-SC9 fibrils or the route of challenge, which was intracerebral (left), intraperitoneal (center), or intragastric (right). Molecular weight is indicated in kilodaltons (kDa).

Neuropathology in brainstem sections from diseased TgM83$^{+/-}$ mice was also analyzed by immunohistochemical staining with the pSyn#64 antibody, which recognizes phosphorylation of serine 129 of α-syn, to detect pathological deposits (Fig. 17). Phosphorylated α-syn was present in neuronal cell bodies and neurites in both vaccinated and non-vaccinated mice. There was no obvious difference in the amount of deposited α-syn pathology between vaccinated and non-vaccinated mice. The pathology was also consistent across injection routes. In summary, dense α-syn pathology was observed in diseased TgM83$^{+/-}$ mice after intracerebral, intraperitoneal, and intragastric challenge regardless of the route of challenge or the vaccination status.

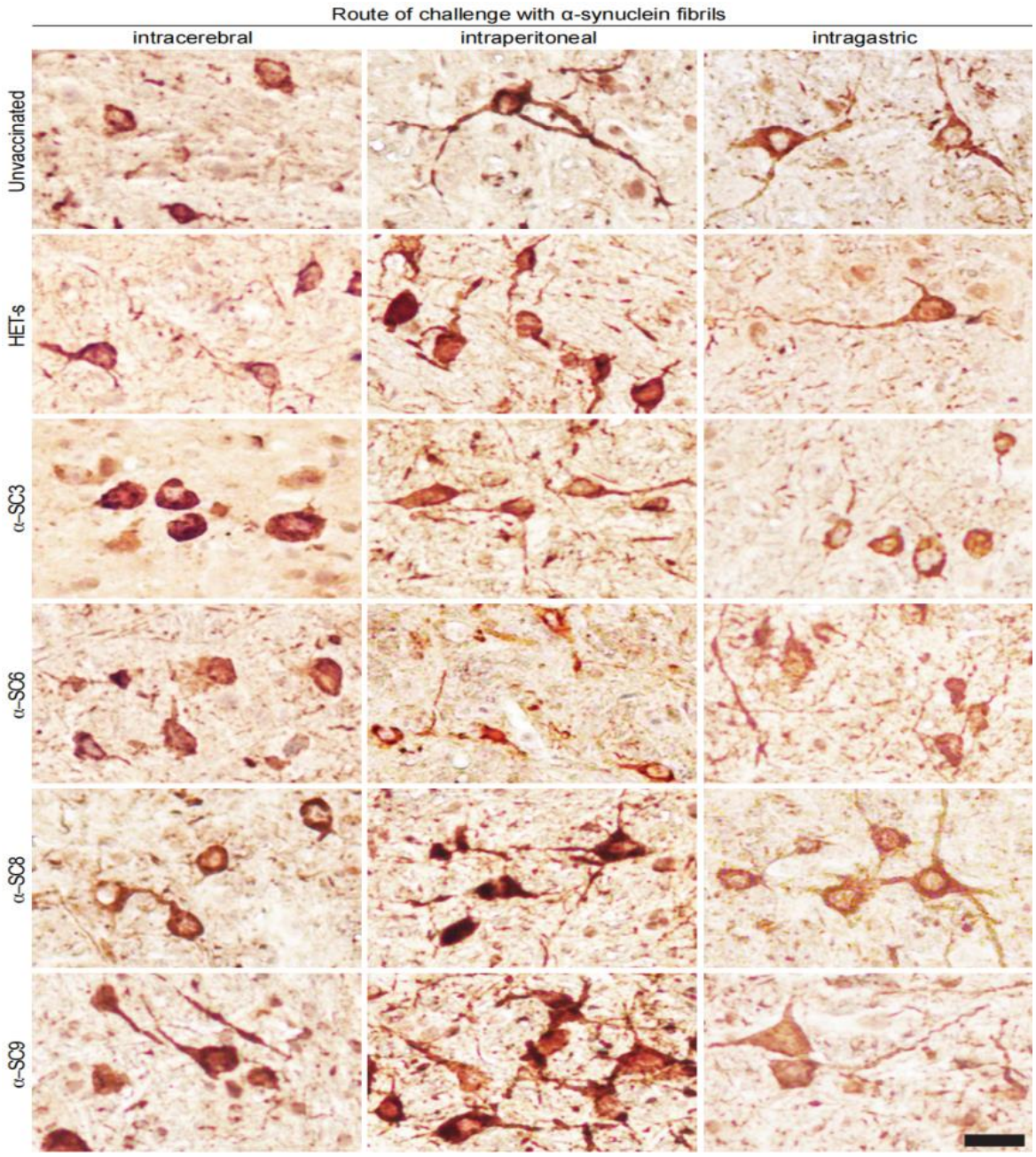

Fig. 4 Immunohistochemical analysis shows neuropathology in the CNS of diseased TgM83$^{+/-}$ mice. In diseased TgM83$^{+/-}$ mice challenged intracerebrally (left column), intraperitoneally (center column), or intragastrically (right column) with α-syn fibrils, deposits of phosphorylated α-syn were present in neuronal cell bodies and neurites as detected in brainstem sections by staining with the pSyn#64 antibody, which recognizes phosphorylation at serine 129 of α-syn. Pathology was observed in non-vaccinated mice (first row) and mice vaccinated with HET-s (second row), α-SC3 (third row), α-SC6 (fourth row), α-SC8 (fifth row), and α-SC9 fibrils (sixth row). The scale bar applies to all eighteen images and corresponds to 50 μm.

Brainstem sections of sick TgM83$^{+/-}$ mice were analyzed by immunofluorescence co-staining for phosphorylated α-syn (pSyn#64) and either ionized calcium-binding adaptor molecule-1 (Iba1) to detect microglia or glial fibrillary acidic protein (GFAP) to detect reactive astrocytes. Activated microglia were found in close proximity to pathological α-syn deposits. Non-

challenged healthy TgM83$^{+/-}$ mice showed no α-syn pathology and only ramified inactive microglia (Fig. 18A). Additionally, strong astrogliosis was observed in diseased mice. Astrocytes were enriched around neurons containing pathological α-syn. Again, the non-challenged healthy control mice showed no α-syn pathology and no pathological enrichment of astrocytes (Fig. 18B).

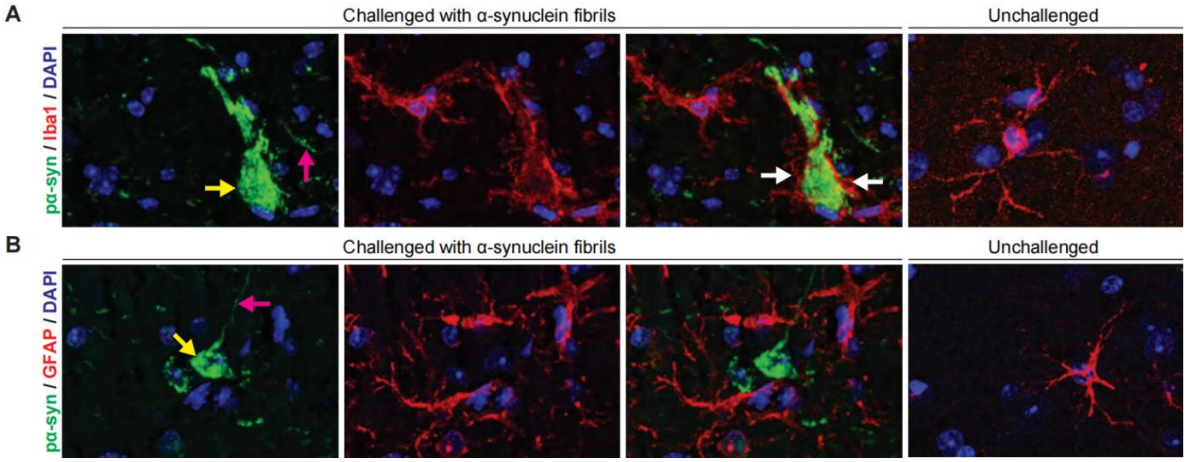

Fig. 5 Immunofluorescence staining shows astrogliosis and microgliosis in the brainstem of diseased mice. (A) Immunofluorescence co-staining of brainstem sections with antibodies against phosphorylated serine 129 of α-syn revealed deposits of pathological α-syn (green) and activated microglia with antibodies against ionized calcium-binding adapter molecule 1 (Iba1, red) in diseased mice. Pathological α-syn inclusions were observed in both neuronal cell bodies (yellow arrows) and dendrites (magenta arrows), surrounded by activated amoeboid microglia (white arrows). **(B)** Immunofluorescence co-staining with an antibody against phosphorylated serine 129 (green) and glial fibrillary acidic protein (GFAP, red) in diseased mice showed that in brainstem areas with deposits of pathological α-syn, neuronal cell bodies (yellow arrow) and neurites (magenta arrow) were enriched with surrounding astrocytes. The control stain showed no pathology and only isolated astrocytes. Cell nuclei were stained in blue with DAPI.

To explore whether the levels of α-syn aggregates differed between vaccinated and non-vaccinated mice, a TR-FRET assay was performed (Fig. 19). This assay was designed to quantify the levels of aggregated α-syn in brain homogenates and to assess how variations in exposure routes and vaccination status might affect the observed outcomes. The results revealed a significant increase in the levels of aggregated α-syn in the CNS of mice challenged with α-syn fibrils, regardless of the route of administration (intracerebral, intraperitoneal, or intragastric). However, statistical analysis did not identify significant differences between vaccinated and non-vaccinated mice, regardless of the route of challenge. It is noteworthy that a trend towards reduced pathology was observed in mice challenged via the intraperitoneal and intragastric routes compared to those challenged via the intracerebral route, which is known for its rapid induction of disease (Breid *et al.*, 2016; Lohmann *et al.*, 2019).

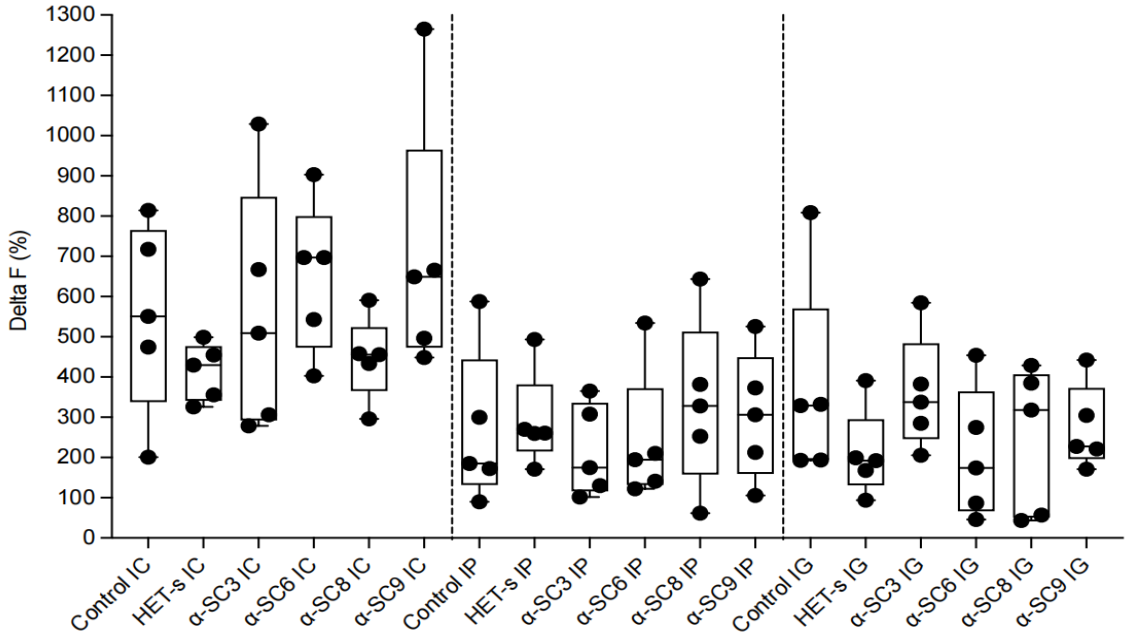

Fig. 19 Quantification of α-syn aggregates in the CNS of TgM83$^{+/-}$ mice challenged with α-syn fibrils. The levels of α-syn aggregates were quantified from brain homogenates of each cohort of intracerebrally, intraperitoneally, and intragastrically challenged TgM83$^{+/-}$ mice using a TR-FRET assay. The mice were either non-vaccinated controls or vaccinated with HET-s fibrils or one of the four HET-s-derived α-SC3, α-SC6, α-SC8, or α-SC9 fibrils. Each route of challenge, intracerebral (IC), intraperitoneal (IP), or intragastric (IG), was assessed separately, and no significant differences in the amount of aggregated α-syn were observed between vaccinated and non-vaccinated control mice for each route of challenge. Bars represent mean ± SD.

In summary, intracerebral, intraperitoneal and intragastric challenge of human α-syn fibrils lead to oligomeric and fibrillar conformations of phosphorylated α-syn in the brain of both vaccinated and non-vaccinated TgM83$^{+/-}$ mice, resulting in insoluble inclusions resembling Lewy bodies. This indicates that the aggregation and spread of pathological α-syn could not be slowed in intracerebrally challenged mice, but could be delayed in peripherally challenged animals.

3.7 Vaccination induces antibodies that recognize α-syn aggregates in patient brain homogenates

The ability of post-immune plasma to recognize pathological α-syn was tested by competitive ELISA. The plasma samples were tested against brain homogenates from patients with DLB (n = 3), MSA (n = 3), and PD (n = 3) and compared with brain homogenates from healthy controls (n=5). Plasma from mice vaccinated with HET-s and α-SC3 fibrils demonstrated superior detection of pathological α-syn in brain homogenates from patients with MSA and PD, but not DLB (Fig. 20A and B). Conversely, plasma samples from mice vaccinated with α-SC6, α-SC8, or α-SC9 fibrils showed better recognition of brain homogenates from patients with DLB, MSA, and PD than from healthy controls. Specifically, plasma from mice immunized

with α-SC6 (Fig. 20C) or α-SC9 fibrils (Fig. 20E) exhibited enhanced recognition of brain homogenates from patients with MSA and PD compared to DLB. Plasma samples from mice vaccinated with α-SC8 fibrils showed better detection of pathological α-syn aggregates in brain homogenates from patients with MSA and DLB and slightly less for PD (Fig. 20D).

These results indicate that fully vaccinated TgM83$^{+/-}$ mice develop antibodies not only against HET-s fibrils, the four vaccine candidates derived from them, but also against synthetic α-syn fibrils and, importantly, against pathological α-syn aggregates in brain homogenates from patients with synucleinopathies.

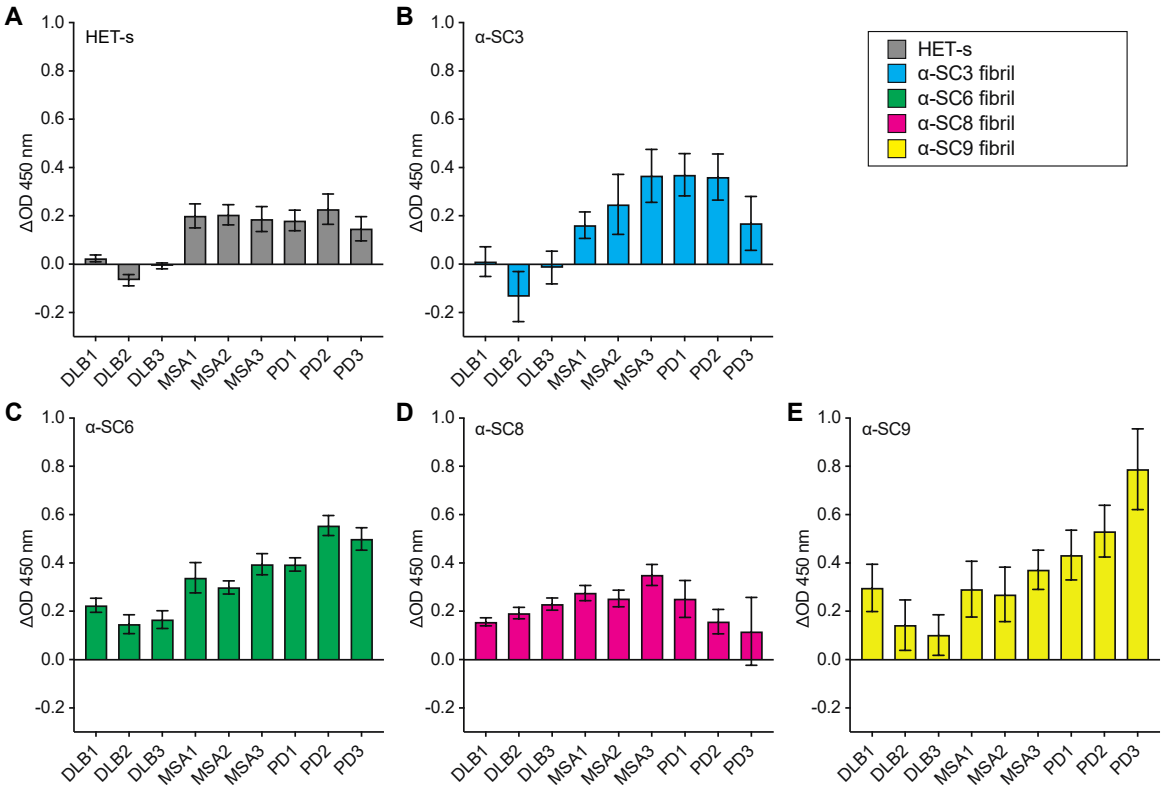

Fig. 20 Vaccinated mice produce antibodies against pathological α-syn present in patient brain homogenates. Using a competitive ELISA, plasma from five TgM83$^{+/-}$ mice each fully vaccinated with HET-s **(A)**, α-SC3 **(B)**, α-SC6 **(C)**, α-SC8 **(D)**, or α-SC9 fibrils **(E)** was tested against brain homogenates from healthy controls (n = 5) and patients with DLB (n = 3), MSA (n = 3), and PD (n = 3). Except for mice vaccinated with HET-s and α-SC3 fibrils and DLB brain homogenates, antibodies from immunized mice recognized brain homogenates from patients better than those from non-neurological controls. Bars represent mean ± SD.

3.8 Vaccinated mice produce antibodies recognizing sarkosyl-insoluble α-syn fibrils purified from patient brain homogenates

Sarkosyl-insoluble α-syn fibrils were extracted from brain homogenates of patients with DLB, PD, and MSA based on protocols to purify ex-vivo α-syn fibrils for cryo-electron microscopy

(Schweighauser *et al*., 2020; Yang *et al*., 2022). To assess the presence of antibodies in plasma of vaccinated mice recognizing α-syn fibrils, an immunoprecipitation assay was performed using pre-immune plasma, plasma from fully vaccinated mice or the MJFR-14-6-4-2 antibody against misfolded α-syn coupled to protein G-coated magnetic beads. After immunoprecipitation, the remaining amount of α-syn fibrils extracted from DLB (Fig. 21A), PD (Fig. 21B) and MSA (Fig. 21C) brains was quantified using TR-FRET analysis. The results demonstrated that vaccinated mice produced antibodies recognizing sarkosyl-insoluble α-syn fibrils from patients with synucleinopathies.

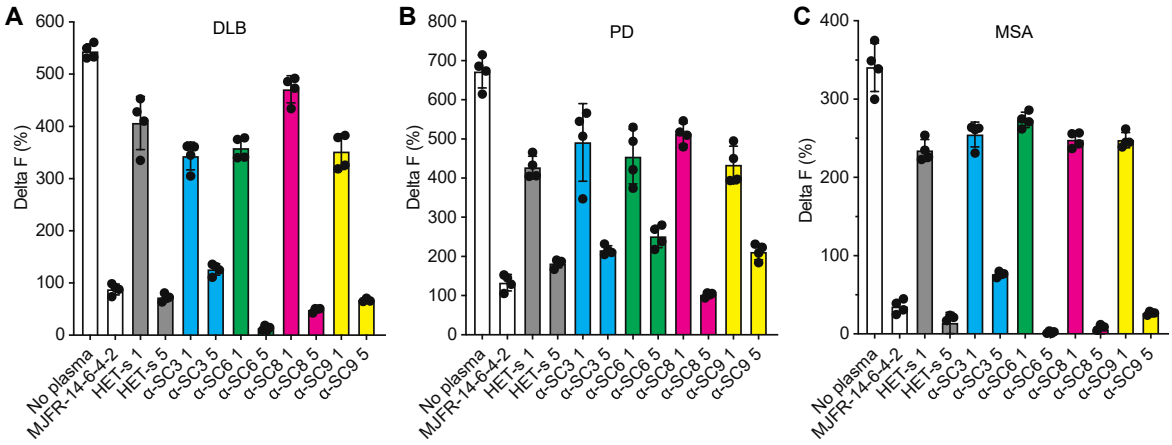

Fig. 6 Vaccinated mice produce antibodies that recognize sarkosyl-insoluble α-syn fibrils isolated from DLB, PD and MSA brains. Antibodies in plasma from four non-vaccinated (1) and TgM83$^{+/-}$ mice each fully vaccinated (5) with HET-s, α-SC3, α-SC6, α-SC8, or α-SC9 fibrils were bound to magnetic beads coated with protein G sepharose to immunodeplete sarkosyl-insoluble α-syn fibrils isolated from brain homogenates of patients with DLB **(A)**, PD **(B)**, and MSA **(C)**. Magnetic beads without plasma treatment (no plasma) and the MJFR-14-6-4-2 antibody directed against pathological α-syn served as negative and positive controls, respectively. Pathological α-syn fibrils left in the extracted samples after immunoprecipitation were measured using a TR-FRET assay for aggregated α-syn. In contrast to plasma from non-immunized mice, antibodies from immunized mice depleted sarkosyl-insoluble α-syn fibrils isolated from brain homogenates of patients. Bars represent mean ± SD.

4. Discussion

The HET-s fibrils and the four thereof derived vaccine candidates α-SC3, α-SC6, α-SC8, and α-SC9 fibrils demonstrated excellent efficacy in two body-first TgM83$^{+/-}$ mouse models. Unlike for previously described vaccine candidates (Masliah *et al.,* 2005), where only small epitopes were employed instead of the full-length α-syn as a vaccine (Ghochikyan *et al.,* 2014). The strategy of this approach was to minimize the risk of autoimmunity, which has been observed in other vaccine trials targeting neurodegenerative diseases, by targeting conformational epitopes present on pathological α-syn fibrils (Orgogozo *et al*., 2003). Therefore, the vaccines developed and tested in this study are likely to be safe for human use. However, this hypothesis needs to be explored in future clinical studies. An important feature of the vaccine candidates used in this study is that they contain epitopes located in the NAC region of α-syn, which are involved in α-syn aggregation. Consequently, the induced antibodies have the potential to block the NAC region, which could also prevent aggregation in vaccinated individuals (Chatterjee *et al.*, 2018).

4.1 In two body-first PD models, vaccinated mice show significantly delayed weight loss, improved behavioral performance and a prolonged lifespan

Weight loss, motor deficits, and shortened lifespan are primary indicators of early PD-like symptoms in TgM83$^{+/-}$ mice following challenge with α-syn fibrils. This study demonstrates the significant impact of the developed vaccines on these critical reference metrics in vaccinated mice.

Vaccinated mice that modeled brain-first PD showed an only minimally delayed onset of weight loss, improvement in motor function, and a trend towards extended median lifespan. However, extension of survival did not reach statistical significance. On the other hand, vaccinated mice that modeled the body-first PD exhibited a significantly prolonged period of weight gain, enhanced motor function, and an extended median lifespan (Fig. 10-12 and 15).

Generally, mice that were vaccinated and then injected with α-syn fibrils into the peritoneum or gut wall showed a significantly delayed onset of early PD-like symptoms compared to those injected into the brain. This suggests that vaccination has a more pronounced effect in the context of the body-first PD compared to the brain-first PD. It should be noted that mice that received intracerebral injections showed earlier disease manifestation compared to those that received intraperitoneal and intragastric injections. This is due to the presence of pathological α-syn fibrils in the brain after intracerebral injections, resulting in an earlier onset of disease and a shorter lifespan, whereas in the model of body-first PD α-syn pathology still has to propagate to the brain (Bae *et al*., 2012). Another contributing factor is that only a limited

amount of antibodies induced from the periphery can penetrate the BBB and reach the brain. Previous studies with antibodies against β-amyloid have demonstrated that antibodies from the bloodstream can enter the brain, albeit to a minimal extent with approximately only 0.1% of the administered dose reaching the brain (Banks *et al.*, 2002).

Compared to our previous results, where we combined 25 µg of each α-SC3, α-SC6, α-SC8 and α-SC9 fibrils into a 100 µg quadrivalent vaccine, the combination vaccine prolonged survival by 21% after intraperitoneal injection challenge and by 22% after intragastric challenge. In this study, we administered 100 µg of only one vaccine candidate, quadrupling the dose. Some vaccine candidates, particularly α-SC8 fibrils, doubled the level of protection and prolonged survival by 42% after intragastric challenge. It is notable that higher levels of protection and health benefits can be achieved by adjusting the dose, timing of boosters, vaccination route, and adjuvant used. PD, DLB, and MSA are primarily age-related diseases, particularly in those over 60 years of age. Studies suggest that body-first PD accounts for 30-50% of all PD cases (Berg *et al.*, 2021; Horsager *et al.*, 2024). If the vaccine candidates developed and tested in this study can provide the same level of protection in humans, the onset of body-first PD could be delayed from 65 to 92 years of age. Given that the average life expectancy in the Western world is nearly 80 years for both men and women, the protection provided by some of the vaccine candidates developed and tested in this study would virtually eradicate body-first PD, reducing the incidence of Parkinson's disease by half.

Overall, these findings suggest that vaccination with any of the vaccine candidates developed here may effectively delay the onset of PD by preventing the spread of α-syn pathology from the periphery to the brain.

4.2 Both vaccinated and non-vaccinated mice display pathology and neuroinflammation in the CNS

Transmission of α-syn fibrils resulted in severe neurological disease regardless of the injection route or vaccination status. Pathological confirmation was achieved through immunohistochemistry or immunofluorescence staining for deposits of pathological α-syn in the brainstem, accompanied by microgliosis and astrogliosis, or via biochemistry using western blot for the accumulation of pathological α-syn aggregates in brain homogenates.

Histological staining and western blot investigations revealed robust α-syn pathology, microgliosis, and astrogliosis (Fig. 16-19). These results show that vaccination delays disease onset in mice but does not prevent it. In contrast, previous vaccine studies have demonstrated a reduction in both pathology and neuroinflammation (Nimmo *et al.*, 2022; Mandler *et al.*, 2014). However, these differences are due to the fact that this study was designed as a

survival study, specifically to assess the extended lifespan of vaccinated mice compared to non-vaccinated mice. It is important to note that the mice in this study were euthanized based on the manifestation of disease signs, such as weight loss exceeding 20% of their maximum weight or decline in behavioral performance, including ataxia, kyphosis, hindlimb paralysis, or general motor impairments. If mice had been sacrificed at a predetermined time point, differences in pathology might have been observed. Previous vaccine studies euthanized both vaccinated and non-vaccinated animals simultaneously after a specific experimental period, enabling a direct comparison of pathology between the two groups. However, this study cannot be directly compared to previous ones as they were not designed as survival studies (Mandler *et al.*, 2015; Sanchez-Guajardo *et al.*, 2013; Ghochikyan *et al.*, 2014).

In summary, pathological α-syn was found in the brains of both vaccinated and non-vaccinated control mice after intracerebral, intraperitoneal, and intragastric challenge with α-syn fibrils. This resulted in insoluble inclusions resembling Lewy body pathology. These findings suggest that vaccination was not able to prevent the aggregation and spread of pathological α-syn, as these oligomers and aggregates were also present in vaccinated mice.

In conclusion, vaccination delayed the spread of α-syn pathology to the CNS in peripherally challenged mice, resulting in a delayed onset of weight loss, enhanced motor function, and extended lifespan.

4.3 HET-s induces immunity and delays the onset of PD

To design vaccines targeting aggregated α-syn, we chose the fungal prion HET-s as a scaffold protein. HET-s possesses a left-handed, two-rung β-solenoid fold structure, with a distance of 4.8 ± 0.2 Å between each β-rung and containing three β-strands per rung. The selection of the HET-s scaffold was based on its innocuous nature, rich β-folding, and structural similarities to α-syn. Additionally, HET-s fibrils are not infectious since they cannot propagate in humans. In the study, specific amino acids were introduced from the surface of α-syn to express antigenic determinants on the scaffold protein, owing to their structural similarities.

TgM83$^{+/-}$ mice were also vaccinated with HET-s fibrils as an additional control for mice vaccinated with HET-s-derived vaccine candidates. Interestingly, mice vaccinated with HET-s fibrils exhibited delayed early weight loss (Fig. 10 and 11), improved behavioral performance (Fig. 12) and extended lifespan (Fig. 15) upon intraperitoneal and intragastric challenge with α-syn fibrils. Additionally, the indirect ELISA results demonstrated that vaccination with HET-s fibrils induced antibodies against HET-s fibrils (Fig. 13) and synthetic α-syn fibrils (Fig. 14). The competitive ELISA showed that the induced antibodies had excellent recognition of pathological α-syn species present in brain homogenates from patients with MSA and PD but

not from patients with DLB (Fig. 20). In contrast, the TR-FRET assay showed that the induced antibodies recognized sarkosyl-insoluble α-syn fibrils purified from all patient brain homogenates with synucleinopathies (Fig. 21).

Not only did the four vaccine candidates presenting grafted conformational epitopes found on α-syn fibrils induce significant immunity in both animal models for body-first PD, but also unmodified HET-s fibrils, which is in line with the findings above. A possible explanation for these findings may be the presence of amino acids in the vaccine and in α-syn fibrils forming continuous stretches of identical amino acids across the backbone of the fibrils. Amino acid residues S227 in the β1a position of the first rung of HET-s and S263 in the β3a position of the second rung of HET-s (Fig. 6C) create a continuous sequence of serine residues, forming a conformational epitope across subunits within the HET-s fibrils (Wasmer *et al*., 2008). Similar stretches of serine residues, forming conformational epitopes across subunits, are also observed in the α-syn fibrils used to challenge TgM83$^{+/-}$ mice (PDB ID: 8OQI), where they are constituted by S42 or S87 in α-syn (Pesch *et al*., 2024). In these fibrils, S87 is exposed when both protofilaments are paired, while S42 is likely accessible only in unpaired protofilaments. Additionally, amino acid residues N243 in the β2b position of the first rung of HET-s and N279 in the β4b position of the second rung of HET-s constitute a continuous sequence of asparagine residues within the HET-s fibrils (Wasmer *et al*., 2008). A continuous sequence of asparagine residues is also present in the α-syn fibrils used to challenge mice, formed by N65 in α-syn, which represents a conformational epitope accessible in paired protofilaments (Pesch *et al*., 2024). Two additional asparagine residues at positions 103 and 122 of α-syn may also potentially form conformational epitopes of this nature, although this remains uncertain.

In conclusion, HET-s fibrils, initially selected only as a scaffold protein for vaccination against aggregated α-syn, also delayed early weight loss, improved behavioral performance, prolonged lifespan after peripheral challenge by inducing an immune response against pathological α-syn fibrils.

4.4 Vaccination induces immune response against all vaccine candidates, synthetic and pathological α-syn fibrils

The indirect ELISA conducted in this study revealed that vaccinated mice generated antibodies targeting each of the four vaccine candidates, HET-s fibrils, and also synthetic α-syn fibrils (Fig. 13 and 14). This indicates that the selected epitopes from the surface of synthetic α-syn fibrils were well-suited to develop effective vaccines. Furthermore, the competitive ELISA showed that the induced antibodies also recognized pathological α-syn aggregates in brain homogenates from patients with various synucleinopathies (Fig. 20). The

immunoprecipitation assay showed that vaccinated mice produced antibodies recognizing sarkosyl-insoluble α-syn fibrils extracted from brain homogenates of patients with DLB, PD and MSA (Fig. 21).

Interestingly, when assessing the ability of induced antibodies in fully vaccinated plasma to recognize pathological α-syn in brain homogenates from patients with DLB, PD and MSA using competitive ELISA, different results were observed compared to testing against sarkosyl-insoluble fractions extracted from brain homogenates that enriched in α-syn fibrils. Antibodies from mice fully immunized with HET-s and α-SC3 fibrils were unable to recognize DLB brain homogenates in the competitive ELISA. However, the antibodies were capable of recognizing α-syn species present in sarkosyl-insoluble fractions extracted from brain homogenates of patients with DLB, PD and MSA. These differences may be due to the fact that recognizable α-syn fibrils in pure brain homogenates from DLB patients are either less abundant or less accessible due to masking compared to those present in sarkosyl-extracted fractions when it comes to detecting them with antibodies generated to HET-s and a-SC3 fibrils. These findings suggest that there are differences in the pathological α-syn species present in DLB, PD, and MSA.

The vaccines developed and tested in this study demonstrated high immunogenicity in mice, inducing an immune response against both synthetic and pathological α-syn. The significance of these results lies in the distinct immune response pattern generated by each vaccine candidate against α-syn aggregates. These findings are promising as they suggest that these vaccines have the potential to elicit immunity to pathologically aggregated α-syn while avoiding autoimmunity. Therefore, these vaccine candidates offer a potential therapeutic avenue for related diseases.

Previous studies have encountered difficulties in developing vaccines for PD and other synucleinopathies due to the use of native α-syn or linear peptides and epitopes without controlling the antigen structure (Masliah *et al.*, 2005; Ghochikyan *et al.*, 2014). This has resulted in difficulties because the immune system cannot distinguish between the native and pathological forms of α-syn, which poses a high risk of autoimmune reactions. This study presents an innovative approach to designing vaccines that mimic regions on the surface of pathological forms of α-syn that are effectively recognized by the immune system. This novel strategy enables vaccines to express specific antigenic determinants of α-syn, resulting in effective active immunization for disease prevention. The induced antibodies were able to identify both synthetic α-syn fibrils and pathological α-syn aggregates in brain homogenates from patients with DLB, MSA, and PD. It is worth noting that the study did not target native α-syn, which demonstrates the effectiveness of this active immunotherapy in a mouse model.

In conclusion, the findings suggest that vaccination could induce an active immune response against pathological α-syn, positioning the vaccine candidates as potential therapeutic interventions against synucleinopathies in humans. Since DLB, MSA and PD primarily affect older individuals, even a small delay in the onset of these disorders could lead to significant benefits in terms of prevention and treatment, ultimately improving the overall well-being of the aging population.

5. Conclusion and Future Perspectives

The study findings indicate that the vaccination experiment demonstrated promising efficacy in TgM83$^{+/-}$ mice. Vaccination induced a robust immune response against all vaccine candidates, the induced antibodies also recognized synthetic α-syn fibrils. Vaccination with α-SC-3, α-SC-6, α-SC-8, α-SC-9 and HET-s fibrils protects from early weight loss and motor impairment and prolongs survival in two body-first PD models. These results show that HET-s fibrils and thereof derived vaccine candidates delay the onset of PD and early symptoms in body-first TgM83$^{+/-}$ mouse models.

However, both vaccinated and non-vaccinated animals displayed α-syn pathology in histological sections and biochemical analyses, along with astrogliosis and microgliosis. Although the vaccines delayed the onset of PD-like symptoms, they were not able to prevent the development or progression of PD in mice, ultimately resulting in both vaccinated and non-vaccinated animals succumbing to the disease.

Importantly, the induced antibodies demonstrated excellent recognition not only of synthetic α-syn but also of pathological α-syn associated with various synucleinopathies. Future research will investigate the efficacy of these vaccines and their prospects in clinical practice, providing crucial insights and guidance towards the development of safer and more effective vaccines.

The vaccine candidates in this study were modeled after only a few conformational epitopes present on two structures of synthetic α-syn fibrils. Thus, the design approach only selected a limited set of conformational epitopes from a larger conformational space. Nevertheless, the vaccines still provided significant protection against disease in TgM83$^{+/-}$ mouse models. Therefore, it is possible that additional or different conformational epitopes could provide even better immunity and greater protection against disease. Importantly, the recent availability of ex-vivo structures of α-syn fibrils isolated from the brains of patients with synucleinopathies now enable the design of disease-specific and potentially more potent vaccine candidates.

Moreover, the method of conformational epitope grafting described in this text is suitable for developing vaccines that target a wide range of pathogenic protein structures and amyloids,

such as amyloid beta and tau in Alzheimer's disease, islet amyloid polypeptide (IAPP) in type II diabetes, and other proteins associated with protein misfolding diseases.

The field of research on PD vaccines is entering a new and exciting era. Future studies on vaccines targeting pathological α-syn species are expected to improve their precision and efficacy and may result in vaccine candidates that fully halt the disease progression.

6. Bibliography

Abouni, S., Bousset, L., Loria, F., Zhu, S., Chaumont, F. D., Pieri, L. *et al.* (2016). Tunneling nanotubes spread fibrillar α-synuclein by intercellular trafficking of lysosomes. *The EMBO journal*, 35 (19), 2120–2138. doi: 10.15252/embj.201593411.

Alborghetti, M., Nicoletti, F. (2019). Different Generations of Type-B Monoamine Oxidase Inhibitors in Parkinson's Disease: From Bench to Bedside. *Current neuropharmacology*, 17 (9), 861–873. doi: 10.2174/1570159X16666180830100754.

Ali, G. N., Wallace, K. L., Schwartz, R., DeCarle, D. J., Zagami, A. S., Cook, I. J. (1996). Mechanisms of oral-pharyngeal dysphagia in patients with Parkinson's disease. *Gastroenterology*, 110 (2), 383–392. doi: 10.1053/gast1996.v110.pm8566584.

Allaman, I., Bélanger, M., and Magistretti, P. J. (2011). Astrocyte-neuron metabolic relationships: For better and for worse. *Trends in Neurosciences*, 34 (2), 76-87. doi: 10.1016/j.tins.2010.12.001.

Anderson, J. P., Walker, D. E., Goldstein, J. M., Laat, R. de., Banducci, K., Caccavello, R. J. *et al*. (2006). Phosphorylation of Ser-129 is the dominant pathological modification of alpha-synuclein in familial and sporadic Lewy body disease. *The Journal of Biological Chemistry,* 281 (40), 29739–29752. doi: 10.1074/jbc.M600933200.

Appel-Cresswell, S., Vilarino-Guell, C., Encarnacion, M., Sherman, H., *et al*. (2013). Alpha-synuclein p.H50Q, a novel pathogenic mutation for Parkinson’s disease. *Movement Disorders*, 28 (6), 811-813. doi: 10.1002/mds.25421.

Annerino, D. M., Arshad, S., Taylor, G. M., Adler, C. H., Beach, T. G., Greene, J. G. (2012). Parkinson's disease is not associated with gastrointestinal myenteric ganglion neuron loss. *Acta Neuropathol* ,124 (5), 665–680. doi: 10.1007/s00401-012-1040-2.

Ascherio, A. and Schwarzschild, M. A. (2016). The epidemiology of Parkinson’s disease: risk factors and prevention, *The Lancet Neurology*, 15 (12), 1257-1272. doi: 10.1016/S1474-4422(16)30230-7.

Baba, M., Nakajo, S., Tu, P. H., Tomita, T., Nakaya, K., Lee, V. M. *et al*. (1998). Aggregation of alpha-synuclein in Lewy bodies of sporadic Parkinson's disease and dementia with Lewy bodies. *The American Journal of Pathology,* 152 (4), 879–884.

Bae, E. J., Lee, H. J., Rockenstein, E., Ho, D. H., Park, E. B., Yang, N. Y. *et al*. (2012). Antibody-aided clearance of extracellular α-synuclein prevents cell-to-cell aggregate transmission. *The Journal of neuroscience*, 32 (39), 13454–13469. doi: 10.1523/JNEUROSCI.1292-12.2012.

Balguerie, A., Dos Reis, S., Ritter, C., Chaignepain, S., Coulary-Salin, B., Forge, V. *et al.* (2003). Domain organization and structure-function relationship of the HET-s prion protein of Podospora anserina. *The EMBO journal* 22 (9), 2071–2081. doi: 10.1093/emboj/cdg213.

Banks, W. A., Terrell, B., Farr, S. A., Robinson, S. M., Nonaka, N., Morley, J. E. (2002) Passage of amyloid beta protein antibody across the blood-brain barrier in a mouse model of Alzheimer's disease. *Peptides,* 23 (12), 2223–2226. doi: 10.1016/S0196-9781(02)00261-9.

Bartels, T., Choi, J. G., Selkoe, D. J. (2011). α-Synuclein occurs physiologically as a helically folded tetramer that resists aggregation. *Nature,* 477 (7362), 107–110. doi: 10.1038/nature10324.

Benabid, A. L. (2003). Deep brain stimulation for Parkinson's disease. *Current Opinion in Neurobiology,* 13 (6), 696–706. doi: 10.1016/j.conb.2003.11.001.

Berg, D., Borghammer, P., Fereshtehnejad, S-M., Heinzel, S., Horsager, J., *et al*. (2021). Prodromal Parkinson disease subtypes- key to understanding heterogeneity. *Nature Reviews Neurology*, 17 (6), 349-361. doi: 10.1038/s41582-021-00486-9.

Bergström, A. L., Kallunki, P., Fog, K. (2016). Development of Passive Immunotherapies for Synucleinopathies. *Movement Disorders,* 31 (2), 203–213. doi: 10.1002/mds.26481.

Braak, H., Rüb, U., Gai, W. P., Del Tredici, K. (2003a). Idiopathic Parkinson's disease: possible routes by which vulnerable neuronal types may be subject to neuroinvasion by an unknown pathogen. *Journal of neural transmission*, 110 (5), 517–536. doi: 10.1007/s00702-002-0808-2.

Braak, H., Del Tredici, K., Rüb, U., Vos, R. I. de., Jansen Steur, E. N. H., Braak, E. (2003b). Staging of brain pathology related to sporadic Parkinson's disease. *Neurobiology of aging* 24 (2), 197–211. doi: 10.1016/s0197-4580(02)00065-9.

Braak, H., Vos, R. A. I. de., Bohl, J., Del Tredici, K. (2006). Gastric alpha-synuclein immunoreactive inclusions in Meissner's and Auerbach's plexuses in cases staged for Parkinson's disease-related brain pathology. *Neuroscience Letters,* 396 (1), 67–72. doi: 10.1016/j.neulet.2005.11.012.

Breid, S., Bernis, M. E., Babila, J. T., Garza, M. C., Wille, H., Tamgüney, G. (2016). Neuroinvasion of alpha-Synuclein Prionoids after Intraperitoneal and Intraglossal Inoculation. *J Virol*, 90(20), 9182-93. doi: 10.1128/JVI.01399-16

Brys, M., Fanning, L., Hung, S., Ellenbogen, A., Penner, N., Yang, M. H. *et al*. (2019). Randomized phase I clinical trial of anti-α-synuclein antibody BIIB054. *Movement Disorders,* 34 (8), 1154–1163. doi: 10.1002/mds.27738.

Burai, R., Ait-Bouziad, N., Chiki, A., Lashuel, H. A. (2015). Elucidating the Role of Site-Specific Nitration of α-Synuclein in the Pathogenesis of Parkinson's Disease via Protein Semisynthesis and Mutagenesis. *Journal of the American Chemical Society,* 137 (15), 5041–5052. doi: 10.1021/ja5131726.

Burré, J., Sharma, M., Tsetsenis, T., Buchman, V., Etherton, M. R., Südhof, T. C. (2010). Alpha-synuclein promotes SNARE-complex assembly in vivo and in vitro. *Science*, 329 (5999), 1663–1667. doi: 10.1126/science.1195227.

Campbell, B. C., McLean, C. A., Culvenor, J. G., Gai, W. P., Blumbergs, P. C., Jäkälä, P. *et al*. (2001). The solubility of alpha-synuclein in multiple system atrophy differs from that of dementia with Lewy bodies and Parkinson's disease. *Journal of neurochemistry,* 76 (1), 87–96. doi: 10.1046/j.1471-4159.2001.00021x.

Chan, D. K. Y., Xu, Y.H.,Chan, L.K.M., Braidy, N., Mellick, G.D. (2017). Mini-review on initiatives to interfere with the propagation and clearance of alpha-synuclein in Parkinson's disease. *Translational Neurodegeneration*, 6 (1). doi: 10.1186/s40035-017-0104-6.

Chandra, S., Chen, X. C., Rizo, J., Jahn, R., *et al*. (2003). A broken α-Helix in Folded α-synuclein. *Journal of Biological Chemistry*, 278 (17), 15313-15318. doi: 10.1074/jbc.M213128200.

Chatterjee, D., Bhatt, M., Butler, D., Genst, E. de., Dobson, C. M., Messer, A., Kordower, J. H. (2018). Proteasome-targeted nanobodies alleviate pathology and functional decline in an

α-synuclein-based Parkinson's disease model. *Parkinson's Disease,* 4 (1), 25. doi: 10.1038/s41531-018-0062-4.

Chavarría, C., Souza, J. M. (2013). Oxidation and nitration of α-synuclein and their implications in neurodegenerative diseases. *Archives of biochemistry and biophysics,* 533 (1-2), 25–32. doi: 10.1016/j.abb.2013.02.009.

Chen, L., Jin, J. H., Davis, J., Zhou, Y., Wang, Y., Liu, J. *et al.* (2007). Oligomeric alpha-synuclein inhibits tubulin polymerization. *Biochemical and biophysical research communications,* 356 (3), 548–553. doi: 10.1016/j.bbrc.2007.02.163.

Choi, B. K., Choi, M. G., Kim, J. Y., Yang, Y., Lai, Y., Kweon, D. H. *et al*. (2013). Large α-synuclein oligomers inhibit neuronal SNARE-mediated vesicle docking. *Proceedings of the National Academy of Sciences of the United States of America,* 110 (10), 4087–4092. doi: 10.1073/pnas.1218424110.

Chung, K. A., Pfeiffer, R. F. (2021): Gastrointestinal dysfunction in the synucleinopathies. *Clin Auton Res,* 31 (1), 77–99. doi: 10.1007/s10286-020-00745-7.

Chung, C. Y., Seo, H., Sonntag, K. C., Brooks, A., *et al*. (2005). Cell type-specific gene expression of midbrain dopaminergic neurons reveals molecules involved in their vulnerability and protection. *Human Molecular Genetics*, 14 (13), 1709-1725. doi: 10.1093/hmg/ddi178.

Colla, E., Jensen, P. H., Pletnikova, O., Troncoso, J. C., Glabe, C., Lee, M. K. (2012). Accumulation of toxic α-synuclein oligomer within endoplasmic reticulum occurs in α-synucleinopathy in vivo. *The Journal of neuroscience: the official journal of the Society for Neuroscience,* 32 (10), 3301–3305. doi: 10.1523/JNEUROSCI.5368-11.2012.

Conway, K. A., Harper, J. D., Lansbury, P. T. (1998). Accelerated in vitro fibril formation by a mutant alpha-synuclein linked to early-onset Parkinson disease. *Nature medicine,* 4 (11), 1318–1320. doi: 10.1038/3311.

Coustou, V., Deleu, C., Saupe, S., Begueret, J. (1997). The protein product of the het-s heterokaryon incompatibility gene of the fungus Podospora anserina behaves as a prion analog. *Proceedings of the National Academy of Sciences of the United States of America,* 94 (18), 9773–9778. doi: 10.1073/pnas.94.18.9773.

Crowther, R. A., Jakes, R., Spillantini, M. G., Goedert, M. (1998). Synthetic filaments assembled from C-terminally truncated alpha-synuclein. *FEBS letters,* 436 (3), 309–312. doi: 10.1016/s0014-5793(98)01146-6.

Daniele, S. G., Béraud, D., Davenport, C., Cheng, K., Yin, H., Maguire-Zeiss, K. A. (2015). Activation of MyD88-dependent TLR1/2 signaling by misfolded α-synuclein, a protein linked to neurodegenerative disorders. *Science signaling,* 8 (376), ra45. doi: 10.1126/scisignal.2005965.

Danielson, S. R., Held, J. M., Schilling, B., Oo, M., Gibson, B. W., Andersen, J. K. (2009). Preferentially increased nitration of alpha-synuclein at tyrosine-39 in a cellular oxidative model of Parkinson's disease. *Analytical chemistry,* 81 (18), 7823–7828. doi: 10.1021/ac901176t.

Danzer, K. M., Haasen, D., Karow, A. R., Moussaud, S., Habeck, M., Giese, A. *et al.* (2007). Different species of alpha-synuclein oligomers induce calcium influx and seeding. *The Journal of neuroscience*: the official journal of the Society for Neuroscience, 27 (34), 9220–9232. doi: 10.1523/JNEUROSCI.2617-07.2007.

Danzer, K. M., Kranich, L. R., Ruf, W. P., Cagsal-Getkin, O., Winslow, A. R., Zhu, L. *et al.* (2012). Exosomal cell-to-cell transmission of alpha synuclein oligomers. *Mol Neurodegeneration,* 7, 42. doi: 10.1186/1750-1326-7-42.

Davidson, W. S., Jonas, A., Clayton, D. F., George, J. M. (1998). Stabilization of alpha-synuclein secondary structure upon binding to synthetic membranes. *Journal of Biological Chemistry*, 273 (16), 9443-9449. doi: 10.1074/jbc.273.16.9443.

Di Maio, R., Barrett, P. J., Hoffman, E. K., Barrett, C. W., Zharikov, A., Borah, A. *et al.* (2016). α-Synuclein binds to TOM20 and inhibits mitochondrial protein import in Parkinson's disease. *Science translational medicine,* 8 (342), 342ra78. doi: 10.1126/scitranslmedaaf3634.

Dickson, D. W. (2018): Neuropathology of Parkinson disease. *Parkinsonism & Related Disorders,* 46 Suppl 1 (Suppl 1), S30-S33. doi: 10.1016/j.parkreldis.2017.07.033.

Dickson, D. W. (2007) Linking selective vulnerability to cell death mechanisms in Parkinson's disease. *American Journal of Pathology*,170 (1), 16-19. doi: 10.2353/ajpath.2007.061011

Eliezer, D., Kutluay, E., Bussell, R., Browne, G. (2001). Conformational properties of alpha-synuclein in its free and lipid-associated states. *Journal of Molecular Biology,* 307 (4), 1061-1073. doi: 10.1006/jmbi.2001.4538.

Ellis, C. E., Schwartzberg, P. L., Grider, T. L., Fink, D. W., Nussbaum, R. L. (2001). alpha-synuclein is phosphorylated by members of the Src family of protein-tyrosine kinases. *The Journal of Biological Chemistry,* 276 (6), 3879–3884. doi: 10.1074/jbc.M010316200.

Farrer, M., Kachergus, J., Forno, L., Lincoln, S., et al. (2004). Comparison of kindreds with parkinsonism and alpha-synuclein genomic multiplications. *Annals of Neurology*, 55 (2), 174-179. doi: 10.1002/ana.10846.

Feany, M. B. and Bender, W. W. (2000). A Drosophila model of Parkinson's disease. *Nature,* 404 (6776), 394-398. doi: 10.1038/35006074.

Fellner, L., Irschick, R., Schanda, K., Reindl, M., *et al*. (2012). Toll-like receptor 4 is required for a-synuclein dependent activation of microglia and astroglia. *GLIA,* 61 (3), 349-360. doi: 10.1002/glia.22437.

Foulds, P.G., Diggle, P., Mitchell, J. D., Parker, A., Hasegawa, M., et al. (2013). A longitudinal study on a-synuclein in blood plasma as a biomarker for Parkinson's disease. *Scientific Reports*. doi: 10.1038/srep02540.

Fujiwara, H., Hasegawa, M., Dohmae, N., Kawashima, A., Masliah, E., Goldberg, M. S. *et al.* (2002). alpha-Synuclein is phosphorylated in synucleinopathy lesions. *Nat Cell Biol,* 4 (2), 160–164. doi: 10.1038/ncb748.

Games, D., Valera, E., Spencer, B., Rockenstein, E., Mante, M., Adame, A. *et al.* (2014). Reducing C-terminal-truncated alpha-synuclein by immunotherapy attenuates neurodegeneration and propagation in Parkinson's disease-like models. *The Journal of neuroscience*: the official journal of the Society for Neuroscience, 34 (28), 9441–9454. doi: 10.1523/JNEUROSCI.5314-13.2014.

George, J. M. (2002). The synucleins. *Genome Biology,* 3 (1), REVIEWS3002. doi: 10.1186/gb-2001-3-1-reviews3002.

Ghochikyan, A., Petrushina, I., Davtyan, H., Hovakimyan, A., Saing, T., Davtyan, A. *et al.* (2014). Immunogenicity of epitope vaccines targeting different B cell antigenic determinants of human α-synuclein: feasibility study. *Neuroscience Letters,* 560, 86–91. doi: 10.1016/j.neulet.2013.12.028.

Giasson, B. I., Duda, J. E., Murray, I. V., Chen, Q., Souza, J. M., Hurtig, H. I. *et al.* (2000). Oxidative damage linked to neurodegeneration by selective alpha-synuclein nitration in synucleinopathy lesions. *Science,* 290 (5493), 985–989. doi: 10.1126/science.290.5493.985.

Giasson, B. I., Duda, J. E., Quinn, S. M., Zhang, B., Trojanowski, J. Q., Lee, Virginia M-Y (2002). Neuronal alpha-synucleinopathy with severe movement disorder in mice expressing A53T human alpha-synuclein. *Neuron,* 34 (4), 521–533. doi: 10.1016/S0896-6273(02)00682-7.

Goedert, M., Falcon, B., Clavaguera, F., Tolnay, M. (2014). Prion-like mechanisms in the pathogenesis of tauopathies and synucleinopathies. *Current Neurology and Neuroscience Reports*, 14 (11), 495. doi: 10.1007/s11910-014-0495-z.

Goedert, M., Clavaguera, F. and Tolnay, M. (2010). The propagation of prion-like protein inclusions in neurodegenerative disease. *Trends in Neurosciences*, 33 (7), 317-325. doi: 10.1016/j.tins.2010.04.003.

Gómez-Benito, M., Granado, N., García-Sanz, P., Michel, A., Dumoulin, M., Moratalla, R. (2020). Modeling Parkinson's Disease with the Alpha-Synuclein Protein. *Frontiers in Pharmacology,* 11, 356. doi: 10.3389/fphar.2020.00356.

Gómez-Tortosa, E., Newell, K., Irizarry, M. C., Sanders, J. L., Hyman, B. T. (2000). α-Synuclein immunoreactivity in dementia with Lewy bodies: morphological staging and comparison with ubiquitin immunostaining. *Acta Neuropathol,* 99 (4), 352–357. doi: 10.1007/s004010051135.

Guardia-Laguarta, C., Area-Gomez, E., Rüb, C., Liu, Y. Y., *et al*. (2014). a-Synuclein is localized to mitochondria-associated ER membranes. *Journal of Neuroscience*, 34 (1), 249-259. doi: 10.1523/JNEUROSCI.2507-13.2014

Guerrero-Ferreira, R., Taylor, N. M., Mona, D., Ringler, P., Lauer, M. E., Riek, R. *et al.* (2018). Cryo-EM structure of alpha-synuclein fibrils. *eLife,* 7. doi: 10.7554/eLife.36402.

Hasegawa, M., Fujiwara, H., Nonaka, T., Wakabayashi, K., Takahashi, H., Lee, Virginia M-Y *et al.* (2002). Phosphorylated alpha-synuclein is ubiquitinated in alpha-synucleinopathy lesions. *The Journal of Biological Chemistry,* 277 (50), 49071–49076. doi: 10.1074/jbc.M208046200.

Hirsch, E. C., Hunot, S. (2009). Neuroinflammation in Parkinson's disease: a target for neuroprotection. *The Lancet Neurology,* 8 (4), 382–397. doi: 10.1016/S1474-4422(09)70062-6.

Hirsch, E. C. (1994). Biochemistry of Parkinson’s disease with special reference to the dopaminergic system. *Molecular Neurobiology*, 9 (1-3), 135-142. doi: 10.1007/BF02816113.

Hirsch, E., Graybiel, A. M. and Agid, Y. A. (1988): Melanized dopaminergic neurons are differentially susceptible to degeneration in Parkinson's disease. *Nature*,334 (6180), 345-348. doi: 10.1038/334345a0.

Hoban, D. B., Shrigley, S., Mattsson, B., Breger, L., et al. (2020). Impact of α-synuclein pathology on transplanted hESC-derived dopaminergic neurons in a humanized α-synuclein rat model of PD. *Proceedings of the National Academt of Sciences of the United States of America*, 117 (26), 15209-15220. doi: 10.1073/pnas.2001305117.

Hodara, R., Norris, E. H., Giasson, B. I., Mishizen-Eberz, A. J., Lynch, D. R., *et al*. (2004). Functional consequences of alpha-synuclein tyrosine nitration: diminished binding to lipid vesicles and increased fibril formation. *The Journal of Biological Chemistry*, 279 (46), 47746-47753. doi: 10.1074/jbc.M408906200.

Horsager, J., Borghammer, P. (2024). Brain-first vs. body-first Parkinson's disease: An update on recent evidence. *Parkinonism Relat Disord*, 15, 106101. doi: 10.1016/j.parkreldis.2024.106101.

Hoyer, W., Cherny, D., Subramaniam, V., Jovin, T. M. (2004). Impact of the acidic C-terminal region comprising amino acids 109-140 on alpha-synuclein aggregation in vitro. *Biochemistry,* 43 (51), 16233–16242. doi: 10.1021/bi048453u.

Hubble, J. P., Cao. T., Hassanein, R. E. S., Neuberger, J. S., Roller, W.C. (1993). Risk factors for Parkinson's disease. *Neurology*, 43(9), 1693-1697. doi: 10.1212/WNL.43.9.1693.

Hughes, C. D., Choi, M. L., Ryten, M., Hopkins, L., Drews, A., Botía, J. A. *et al.* (2019). Picomolar concentrations of oligomeric alpha-synuclein sensitizes TLR4 to play an initiating role in Parkinson's disease pathogenesis. *Acta Neuropathol,* 137 (1), 103–120. doi: 10.1007/s00401-018-1907-y.

Hyun, C. H., Yoon, C.Y., Lee, H-J., Lee, S-J. (2013). LRRK2 as a Potential Genetic Modifier of Synucleinoathies: Interlacing the Two Major Genetic Factors of Parkinson's Disease. *Experimental Neurobiology*, 22 (4), 249-257. doi: 10.5607/en.2013.22.4.249.

Inglis, K. J., Chereau, D., Brigham, E. F., Chiou, S., Schöbel, S., Frigon, N. L. *et al.* (2009). Polo-like kinase 2 (PLK2) phosphorylates alpha-synuclein at serine 129 in central nervous system. *The Journal of Biological Chemistry,* 284 (5), 2598–2602. doi: 10.1074/jbc.C800206200.

Iwatsubo, T. (2003). Aggregation of alpha-synuclein in the pathogenesis of Parkinson's disease. *Journal of neurology,* 250 Suppl 3, III11-4. doi: 10.1007/s00415-003-1303-x.

Iwai, A., Masliah, E., Yoshimoto, M., Ge, L. F., Flanagan, H. A., *et al*. (1995). The precursor protein of non-Abeta component of Alzheimer's disease amyloid is a presynaptic protein of the central nervous system. *Neuron*, 14 (2), 467-475. doi: 10.1016/0896-6273(95)90302-x.

Jakes, R., Spillantini, M. G., Goedert, M. (1994). Identification of two distinct synucleins from human brain. *FEBS letters,* 345 (1), 27–32. doi: 10.1016/0014-5793(94)00395-5.

Jankovic, J. (2008). Parkinson's disease: clinical features and diagnosis. *Journal of Neurology, Neurosurgery & Psychiatry,* 79 (4), 368–376. doi: 10.1136/jnnp.2007.131045.

Jankovic, J., Goodman, I., Safirstein, B., Marmon, T. K., Schenk, D. B., Koller, M. *et al.* (2018). Safety and Tolerability of Multiple Ascending Doses of PRX002/RG7935, an Anti-α-Synuclein Monoclonal Antibody, in Patients with Parkinson Disease: A Randomized Clinical Trial. *JAMA neurology,* 75 (10), 1206–1214. doi: 10.1001/jamaneurol.2018.1487.

Jiang, P. Z., Gan, M., Ebrahim, A. S., Lin, W., Melrose, H. L., Yen, S. C. (2010). ER stress response plays an important role in aggregation of α-synuclein. *Mol Neurodegeneration,* 5 (1), 56. doi: 10.1186/1750-1326-5-56.

Johnson, M., Coulton, A. T., Geeves, M. A., Mulvihill, D. P. (2010). Targeted amino-terminal acetylation of recombinant proteins in E. coli. *PLOS ONE,* 5 (12), e15801. doi: 10.1371/journal.pone.0015801.

Kalia, S. K., Sankar, T., Lozano, A. M. (2013). Deep brain stimulation for Parkinson's disease and other movement disorders. *Current opinion in neurology,* 26 (4), S. 374–380. doi: 10.1097/WCO.0b013e3283632d08.

Katzenschlager, R., Lees, A. J. (2002). Treatment of Parkinson's disease: levodopa as the first choice. *J Neurol,* 249 Suppl 2 (2), II19-24. doi: 10.1007/s00415-002-1204-4.

Khalaf, O., Fauvet, B., Oueslati, A., et al. (2014). The H50Q Mutation Enhances α-Synuclein Aggregation, Secretion, and Toxicity. *Journal of Biological Chemistry*, 289 (32), 21856-21876. doi: 10.1074/jbc.M114.553297.

Kiely, A. P.; Asi, Yasmine T., Kara, E., Limousin, P., Ling, H., Lewis, P. *et al.* (2013). α-Synucleinopathy associated with G51D SNCA mutation: a link between Parkinson's disease and multiple system atrophy. *Acta Neuropathol,* 125 (5), 753–769. doi: 10.1007/s00401-013-1096-7.

Kim, S., Kwon, S. H., Kam, T., Panicker, N., Karuppagounder, S. S., Lee, S. *et al*. (2019). Transneuronal Propagation of Pathologic α-Synuclein from the Gut to the Brain Models Parkinson's Disease. *Neuron,* 103 (4), 627-641.e7. doi: 10.1016/j.neuron.2019.05.035.

Knecht, L., Folke, J., Dodel, R., Ross, J. A., Albus, A. (2022). Alpha-synuclein Immunization Strategies for Synucleinopathies in Clinical Studies: A Biological Perspective. *Neurotherapeutics: the journal of the American Society for Experimental NeuroTherapeutics,* 19 (5), 1489–1502. doi: 10.1007/s13311-022-01288-7.

Koga, S., Sekiya, H., Kondru, N., Ross, O. A., Dickson, D. W. (2021). Neuropathology and molecular diagnosis of Synucleinopathies. *Molecular Neurodegeneration,* 16 (1), 83. doi: 10.1186/s13024-021-00501-z.

Krüger, R.; Kuhn, W.; Müller, T.; Woitalla, D.; Graeber, M.; Kösel, S. et al. (1998). Ala30Pro mutation in the gene encoding alpha-synuclein in Parkinson's disease. *Nature genetics,* 18 (2), 106–108. doi: 10.1038/ng0298-106.

Kumar, S. T., Mahul-Mellier, A. L., Hegde, R. N., Rivière, G., Moons, R., Ibáñez de Opakua, A. *et al.* (2022). A NAC domain mutation (E83Q) unlocks the pathogenicity of human alpha-synuclein and recapitulates its pathological diversity. *Science Advances,* 8 (17), eabn0044. doi: 10.1126/sciadvabn0044.

Kuzuhara, S., Mori, H., Izumiyama, N., Yoshimura, M., Ihara, Y. (1988). Lewy bodies are ubiquitinated. A light and electron microscopic immunocytochemical study. *Acta Neuropathol,* 75 (4), 345–353. doi: 10.1007/BF00687787.

Lakso, M., Vartiainen, S., Moilanen, A-M., *et al*. (2003). Dopaminergic neuronal loss and motor deficits in Caenorhabditis elegans overexpressing human alpha-synuclein. *Journal of Neurochemistry*, 86 (1), 165-172. doi: 10.1046/j.1471-4159.2003.01809x.

Lavedan, C., Leroy, E., Dehejia, A., Buchholtz, S., Dutra, A., *et al.* (1998). Identification, localization and characterization of the human γ-synuclein gene. *Human Genetics,* 103, 106-112. doi: 10.1007/s004390050792.

Lee, A., Gilbert, R. M. (2016). Epidemiology of Parkinson Disease. *Neurologic Clinics,* 34 (4), 955–965. doi: 10.1016/j.ncl.2016.06.012.

Lee, M. K., Stirling W., Xu, Y. G., Price, D. L. (2002). Human α-synuclein-harboring familial Parkinson's disease-linked Ala-53 → Thr mutation causes neurodegenerative disease with α-synuclein aggregation in transgenic mice. *Proceedings of the National Academy of Sciences of the United States of America*, 99 (13), 8968-8973. doi: 10.1073/pnas.132197599.

Lee, H. J., Suk, J. E., Bae, E. J., Lee, J. H., Paik, S. R., Lee, S. J. (2008a). Assembly-dependent endocytosis and clearance of extracellular alpha-synuclein. *The international journal of biochemistry & cell biology,* 40 (9), 1835–1849. doi: 10.1016/j.biocel.2008.01.017.

Lee, H. J.,Suk, J. E., Patrick, C., Bae, E. J., Cho, J. H., Rho, S. *et al.* (2010). Direct transfer of alpha-synuclein from neuron to astroglia causes inflammatory responses in synucleinopathies. *Journal of Biological Chemistry,* 285 (12), 9262–9272. doi: 10.1074/jbc.M109.081125.

Lee, J. T., Wheeler, T. C., Li, L., Chin, L. S. (2008b). Ubiquitination of alpha-synuclein by Siah-1 promotes alpha-synuclein aggregation and apoptotic cell death. *Human molecular genetics,* 17 (6), 906–917. doi: 10.1093/hmg/ddm363.

Li, H. T., Du, H. N., Tang, L., Hu, J., Hu, H. Y. (2002). Structural transformation and aggregation of human alpha-synuclein in trifluoroethanol: non-amyloid component sequence is essential and beta-sheet formation is prerequisite to aggregation. *Biopolymers,* 64 (4), 221–226. doi: 10.1002/bip.10179.

Li, Y. W., Zhao, C. Y., Luo, F., Liu, Z. Y., Gui, X. R., *et al*. (2018). Amyloid fibril structure of α-synuclein determined by cryo-electron microscopy. *Cell Reseach*, 18, 897–903. doi: 10.1038/s41422-018-0075-x.

Lohmann, S., Bernis, M E., Tachu, B. J., Ziemski, A., Grigoletto, J., Tamgüney, G. (2019). Oral and intravenous transmission of α-synuclein fibrils to mice. *Acta Neuropathol,* 138 (4), 515–533. doi: 10.1007/s00401-019-02037-5.

Ludtmann, Marthe H. R., Angelova, P. R., Horrocks, M. H., Choi, M. L., Rodrigues, M., Baev, A. Y. *et al.* (2018). α-synuclein oligomers interact with ATP synthase and open the permeability transition pore in Parkinson's disease. *Nat Commun,* 9 (1), 2293. doi: 10.1038/s41467-018-04422-2.

Luk, K. C., Kehm, V., Carroll, J., Zhang, B., O'Brien, P., Trojanowski, J. Q., Lee, Virginia M-Y (2012a). Pathological α-synuclein transmission initiates Parkinson-like neurodegeneration in nontransgenic mice. *Science*, 338 (6109), 949–953. doi: 10.1126/science.1227157.

Luk, K. C.; Kehm, V. M., Zhang, B., O'Brien, P., Trojanowski, J. Q., Lee, Virginia M. Y. (2012b). Intracerebral inoculation of pathological α-synuclein initiates a rapidly progressive neurodegenerative α-synucleinopathy in mice. *The Journal of experimental medicine,* 209 (5), 975–986. doi: 10.1084/jem.20112457.

Luk, K. C., Song, C., O'Brien, P., Stieber, A., Branch, J. R., Brunden, K. R. *et al.* (2009). Exogenous alpha-synuclein fibrils seed the formation of Lewy body-like intracellular inclusions in cultured cells. *Proceedings of the National Academy of Sciences of the United States of America,* 106 (47), 20051–20056. doi: 10.1073/pnas.0908005106.

Mahul-Mellier, A. L., Fauvet, B., Gysbers, A., Dikiy, I., Oueslati, A., Georgeon, S. *et al.* (2014). c-Abl phosphorylates α-synuclein and regulates its degradation: implication for α-synuclein clearance and contribution to the pathogenesis of Parkinson's disease. *Human molecular genetics,* 23 (11), 2858–2879. doi: 10.1093/hmg/ddt674.

Mandler, M., Valera, E., Rockenstein, E., Mante, M., Weninger, H., Patrick, C. *et al.* (2015). Active immunization against alpha-synuclein ameliorates the degenerative pathology and prevents demyelination in a model of multiple system atrophy. *Mol Neurodegeneration,* 10, 10. doi: 10.1186/s13024-015-0008-9.

Mandler, M., Valera, E., Rockenstein, E., Weninger, H., Patrick, C., Adame, A. *et al.* (2014). Next-generation active immunization approach for synucleinopathies: implications for Parkinson's disease clinical trials. *Acta Neuropathol,* 127 (6), 861–879. doi: 10.1007/s00401-014-1256-4.

Mandler, M., Rockenstein, E., Overk, C. *et al*. (2019). Effects of single and combined immunotherapy approach targeting amyloid beta protein and alpha-synuclein in a dementia with Lewy bodies-like model. *Alzheimers Dement*, 15(9), 1133-1148. doi: 10.1016/jjalz.2019.02.002.

Meade, R. M., Fairlie, D. P. and Mason, J. M. (2019). Alpha-synuclein structure and Parkinson’s disease – lessons and emerging principles. *Molecular Neurodefeneration*, 14(1), 29. doi: 10.1186/s13024-019-0329-1.

Mao, X. B., Ou, M. T., Karuppagounder, S. S., Kam, T. I., Yin, X. L., Xiong, Y. L. *et al.* (2016). Pathological α-synuclein transmission initiated by binding lymphocyte-activation gene 3. *Science*, 353 (6307), aah3374. doi: 10.1126/scienceaah3374.

Maroteaux, L., Campanelli, J. T., Scheller, R. H. (1988). Synuclein: a neuron-specific protein localized to the nucleus and presynaptic nerve terminal. *The Journal of neuroscience: the official journal of the Society for Neuroscience,* 8 (8), 2804–2815. doi: 10.1523/JNEUROSCI.08-08-02804.1988.

Masliah, E., Rockenstein, E., Adame, A., Alford, M., Crews, L., Hashimoto, M. *et al*. (2005). Effects of alpha-synuclein immunization in a mouse model of Parkinson's disease. *Neuron,* 46 (6), 857–868. doi: 10.1016/j.neuron.2005.05.010.

Masliah, E., Rockenstein, E., Mante, M., Crews, L., Spencer, B., Adame, A. *et al.* (2011). Passive immunization reduces behavioral and neuropathological deficits in an alpha-synuclein transgenic model of Lewy body disease. *PLOS ONE,* 6 (4), e19338. doi: 10.1371/journal.pone.0019338.

Masliah, E., Rockenstein, E., Veinbergs, I., Mallory, M., *et al*. (2000a). Dopaminergic loss and inclusion body formation in alpha-synuclein mice: implications for neurodegenerative disorders. *Science*, 287 (5456), 1265-1269. doi:10.1126/science.287.5456.1265.
Masuda-Suzukake, M., Nonaka, T., Hosokawa, M., Oikawa, T., Arai, T., Akiyama, H. *et al.* (2013). Prion-like spreading of pathological α-synuclein in brain. *Brain* 136 (Pt 4), 1128–1138. DOI: 10.1093/brain/awt037.

Michel, P. P., Hirsch, E. C. and Hunot, S. (2016). Understanding Dopaminergic Cell Death Pathways in Parkinson Disease. *Neuron*, 90 (4), 675-691. DOI: 10.1016/j.neuron.2016.03.038.
Mitra, S., Chakrabarti, N., Bhattacharyya, A. (2011). Differential regional expression patterns of α-synuclein, TNF-α, and IL-1β; and variable status of dopaminergic neurotoxicity in mouse brain after Paraquat treatment. *J Neuroinflammation,* 8 (1), 163. doi:10.1186/1742-2094-8-163.

Murray, Ian V. J., Giasson, B. I., Quinn, S. M., Koppaka, V., Axelsen, P. H., Ischiropoulos, H. *et al.* (2003). Role of alpha-synuclein carboxy-terminus on fibril formation in vitro. *Biochemistry,* 42 (28), 8530–8540. doi:10.1021/bi027363r.

Nakajo, S., Tsukada, K., Omata, K., Nakamura, Y., Nakaya, K. (1993). A new brain-specific 14-kDa protein is a phosphoprotein. Its complete amino acid sequence and evidence for phosphorylation. *European journal of biochemistry,* 217 (3), 1057–1063. doi:10.1111/j.1432-1033.1993. tb 18337.x.

Negro, A., Brunati, A. M., Donella-Deana, A., Massimino, M. L., Pinna, L. A. (2002). Multiple phosphorylation of alpha-synuclein by protein tyrosine kinase Syk prevents eosin-induced aggregation. *FASEB journal*: official publication of the Federation of American Societies for Experimental Biology, 16 (2), 210–212. doi: 10.1096/fj.01-0517fje.

Nemani, V. M., Lu, W., Berge, V., Nakamura, K., *et al*. (2010). Increased expression of alpha-synuclein reduces neurotransmitter release by inhibiting synaptic vesicle reclustering after endocytosis*. Neuron*, 65 (1), 66-79. doi: 10.1016/j.neuron.2009.12.023.

Neumann, M., Müller, V., Kretzschmar, H. A., Haass, C., Kahle, P. J. (2004). Regional distribution of proteinase K-resistant alpha-synuclein correlates with Lewy body disease stage. *Journal of neuropathology and experimental neurology,* 63 (12), 1225–1235. doi: 10.1093/jnen/63.12.1225.

Nielsen, M. S., Vorum, H., Lindersson, E., Jensen, P. H. (2001). Ca2+ binding to alpha-synuclein regulates ligand binding and oligomerization. *The Journal of Biological Chemistry,* 276 (25), 22680–22684. doi: 10.1074/jbc.M101181200.

Nimmo, Jacqui T., Smith, H., Wang, C. Y., Teeling, J. L., Nicoll, J. A. R.; Verma, A. *et al*. (2022). Immunisation with UB-312 in the Thy1SNCA mouse prevents motor performance deficits and oligomeric α-synuclein accumulation in the brain and gut. *Acta Neuropathol,* 143 (1), 55–73. doi: 10.1007/s00401-021-02381-5.

Nonaka, T., Iwatsubo, T., Hasegawa, M. (2005). Ubiquitination of alpha-synuclein. *Biochemistry,* 44 (1), 361–368. doi: 10.1021/bi0485528.

Okochi, M., Walter, J., Koyama, A., Nakajo, S., Baba, M., Iwatsubo, T. *et al.* (2000). Constitutive phosphorylation of the Parkinson's disease associated alpha-synuclein. *The Journal of Biological Chemistry,* 275 (1), 390–397. doi: 10.1074/jbc.275.1.390.

Orgogozo, J-M., Gilman, S., Dartigues, J-F., Laurent, B., Puel, M., Kirby, L. C. *et al.* (2003). Subacute meningoencephalitis in a subset of patients with AD after Abeta42 immunization. *Neurology,* 61 (1), 46–54. doi: 10.1212/01.wnl.0000073623.84147a8.

Oueslatti, A., Fournier, M. and Lashuel, H. A. (2010). Role of post-translational modifications in modulating the structure, function and toxity of a-synuclein. *Implications for Parkinson's disease pathogenesis and therapies in Progress in Brain Research*, 183, 115-145. doi: 10.1016/S0079-6123(10)83007-9.

Paleologou, K. E., Oueslati, A., Shakked, G., Rospigliosi, C. C., Kim, H-Y., Lamberto, G. R. *et al.* (2010). Phosphorylation at S87 is enhanced in synucleinopathies, inhibits alpha-synuclein oligomerization, and influences synuclein-membrane interactions. *The Journal of neuroscience: the official journal of the Society for Neuroscience,* 30 (9), 3184–3198. doi:10.1523/JNEUROSCI.5922-09.2010.

Park, M. Ross, G.W., Petrovitch, H., White, L.R., Masaki, K.H., *et al*. (2005). Consumption of milk and calcium in midlife and the future risk of Parkinson's disease. *Neurology,* 64 (6), 1047-1051. doi: 10.1212/01.WNL.0000154532.98495.

Pankratz, N. and Foroud, T. (2004). Genetics of Parkinson's disease. *NeuriRx,* 1, 235-242. doi: 10.1602/neurorx.1.2.235.

Pasanen, P., Myllykangas, L., Siitonen, M., Raunio, A., Kaakkola, S., Lyytinen, J. *et al.* (2014). Novel α-synuclein mutation A53E associated with atypical multiple system atrophy and Parkinson's disease-type pathology. *Neurobiology of aging,* 35 (9), 2180.e1-5. doi: 10.1016/j.neurobiolaging.2014.03.024.

Peelaerts, W., Bousset, L., van der Perren, A., Moskalyuk, A., Pulizzi, R., Giugliano, M. *et al.* (2015). α-Synuclein strains cause distinct synucleinopathies after local and systemic administration. *Nature,* 522 (7556), 340–344. doi: 10.1038/nature14547.

Perfeito, R., Lázaro, D. F., Outeriro, T. F., Rego, A. C. (2014). Lingking alpha-synuclein phosphorylation to reactive oxygen species formation and mitochondrial dysfunction in SH-SY5Y cells. *Molecular and Cellular Neuroscience*, 62, 51-59. doi: 10.1016/j.mcn.2014.08.002.

Peteucelli, L., O'Farrell,C., Lockhart, P. J., Baptista, M., et al. (2002). Parkin protects against the toxicity associated with mutant alpha-synuclein: proteasome dysfunction selectively affects catecholaminergic neurons. *Neuron*, 36 (6), 1007-1019. doi: 10.1016/s0896-6273(02)01125-x.

Pesch, V., Flores-Fernandez, JM., Reithofer, S., Ma, L., *et al*. (2024). Vaccination with structurally adapted fungal protein fibrils induces immunity to Parkinson's disease. *Brain.* doi: 10.1093/brain/awae061.

Plotegher, N., Gratton, E., Bubacco, L. (2014). Number and Brightness analysis of alpha-synuclein oligomerization and the associated mitochondrial morphology alterations in live cells. *Biochimica et biophysica acta,* 1840 (6), 2014–2024. doi: 10.1016/j.bbagen.2014.02.013.

Poewe, W., Volc, D., Seppi, K., Medori, R., Lührs, P., Kutzelnigg, A. *et al.* (2021). Safety and Tolerability of Active Immunotherapy Targeting α-Synuclein with PD03A in Patients with Early Parkinson's Disease: A Randomized, Placebo-Controlled, Phase 1 Study. *Journal of Parkinson's disease,* 11 (3), 1079–1089. doi: 10.3233/JPD-212594.

Polymeropoulos, M. H., Lavedan, C., Leroy, E., Ide, S. E., Dehejia, A., Dutra, A. *et al.* (1997). Mutation in the alpha-synuclein gene identified in families with Parkinson's disease. *Science,* 276 (5321), 2045–2047. doi: 10.1126/science.276.5321.2045.

Pratt, M. R., Abeywardana, T., Marotta, N. P. (2015). Synthetic Proteins and Peptides for the Direct Interrogation of α-Synuclein Posttranslational Modifications. *Biomolecules,* 5 (3), 1210–1227. doi: 10.3390/biom5031210.

Pringsheim, T., Jette, N., Frolkis, A., Steeves, T. D. L. (2014). The prevalence of Parkinson's disease: a systematic review and meta-analysis. *Movement Disorders,* 29 (13), 1583–1590. doi: 10.1002/mds.25945.

Pronin, A. N., Morris, A. J., Surguchov, A., Benovic, J. L. (2000). Synucleins are a novel class of substrates for G protein-coupled receptor kinases. *The Journal of Biological Chemistry,* 275 (34), 26515–26522. doi: 10.1074/jbc.M003542200.

Prots, I., Veber, V., Brey, S., Campioni, S., Buder, K., Riek, R. *et al.* (2013). α-Synuclein oligomers impair neuronal microtubule-kinesin interplay. *Journal of Biological Chemistry,* 288 (30), 21742–21754. DOI: 10.1074/jbc.M113.451815.

Proukakis, C., Dudzik, C. G., Brier, T., MacKay, D. S., Cooper, J. M., Millhauser, G. L. *et al*. (2013). A novel α-synuclein missense mutation in Parkinson disease. *Neurology,* 80 (11), 1062–1064. doi: 10.1212/WNL.0b013e31828727ba.

Rannikko, E. H., Weber, S. S., and Kahle, P. J. (2015). Exogenpus a-synuclein induces toll-like receptor 4 dependent inflammatory responses in astrocytes. *BMC Neuroseience,* 16:57. doi: 10.1186/s12868-015-0192-0.

Recasens, A., Dehay, B. (2014). Alpha-synuclein spreading in Parkinson's disease. *Frontiers in neuroanatomy,* 8, 159. doi: 10.3389/fnana.2014.00159.

Rey, N. L., Petit, G. H., Bousset, L., Melki, R., Brundin, P. (2013). Transfer of human α-synuclein from the olfactory bulb to interconnected brain regions in mice. *Acta Neuropathol,* 126 (4), 555–573. doi: 10.1007/s00401-013-1160-3.

Rott, R., Szargel, R., Haskin, J., Shani, V., Shainskaya, A., Manov, I. *et al.* (2008). Monoubiquitylation of alpha-synuclein by seven in absentia homolog (SIAH) promotes its aggregation in dopaminergic cells. *The Journal of Biological Chemistry,* 283 (6), 3316–3328. doi: 10.1074/jbc.M704809200.

Rott, R., Szargel, R., Shani, V., Hamza, H., Savyon, M., Abd Elghani, F. *et al.* (2017). SUMOylation and ubiquitination reciprocally regulate α-synuclein degradation and pathological aggregation. *Proceedings of the National Academy of Sciences of the United States of America,* 114 (50), 13176–13181. doi: 10.1073/pnas.1704351114.

Sacino, A. N., Brooks, M., Thomas, M. A., McKinney, A. B., Lee, S., Regenhardt, R. W. *et al*. (2014). Intramuscular injection of α-synuclein induces CNS α-synuclein pathology and a rapid-onset motor phenotype in transgenic mice. *Proceedings of the National Academy of Sciences of the United States of America, 111 (*29), 10732–10737. doi: 10.1073/pnas.1321785111.

Sampathu, D. M., Giasson, B. I., Pawlyk, A. C., Trojanowski, J. Q., Lee, V. M-Y (2003). Ubiquitination of alpha-synuclein is not required for formation of pathological inclusions in alpha-synucleinopathies. *The American Journal of Pathology,* 163 (1), 91–100. doi: 10.1016/s0002-9440(10)63633-4.

Sanchez-Guajardo, V., Annibali, A., Jensen, P. H., Romero-Ramos, M. (2013). α-Synuclein vaccination prevents the accumulation of parkinson disease-like pathologic inclusions in striatum in association with regulatory T cell recruitment in a rat model. *Journal of neuropathology and experimental neurology,* 72 (7), 624–645. doi: 10.1097/NEN.0b013e31829768d2.

Schapira, A. H. V., Emre, M., Jenner, P., Poewe, W. (2009). Levodopa in the treatment of Parkinson's disease. *European journal of neurology,* 16 (9), 982–989. doi: 10.1111/j.1468-1331.2009.02697x.

Schneeberger, A., Tierney, L., Mandler, M. (2016). Active immunization therapies for Parkinson's disease and multiple system atrophy. *Movement Disorders,* 31 (2), 214–224. doi: 10.1002/mds.26377.

Schweighauser, M., Shi, Y., Tarutani, A. *et al*. (2020). Structures of alpha-synuclein filaments from multiple system atrophy. *Nature*, 585(7825), 464-469. doi:10.1038/s41586-020-2317-6

Sevcsik, E., Trexler, A. J., Dunn, J. M., Rhoades, E. (2011). Allostery in a disordered protein: oxidative modifications to α-synuclein act distally to regulate membrane binding. *Journal of the American Chemical Society,* 133 (18), 7152–7158. doi: 10.1021/ja2009554.

Shavali, S., Combs, C. K., Ebadi, M. (2006). Reactive macrophages increase oxidative stress and alpha-synuclein nitration during death of dopaminergic neuronal cells in co-culture: relevance to Parkinson's disease. *Neurochemical research,* 31 (1), 85–94. doi: 10.1007/s11064-005-9233-x.

Singleton, A. B., Farrer, M., Johnson, J., Singleton, A., et al. (2003). alpha-Synuclein locus triplication causes Parkinson's disease. *Science*, 302 (5646), 841. doi: 10.1126/science.1090278.

Smith, J. F., Tuomas, P. J. K., Christopher, M. D., *et al*. (2006). Characterization of the nanoscale properties of individual amyloid fibrils. *Proceedings of the National Academy of Sciences of the United States of American,* 103 (43), 15806-15811. doi:10.1073/pnas.0604035103.

Sofroniew, M. V. and Vinters, H. V. (2010). Astrocytes: biology and pathology. *Acta Neuropathologica*, 119 (1), 7-35. DOI: 10.1007/s00401-009-0618-8

Spillantini, M. G., Croher, R. A., Jakes, R., Hasegawa, M., Goedert, M. (1998). alpha-Synuclein in filamentous inclusions of Lewy bodies from Parkinson's disease and dementia with lewy bodies. *Proceedings of the National Academy of Sciences of the United States of America,* 95 (11), 6469–6473. doi: 10.1073/pnas.95.11.6469.

Spillantini, M. G., Goedert, M. (2000). The alpha-synucleinopathies: Parkinson's disease, dementia with Lewy bodies, and multiple system atrophy. *Annals of the New York Academy of Sciences,* 920, 16–27. doi: 10.1111/j.1749-6632.2000tb06900x.

Spillantini, M. G., Schmidt, M. L., Lee, V. M., Trojanowski, J. Q., Jakes, R., Goedert, M. (1997). Alpha-synuclein in Lewy bodies. *Nature,* 388 (6645), 839–840. doi: 10.1038/42166.

Spillantini, M. G., Crowther, R. A., Jakes, R., Cairns, N. J., Lantos, P. L., Goedert, M. Filamentous. (1998). alpha-synuclein inclusions link multiple system atrophy with Parkinson's disease and dementia with Lewy bodies. *Neurosci Lett*, 251(3), 205-208. doi:10.1016/S0304-3940(98)00504-7

Stefanovic, A. N. D., Söckl, M. T., Claessens, M. M. A., Subramaniam, V. (2014). a-Synuclein oligomers distinctively permeabilize complex model membranes. *FEBS Journal*, 281 (12), 2838-2350. doi: 10.1111/febs.12824.

Subramaniam, S. R., Vergnes, L., Franich, N. R., Rene, K., Chesselet, M-F. (2014). Region specific mitochondrial impairment in mice with widespread overexpression of alpha-synuclein. *Neurobiology of Disease,* 70, 204-213. doi: 10.1016/j.nbd.2014.06.017.

Sung, J. Y., Kim, J., Paik, S. R., Park, J. H., Ahn, Y. S., Chung, K. C. (2001). Induction of neuronal cell death by Rab5A-dependent endocytosis of alpha-synuclein. *The Journal of Biological Chemistry,* 276 (29), 27441–27448. doi: 10.1074/jbc.M101318200.

Sulzer, D. and Surmeier, D. J. (2013). Neuronal vulnerability, pathogenesis, and Parkinson's disease. Moment Disorders, 28(1), 41-50. doi: 10.1002/mds.25095.

Tamgüney, G., Giles, K., Bouzamondo-Bernstein, E., Bosque, P. J., Miller, M. W., Safar, J. *et al.* (2006). Transmission of elk and deer prions to transgenic mice. *Journal of virology*, 80 (18), 9104–9114. doi: 10.1128/JVI.00098-06.

Tamgüney, G., Korczyn, A. D. (2018). A critical review of the prion hypothesis of human synucleinopathies. *Cell Tissue Res,* 373 (1), 213–220. doi: 10.1007/s00441-017-2712-y.

Taschenberger, G., Garrido, M., Tereshchenko, Y., Bähr, M., Zweckstetter, M., Kügler, S. (2012). Aggregation of αSynuclein promotes progressive in vivo neurotoxicity in adult rat dopaminergic neurons. *Acta Neuropathologica,* 123 (5), 671–683. doi: 10.1007/s00401-011-0926-8.

Theodore, S., Cao, S. W., McLean, P. J., Standaert, D. G. (2008). Targeted overexpression of human alpha-synuclein triggers microglial activation and an adaptive immune response in a mouse model of Parkinson disease. *Journal of neuropathology and experimental neurology,* 67 (12), 1149–1158. doi: 10.1097/NEN.0b013e31818e5e99.

Tofaris, G. K., Garcia Reitböck, P., Humby, T., Lambourne, S. L., O'Connell, M., Ghetti, B. *et al.* (2006). Pathological changes in dopaminergic nerve cells of the substantia nigra and olfactory bulb in mice transgenic for truncated human alpha-synuclein (1-120): implications for Lewy body disorders. *The Journal of neuroscience: the official journal of the Society for Neuroscience,* 26 (15), 3942–3950. doi: 10.1523/JNEUROSCI.4965-05.2006.

Tolosa, E., Garrido, A., Scholz, S. W., Poewe, W. (2021), Challenges in the diagnosis of Parkinson's disease. *The Lancet. Neurology,* 20 (5), 385–397. doi: 10.1016/S1474-4422(21)00030-2.

Tong, J. X., Wong, H., Guttman, M., Ang, L. C., Forno, L. S., Shimadzu, M. *et al.* (2010). Brain alpha-synuclein accumulation in multiple system atrophy, Parkinson's disease and progressive supranuclear palsy: a comparative investigation. *Brain: a journal of neurology,* 133 (Pt 1), 172–188. doi: 10.1093/brain/awp282.

Tran, H. T., Chung, C H-Y., Iba, M., Zhang, B., Trojanowski, J. Q., Luk, K. C., Lee, V. M. Y. (2014). A-synuclein immunotherapy blocks uptake and templated propagation of misfolded α-synuclein and neurodegeneration. *Cell Reports,* 7 (6), 2054–2065. doi: 10.1016/j.celrep.2014.05.033.

Tuttle, M. D.; Comellas, G., Nieuwkoop, A. J., Covell, D J., Berthold, D. A., Kloepper, K. D. *et al.* (2016). Solid-state NMR structure of a pathogenic fibril of full-length human α-synuclein. *Nature structural & molecular biology,* 23 (5), 409–415. doi: 10.1038/nsmb.3194.

Tysnes, O. B. and Storstein, A. (2017). Epidemiology of Parkinson's disease. *Journal of Neural Transmission,* 124(8), 901-905. doi: 10.1007/s00702-017-1686-y.

Uéda, K., Fukushima, H., Masliah, E., Xia, Y., Iwai, A., Yoshimoto, M. *et al.* (1993). Molecular cloning of cDNA encoding an unrecognized component of amyloid in Alzheimer disease. *Proceedings of the National Academy of Sciences of the United States of America,* 90 (23), 11282–11286. doi: 10.1073/pnas.90.23.11282.

Uemura, N., Yagi, H., Uemura, M. T., Hatanaka, Y., Yamakado, H., Takahashi, R. (2018). Inoculation of α-synuclein preformed fibrils into the mouse gastrointestinal tract induces Lewy body-like aggregates in the brainstem via the vagus nerve. *Mol Neurodegeneration,* 13 (1), 21. doi: 10.1186/s13024-018-0257-5.

Uversky, V. and Eliezer, D. (2009). Biophysics of Parkinson's Disease: Structure and Aggregation of α-Synuclein. *Current Protein & Peptide Science*, 10 (5), 483-499. doi: 10.2174/138920309789351921.

Van den Berge, N., Ferreira, N., Gram, H., Mikkelsen, T. W., Alstrup, A. K. O., Casadei, N. *et al.* (2019a). Evidence for bidirectional and trans-synaptic parasympathetic and sympathetic propagation of alpha-synuclein in rats. *Acta Neuropathol,* 138 (4), 535–550. doi: 10.1007/s00401-019-02040-w.

Volc, D., Poewe, W., Kutzelnigg, A., Lührs, P., Thun-Hohenstein, C., Schneeberger, A. *et al.* (2020). Safety and immunogenicity of the α-synuclein active immunotherapeutic PD01A in patients with Parkinson's disease: a randomised, single-blinded, phase 1 trial. *The Lancet. Neurology,* 19 (7), 591–600. doi: 10.1016/S1474-4422(20)30136-8.

Volpicelli-Daley, L. A., Luk, K. C., Patel, T. P., Tanik, S. A., *et al*. (2011). Exogenous α-synuclein fibrils induce Lewy body pathology leading to synaptic dysfunction and neuron death. *Neuron*, 72 (1), 57-71. doi: 10.1016/j.neuron.2011.08.033.

Wasmer, C., Lange, A., van Melckebeke, H., Siemer, A. B., Riek, R., Meier, B. H. (2008). Amyloid fibrils of the HET-s (218-289) prion form a beta solenoid with a triangular hydrophobic core. *Science*, 319 (5869), 1523–1526. doi: 10.1126/science.1151839.

Watts, J. C., Giles, K., Oehler, A., et al. (2013). Transmission of multiple system atrophy prions to transgenic mice. *Proceedings of National Sciences and Academy of the United States of America*, 110 (48), 19555-19560. doi: 10.1073/pnas.1318268110.

Welchman, R. L., Gordon, C., Mayer, R. J. (2005). Ubiquitin and ubiquitin-like proteins as multifunctional signals. *Nat Rev Mol Cell Biol*, 6 (8), 599–609. doi: 10.1038/nrm1700.

Wilms, H., Rosenstiel, P., Romero-Ramos, M., Arlt, A., Schäfer, H., Seegert, D. *et al.* (2009). Suppression of MAP kinases inhibits microglial activation and attenuates neuronal cell death induced by alpha-synuclein protofibrils. *International journal of immunopathology and pharmacology,* 22 (4), 897–909. doi: 10.1177/039463200902200405.

Wilton, D. K., Dissing-Olesen, L. and Stevens, B. (2019). Neuron-Glia Signaling in Synapse Elimination. *Annual Review of Neuroscience*, 42, 107-127. doi: 10.1146/annurev-neuro-070918-050306.

Winner, B., Jappelli, R., Maji, S. K., Desplats, P. A., Boyer, L., Aigner, S. *et al*. (2011). In vivo demonstration that α-synuclein oligomers are toxic. *Proceedings of the National Academy of Sciences of the United States of America,* 108 (10), 4194–4199. doi: 10.1073/pnas.1100976108.

Wu, D. C., Jackson-Lewis, V., Vila, M., Tieu, K., Teismann, P., Vadseth, C. *et al.* (2002). Blockade of microglial activation is neuroprotective in the 1-methyl-4-phenyl-1,2,3,6-tetrahydropyridine mouse model of Parkinson disease. *The Journal of neuroscience: the official journal of the Society for Neuroscience,* 22 (5), 1763–1771. doi: 10.1523/JNEUROSCI.22-05-01763.2002.

Yang, Y., Shi, Y., Schweighauser, M., *et al*. (2022). Structures of alpha-synuclein filaments from human brains with Lewy pathology. *Nature*, 610(7933), 791-795. doi:10.1038/s41586-022-05319-3

Young, B. K., Camicioli, R., Ganzini, L. (1997). Neuropsychiatric adverse effects of antiparkinsonian drugs. Characteristics, evaluation and treatment. *Drugs & aging,* 10 (5), 367–383. doi: 10.2165/00002512-199710050-00005.

Zarranz, J. J., Alegre, J., Gómez-Esteban, J. C., Lezcano, E., Ros, R., Ampuero, I. *et al.* (2004). The new mutation, E46K, of alpha-synuclein causes Parkinson and Lewy body dementia. *Annals of neurology,* 55 (2), 164–173. doi: 10.1002/ana.10795.

Zhang, W., Wang, T. G., Pei, Z., Miller, D. S., Wu, X. F., Block, M. L. *et al.* (2005): Aggregated alpha-synuclein activates microglia: a process leading to disease progression in Parkinson's disease. *FASEB journal: official publication of the Federation of American Societies for Experimental Biology,* 19 (6), 533–542. doi: 10.1096/fj.04-2751com.

Zhou, W., Hurlbert, M. S., Schaack, J., Prasad, K. N., et al. (2000). Overexpression of human alpha-synuclein causes dopamine neuron death in rat primary culture and immortalized mesencephalon-derived cells. *Brain Research*, 866 (1-2), 33-43. doi: 10.1016/s0006-8993(00)02215-0.

7. Work Involvement

The vaccine candidates employed in this study were designed and developed by Dr José Miguel Flores-Fernandez in the laboratory of Prof Dr Holger Wille at the University of Alberta. Dr. Verena Pesch administered the intracerebral injections and prepared α-syn monomers and fibrils. Most of the indirect ELISA assays, as well as all comprehensive ELISA tests, were conducted in collaboration with Sara Reithofer. The TR-FRET assay was performed by Laura Müller.

8. Acknowledgements

Firstly, I would like to express my sincere gratitude to my supervisor, Prof. Dr. Erdem Tamgüney, for the opportunity to work on several interesting projects in his lab and for supporting me through my PhD. I am deeply grateful for your invaluable professional guidance throughout my experiments and thesis writing. Your insightful advice has been instrumental in shaping me into a proficient scientist. Moreover, I am deeply thankful for the personal support and care provided to my family members during challenging periods of the pandemic.

I would also like to express my gratitude to Prof. Dr. Dieter Willbold for agreeing to be my mentor and for allowing me to pursue my doctoral thesis in his institute.

My appreciation extends to my colleagues, Dr. Verena Pesch and Sara Reithofer, for their unwavering support and invaluable assistance during challenging phases of this project. Also, I am very thankful to everyone who contributed to this thesis: Pelin Özdüzenciler, Laura Müller, Yanik Busch, and my bachelor student Karl Werner.

I would also like to acknowledge the dedication of the animal house team, including the animal caretakers and Mrs. Kornadt-Beck. Regardless of weekends or public holidays, the animal caretakers consistently provided exemplary care for my laboratory animals. Mrs. Kornadt-Beck and all the caretakers were always available to assist with urgent animal-related matters.

Additionally, I would like to express my gratitude to my colleagues at IBI-7 and INM-2, who generously offered their assistance whenever I had questions. My gratitude also goes out to all the other current and former members of the Tamgüney lab for the great working atmosphere. Special recognition goes to Dr. Abhishek Cukkemane who has always been and still is open for scientific and non-scientific discussions, but also for welcoming me into his family. I would like to thank Yi Lien and Dila Kurtul for their invaluable support, evolving from colleagues to close friends.

I would also like to thank our secretaries Dorothea Stobbe and Sabine Werths. Thank you to them for providing me with all the help, especially for sending me birthday and New Year wishes every year. I am grateful to IT technician Volker Söhnitz for his assistance in resolving all my technical issues.

I would like to seize this chance to express my gratitude to my family, including my mother and wife, for their unwavering motivation and support throughout my four years of PhD studies. I cannot be myself without their emotional support. I deeply appreciate it.

My sincere acknowledgment also goes out to all of you whose names I couldn't mention individually for helping, supporting, advising, and motivating me in the past years.

9. List of Publications

Ma L*, Reithofer S*, Pesch V*, Miguel Flores-Fernandez JM*, Özdüzenciler P, Müller L, Werner K, Sriraman A, Wang YL, Amidian S, Camino JD, Schröder GF, Wille H, Tamgüney G. **(*equal contribution)**

Vaccines mimicking conformational epitopes on α-synuclein fibrils provide immunity to Parkinson's disease (In preparation)

Pesch V*, Flores-Fernandez JM*, Reithofer S*, **Ma L***, Özdüzenciler P, Busch Y, Sriraman A, Wang YL, Amidian S, Kroepel CVM, Müller L, Lien Y, Rudtke O, Frieg B, Schröder GF, Wille H, Tamgüney G. **(*equal contribution)**

Vaccination with structurally adapted fungal protein fibrils induces immunity to Parkinson's disease

Brain, Published: 01 March 2024, doi.org/10.1093/brai

Flores-Fernandez JM, Pesch V, Sriraman A, Chimal Juarez E, Amidian S, Wang XY, Duckering C, Fang A, Reithofer S, **Ma L,** Cortez LM, Sim VL, Tamgüney G, Wille H

Rational design of structure-based vaccines targeting misfolded alpha-synuclein conformers of Parkinson's disease and related disorders

Bioeng Transl Med, Published: 09 April 2024, doi.org/10.1002/btm2.10665

Lohmann S, Grigoletto J, Bernis ME, Pesch V, **Ma L**, Reithofer S, Tamgüney G

Ischemic stroke causes Parkinson's disease-like pathology and symptoms in transgenic mice overexpressing alpha-synuclein

Acta Neuropathol Commun, 10, 26 (2022), https://rdcu.be/cHITe